CAPITAL UNIVERSITY OF SCIENCE AND TECHNOLOGY, ISLAMABAD

Rhomboidal Restricted Six Body Problem

by

Muhammad Ateeq ur Rehman Siddique

A dissertation submitted in partial fulfillment for the degree of Doctor of Philosophy

in the

Faculty of Computing
Department of Mathematics

2023

Rhomboidal Restricted Six Body Problem

By

Muhammad Ateeq ur Rehman Siddique

(DMT163002)

Dr. Fazal Mehmood Mahomed, Professor

University of the Witwatersrand, Johannesburg, South Africa

(Foreign Evaluator 1)

Dr. Ugur Camci, Professor

Roger Williams University, Bristol, Rhode Island, USA

(Foreign Evaluator 2)

Dr. Abdul Rehman Kashif

(Research Supervisor)

Dr. Muhammad Sagheer

(Head, Department of Mathematics)

Dr. Muhammad Abdul Qadir

(Dean, Faculty of Computing)

DEPARTMENT OF MATHEMATICS

CAPITAL UNIVERSITY OF SCIENCE AND TECHNOLOGY

ISLAMABAD

2023

To my late parents, who unfortunately didn't stay in this world long enough to see their son become a doctor.

CAPITAL UNIVERSITY OF SCIENCE & TECHNOLOGY
ISLAMABAD

Expressway, Kahuta Road, Zone-V, Islamabad
Phone:+92-51-111-555-666 Fax: +92-51-4486705
Email: info@cust.edu.pk Website: https://www.cust.edu.pk

CERTIFICATE OF APPROVAL

This is to certify that the research work presented in the dissertation, entitled "**Rhomboidal Restricted Six Body Problem**" was conducted under the supervision of **Dr. Abdul Rehman Kashif**. No part of this dissertation has been submitted anywhere else for any other degree. This dissertation is submitted to the **Department of Mathematics, Capital University of Science and Technology** in partial fulfillment of the requirements for the degree of Doctor in Philosophy in the field of **Mathematics.** The open defence of the dissertation was conducted on **September 13, 2023**.

Student Name :	Muhammad Ateeq ur Rehman Siddique (DMT163002)	

The Examination Committee unanimously agrees to award PhD degree in the mentioned field.

Examination Committee :

(a)	External Examiner 1:	Dr. Zahid Ahmad Professor COMSATS University, Islamabad	
(b)	External Examiner 2:	Dr. Ibrar Hussain, Professor SEECS, NUST, Islamabad	
(c)	Internal Examiner :	Dr. Rashid Ali Professor CUST, Islamabad	
Supervisor Name :		Dr. Abdul Rehman Kashif Associate Professor CUST, Islamabad	
Name of HoD :		Dr. Muhammad Sagheer Professor CUST, Islamabad	
Name of Dean :		Dr. Muhammad Abdul Qadir Professor CUST, Islamabad	

AUTHOR'S DECLARATION

I, **Muhammad Ateeq ur Rehman Siddique (Registration No. DMT163002)**, hereby state that my dissertation titled, '**Rhomboidal Restricted Six Body Problem**' is my own work and has not been submitted previously by me for taking any degree from Capital University of Science and Technology, Islamabad or anywhere else in the country/ world.

At any time, if my statement is found to be incorrect even after my graduation, the University has the right to withdraw my PhD Degree.

(Muhammad Ateeq ur Rehman Siddique)

Dated: 13/ September, 2023

Registration No: DMT163002

PLAGIARISM UNDERTAKING

I solemnly declare that research work presented in the dissertation titled "**Rhomboidal Restricted Six Body Problem**" is solely my research work with no significant contribution from any other person. Small contribution/ help wherever taken has been duly acknowledged and that complete dissertation has been written by me.

I understand the zero-tolerance policy of the HEC and Capital University of Science and Technology towards plagiarism. Therefore, I as an author of the above titled dissertation declare that no portion of my dissertation has been plagiarized and any material used as reference is properly referred/ cited.

I undertake that if I am found guilty of any formal plagiarism in the above titled dissertation even after award of PhD Degree, the University reserves the right to withdraw/ revoke my PhD degree and that HEC and the University have the right to publish my name on the HEC/ University Website on which names of students are placed who submitted plagiarized dissertation.

(Muhammad Ateeq ur Rehman Siddique)

Dated: 13 September, 2023

Registration No: DMT163002

List of Publications

It is certified that following publication(s) have been made out of the research work that has been carried out for this dissertation:-

1. **M. A. R. Siddique**, A. R. Kashif, "The Restricted Six-Body Problem with Stable Equilibrium Points and a Rhomboidal Configuration", Advances in Astronomy, vol. 2022, Article ID 8100523, pages 1-17, 2022. https://doi.org/10.1155/2022/8100523

2. **M. A. R. Siddique**, A. R. Kashif, M. Shoaib, S. Hussain, "Stability Analysis of the Rhomboidal Restricted Six-Body Problem", Advances in Astronomy, vol. 2021, Article ID 5575826, pages 1-15, 2021. https://doi.org/10.1155/2021/5575826

Muhammad Ateeq ur Rehman Siddique
(DMT163002)

Acknowledgements

I give all praise and thanks to **Allah Almighty**, who has showered me with many favours and given me the fortitude to accomplish my aims and this task. With Allah's help, I hope to make the right decisions (ameen). The Holy Prophet **Hazrat Muhammad (PBUH)** was the most flawless human being to have ever lived, and he taught his followers the importance of learning.

My sincere gratitude goes out to **Dr. Abdul Rehman Kashif**, my supervisor, whose unwavering support and insightful feedback were invaluable to my success in completing this project. Thanks to his wisdom, kind assistance, and insightful critiques, I was able to finish my dissertation.

I would like to extend my gratitude to **Dr. Muhammad Sagheer**, head of the mathematics department, for all the support he has given me as a student, from a stimulating learning environment to academic direction and motivation, as well as insightful advice.

I will always be grateful to my parents, **Muhammad Siddique (Late)** and **Parveen Akhtar (Late)**, for their prayers and tireless support. They never stopped believing in me and were willing to make sacrifices for my success. Their boundless affection and fervent prayers have been my compass ever since I was a little child. To my wife, *Zareeda Ateeq*, and my dear brothers, *Dr. Muhammad Laiq ur Rehman* and *Muhammad Khaliq ur Rehman*, I am eternally grateful for the unending love and encouragement they have given me throughout my life.

I wish to express my appreciation to my co-authors, **Dr. Muhammad Shoaib** and **Dr. Shafqat Hussain**, for their inspiration, assistance, and direction for the publication of my research articles. I owe a great obligation of gratitude to my PhD colleagues, without whom I would not have been able to finish my dissertation. I also want to express my gratitude to Dr. Sohail Ashraf, Dr. Tahir Imran, Farooq Abdullah, Zaheer Ahmed and Amir Shahzad for their help and cooperation.

Muhammad Ateeq ur Rehman Siddique

Abstract

We discuss the restricted rhomboidal six-body problem (RR6BP), which has four positive masses at the vertices of the rhombus, and the fifth mass is at the intersection of the two diagonals. These masses always move in rhomboidal central configuration with diagonals 2a and 2b. The sixth body, having a very small mass, does not influence the motion of the five masses, also called primaries. In this capacity we discuss two cases of primaries with different masses. Case-I holds the families of rhomboidal central configuration for the mass parameters $a = 1$ and $b \in (1/\sqrt{3}, 1.1394282249562009)$ when the masses along horizontal axis are assumed to be same, i.e., $m_0 = m_1 = m_2 = m$ and the masses along the vertical axis are same, i.e., $m_3 = m_4 = \widetilde{m}$. The Case-II holds the families of rhomboidal central configuration for the mass parameters a and b both vary in the interval (0.5, 1) when masses along the horizontal axis at the edge of rhombus other than m_0 are taken same, i.e., $m_1 = m_2 = m$ and the masses along the vertical axis m_3 and m_4 are taken same, i.e., $m_3 = m_4 = \widetilde{m}$. The equilibrium points for the test mass m_5 of a very small mass as compared to the primaries whose motion is influenced by the gravitational attraction of the primaries are found in both the cases. Case-I yielded that there are always 12 unstable equilibrium points, while the Case-II have further four sub-cases in the interval (0.5, 1) regarding the mass parameters a and b. These sub-cases have 16, 20, 12 and 12 equilibrium points respectively. The first sub-case contains 8 off the coordinate axis stable equilibrium points; second sub-case also contains 8 off the coordinate axis stable equilibrium points; third sub-case contains 4 off the coordinate axis equilibrium points; the fourth sub-case has no stable equilibrium points. Further, using the first integral of motion, we derive the region of possible motion of test particle m_5 and identify the value of Jacobian constant C for different energy intervals at which these regions become disconnected or partially disconnected.

Contents

List of Figures

List of Tables

Abbreviations

ATHENA	Advanced Telescope for High Energy Astrophysics
ACE	Advance Composition Explorer
CSA	Canadian Space Agency
CR3BP	Circular Restricted Three-Body Problem
CC	Central Configuration
DSCOVR	Deep Space Climate Observatory
ESA	European Space Agency
G3BP	General Three-Body Problem
IMAP	Interstellar Mapping and Acceleration Probe
JWST	James Webb Space Telescope
NASA	The National Aeronautics and Space Administration
R3BP	Restricted Three Body Problem
RR6BP	Restricted Rhomboidal Six-Body Problem
SOHO	Solar and Heliosphere Observatory

Symbols

A	Area
C	Jacobian constant
$\boldsymbol{a}_0$	Constant acceleration vector with respect to time
C_i	Concentric circles $(i = 1, 2, 3, ..., n)$
$\boldsymbol{c}$	Constant vector
e	Eccentricity
E_p	Potential Energy
f	True anomaly
h	Height above floor level
$\boldsymbol{L}$	Angular momentum vector
L_i	Lagrange points $(i = 1, 2, 3, ..., n)$
l	Latus rectum
m_0	Mass of the object positioned on the point of intersection of the two diagonals of rhombus.
m_i	Mass of the objects positioned at the vertices of rhombus $(i = 1, 2, ..., 4)$
m	Mass of the objects placed along the horizontal axis
$\widetilde{m}$	Mass of the objects placed along the vertical axis
M	Mass of Sun
λ	Mass parameter (ratio of the diagonal lengths of rhombus)
μ	Mass parameter
μ_c	Critical mass parameter
T	Time period
k	The number of restricted bodies
n	The number of heavenly bodies other than the primaries

N	Number of the heavenly bodies, called primaries
$\mathbf{p}$	Linear momentum vector
J	Joule
π	The ratio of a circle's circumference to its diameter
α	Angle of the rotating vector with respect to the axis of rotation
r_i	Positions of objects $(i = 0, 1, ..., n)$
F	Force
G	Universal gravitational constant
g	Acceleration due to gravity
r	Distance between the objects
$\mathbf{R}$	Position vector from the inertial frame of reference to the non-inertial frame of reference
$\mathbf{r}'$	Position vector relative to the translating frame of reference
$\boldsymbol{r}$	Position vector of the earth from the sun
r_H	Hill radius
$\boldsymbol{v}$	Velocity vector of an object
$\boldsymbol{v}_0$	Constant velocity vector
$\mathbf{V}$	Velocity of an object relative to inertial frame
$\hat{\boldsymbol{r}}$	Unit vector in radial direction
θ	Angle spanned by frame rotation
θ^*	Constant of integration
$\hat{\boldsymbol{\theta}}$	Unit vector in angular direction
$\boldsymbol{\Upsilon}$	Vector inscribed in the rigid body B
U	Effective potential
V	Gravitational potential
W	Work done
$\boldsymbol{\omega}$	Angular velocity vector
x, y, z	Rectangular coordinates of point particles.
$\mathring{x}, \mathring{y}, \mathring{z}$	Rectangular coordinates of the center of mass
ξ_i, η_i, ζ_i	Rectangular coordinates with respect to the mass and $i = 1, ..., N$
x, y, z	Coordinates of rotating as well as translating frame of reference.

Chapter 1

Introduction

Clusters of objects can be found anywhere in the Universe. Specific stars, star clusters, clouds of hydrogen, and sets of galaxies are all compelled to move relative to one another by the law of gravitation. The N-body problem has been researched extensively in relation to the motion of these clusters of particles throughout history. For the problems with one body and two bodies, there is a well-known solution in closed form [1]. The general three-body problem (G3BP), which arises when $N = 3$, is one of the most interesting unsolved dynamical problems. This problem for $N = 3$ proved to be a cornerstone for celestial mechanics. The ethereal beauty of the night sky and the motion of the Sun influenced this branch of science to begin its quest. In recent years, this field of research has made considerable strides in solving N-body problems.

The quest began with Sir Isaac Newton, who published a work in Principia [2] (1685) on the motion of three bodies subject to the mutual gravitational force but he limited himself to verbal descriptions and geometric drawings. Euler and Lagrange provided the particular solutions to the G3BP. Euler, in 1767 [3], discovered the first three-particle Central Configuration (CC). The three particles in this configuration move in a proportional manner along a fixed straight line (collinear). *A central configuration of N-bodies is a geometric arrangement of N-bodies in which the gravitational and centrifugal forces are equal and preserve the configuration forever.* The triangular CC was discovered by Lagrange (1772) [4],

in which the three bodies move by retaining an equilateral triangle throughout their motion. Additionally, Euler was the first to suggest the circular restricted 3-body problem (CR3BP). Lagrange, on the other hand, focused at the CR3BP and discovered five equilibrium points that are now referred to as Lagrange points, which can be seen in Figure 1.1 for the Earth-Sun system. The James Webb Space Telescope (JWST) [5] was recently directed to park at L_2 of the Earth-Sun system. Its main objective is to observe the Universe's first galaxies after the big bang and the origin of the Universe. It will also observe the birth of early stars and exoplanets with the potential for life.

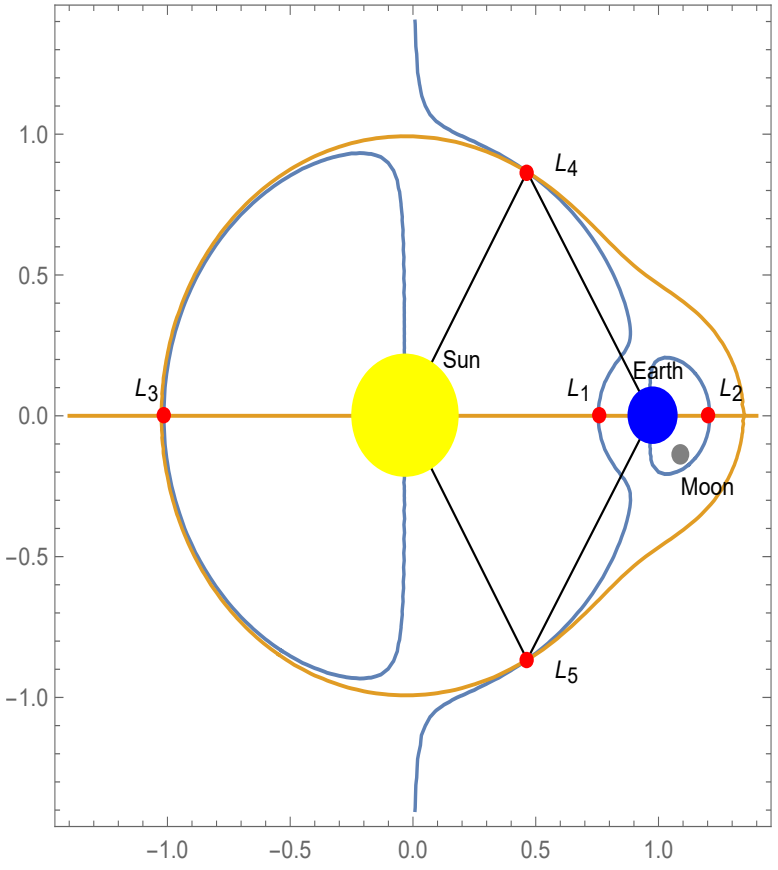

FIGURE 1.1: The Lagrange Points L_1,...,L_5 for the Sun-Earth System are shown as red dots.

Lagrange found that if a test particle (matroids, asteroids, artificial satellite, etc) is placed at one of the two stable points L_4 or L_5, of two celestial objects, then this test particle would remain stationary in its orbit relative to these objects. This phenomenon happened due to the combined forces of the two celestial objects. In

1906 [6], Professor Wolf discovered asteroids (named Trojan and Greek asteroids) in the orbit of Jupiter which is at L_4 and L_5 of the Sun-Jupiter system.

Over the past century, the 3-body problem has received the most attention of celestial mechanics research. A lot of research has been done in the last two centuries on R3BP. The interested reader can see more literature on R3BP [7–22]. Because of the challenges of handling the extra parameters in four and five body problems, relatively little analytical work has been conducted on problems involving more than three bodies. Apart from historical grounds, there are several other reasons to investigate the $N \geqslant 4$-body problem, since it is estimated that in our galaxy, multistellar systems make up around two thirds of the stars. Around one-fifth of these belong to triple systems, with another one-fifth belonging to quadruple or higher systems [23].

A fundamental approach in astronomy and astrophysics is the few-body problem, ranging from solar dynamic systems to galactic dynamics [24]. Due to the increased complexity of having a larger number of bodies, the majority of research on the four, five, and six body problems has focused on their CCs and the presence and stability of equilibrium solutions.

1.1 Central Configurations

The particular geometric compositions of the bodies are known as *Central Configurations* that maintain the shape of their configurations throughout their motion, regardless of their configuration size. The very first contribution to the CC was made by Euler and Lagrange, which paved the way for the present research in celestial mechanics. Euler gave the collinear CC while Lagrange introduced the triangular CC of the three body system of point masses [3, 4].

Lots of work has been done on CCs after Euler and Lagrange and has revealed very interesting results regarding the configuration of CC and the existence and stability of the equilibrium solutions. Saari [25], discussed the role of CCs in the N-body system analysis and he highlighted N-body zero redial velocity surfaces, extending

gravitational systems, and collision orbits. The properties of CC are discussed in the second half of the paper and the the focus is on outlining a distinct approach for analysing these configurations. This approach is demonstrated by discussing Central Configuration nondegeneracy and describing CCs in various dimensions. Using equivariant Morse theory, Pacella [26] determined the least number of N-body problem CCs in $\mathbb{R}^3$ in the case of equal masses, he demonstrated that the planar CCs are potential energy saddle points. The author also deduced that there exist non-planar CCs for every $N \geq 4$.

Moeckel [27], highlighted that CCs are of relevance to celestial mechanics for several reasons. He discussed that what will occur when masses with zero initial velocity are released from a CC ? The arrangement collapses homothetically as all particles speed toward the origin and there is a collision singularity as a result.
As stated by Euler in 1767, the earliest clearly identified approaches to the 3-body problem were simple collision trajectories of this kind. It can be demonstrated that, every such orbit has an asymptotically CC. Additionally, a planar centre arrangement generates a family of periodic solutions. The central arrangement releases the particles with starting velocities that are always perpendicular to their position vectors and the magnitude of a particle's velocity is in proportion to its distance from the origin. The orbit of each particle will be elliptical, similar to the Kepler problem; however, the configuration remains comparable to the original configuration during the whole motion, with just the size changing. If the velocity of particles is just sufficient, there will be circular orbits. As velocities approach zero, the eccentricity of ellipses increases, and periodic solutions approach collision solutions.

According to Slaminka and Woerner [28] , the N-body problem's relative equilibrium state for a rotating system as well as the analysis of total collisions, both require consideration of the CC approach. However, only few arrangements of this nature are known. With the use of a novel global optimizer, they have been able to design new families of coplanar CC with equal-mass particles, as well as extend these constructions to configurations with varying masses and the non-coplanar situation.

Xia [29] conducted research and discovered the precise numbers of CC's for a few open collections of N positive masses for every given N value. It turns out that the numbers are directly proportional to N; for example, given an open set of eighteen positive masses, there are about 2.08766×10^{20} classes of different CCs. He also came upon a few findings regarding the Hausdorff measure for the group of N positive masses that had a degenerate CC. Casasayas et al. [30] developed a novel derivation for the CC equations of the $1 + N$ body problem and showed that there is only one solution for equal masses and large value of N. For more understanding of the CC one should see [31–58].

The most recent work on CC includes the equilateral pentagonal configurations of the 5-body problem, that consisted a cycle of five equal edges, which were the focus of Deng and Hampton's research [59]. They established a number of conclusions pertaining to CC with this property, that include a computer based demonstration of the the boundedness of such arrangements for any set of five positive masses with a range of homogeneous potentials with rational exponents.

Fernandes et al. [60] investigated central six-body planar configurations with specific symmetries, and using analytic evidences, the authors demonstrated the existence of a novel non-absolute convex CC, a non-symmetric concave instance of CC, and various situations of stacked CC, that are CCs with subgroups of the bodies also generating CCs.

Wang [61] investigated a kind of CC in which all of the masses are arranged in a circle and the centre of the mass matches with the centre of the circle named as the"centred co-circular CC." The author discovered several symmetry results for these kind of CCs and also established that for positive numbers $\alpha > 0$ and integers $N \geq 3$ that satisfies $\frac{1}{N}\sum_{j=1}^{N-1} \csc^{\alpha}\frac{j\pi}{N} \leq 1 + \frac{\alpha}{4}$, the regular N-gon with equal masses is the only CC (centered co-cicular) for the N-body problem having power-law potential. The standard N-gon is the distinct centering co-circular CC for the Newtonian N-body problem when $\alpha = 1$ and $N \leq 6$.

Xian and Deng [62] investigated the link between the masses of five satellites and certain symmetric configurations with one satellite on the symmetry axis.

Analysing several CCs for adequate positive masses under particular assumptions, the authors discovered some CCs.

They further showed that in particular cases of symmetrical satellite configurations, there exists a family of mass vectors that can be described by a single parameter, resulting in the configuration being a CC. In addition, the authors showed some numerical findings for configurations and deduced the positive masses for these satellites, indicating that these configurations are CCs.

1.2 The Restricted N-Body Problems and Lagrange Points

In comparison to the N-bodies (known as primaries) problem, the restricted N-body problem is defined as one of the bodies from N-bodies is infinitesimal, which is sometimes called secondary, and its mass is negligible as compared with the rest of $N-1$ primaries i.e., Mass of secondary $<<$ Mass of the Primaries. In other words, the secondary mass will move in the gravitational field of the primaries but it will not affect the gravitational field of the primaries. It will always act as a test particle in the field of $N-1$ primaries. This constraint gave rise to specific solutions to N-body problems, which remained unsolved for centuries.

When moving under the gravitational influence of the primary, the secondary body encounters certain spots between them where the gravitational pull of the primaries becomes equal, and these points are known as Lagrange (equilibrium) points. These equilibrium points are rather stable or unstable, which means that when the secondary body reaches a stable point, it will remain there for ever until some other force displaces them. Trojan and Greek asteroids have been discovered in Jupiter's orbit at L_4 and L_5 in the Sun-Jupiter restricted three body system [63]. Recently James Webb Space Telescope [64] has been sent at L_2 of the Earth-Sun restricted three body system to provide a view of the immense galaxy cluster.

Belbruno [65] developed and quantitatively examined a novel family consisting of periodic orbits extending out from a successive collision orbit in the restricted 3-body problem in three dimension. A countable collection of resonant energy values is associated with the Sun-Earth system, and the energy each time cuts across one of them, the periodic orbit creates a loop through intersecting its own orbits.

Ansari and Alhussain [66] investigated "The Restricted Five-Body Problem With Cyclic Kite Configuration," and discovered that in-plane motion has four equilibrium points, but there are only two equilibrium points for out-of-plane motion. They discovered several forms by drawing zero-velocity curves for both in-plane and out-of-plane motions with respect to each Jacobi constant. They also coloured the motion zones for each Jacobi constant to show that motion is restricted in the coloured regions, while small objects have the ability to move unrestrictedly within the remaining regions. The Poincaré surfaces have the form of butterfly wings, and there is no chaos.

Ollongren [67] developed a generalisation of the well-known restricted problem of three bodies in celestial mechanics, for which Lagrangian points of equilibrium are shown to exist, their locations are determined, and a linear stability analysis is carried out using computer algebra. Liu and Dong [68] re-framed the CR3BP using the port-Hamiltonian technique, and they got the closed loop system Hamiltonian by developing a control scheme as a choice of Lyapunov function that guarantees asymptotic stability. Within the domain of application of the CR3BP model, this method of control also showed global stability.

Lara and Bengochea [69] studied the restricted problem of N-bodies when $N = 2n + k$. They found the existence of reverse symmetry for all $2n$ pairs of bodies having the same mass, where k is the number of restricted bodies. The authors calculated a portion with respect to the sets from which symmetric orbits emerge with the aid of inverting symmetries. The presence of equilibrium points (equilibrium points) and the associated first-order stability analysis of the restricted 4-body problem on an elliptic planar domain subject to radiation pressure owing to radiating primaries were examined by Meena and Kishor [70]. When the radiation pressure from the radiating primaries is present, there are significant

shifts in the location, coordinates, and stability regions of the equilibrium points. Additionally, the quantity of equilibrium points within the range $0 < e < 1$ for eccentricity has been studied, and it has been found to decrease with increasing eccentricity. This holds true for the range of true anomaly f as well, while true anomaly $f \in [0, 2]$ exhibits random variation.

The equilibrium points dependent on the primary masses were investigated by Alvarez-Ramrez and Medina [71] for the planar restricted five body problem with the four pirmaries construct an axisymmetric 4-body CC. Zepeda et al. [72] analysed the restricted equilateral 4-body problem for equilibrium points in a planar sense, where one particle with insignificant mass moves in the gravitational field consistent with Newton's laws of three primaries with the three positive masses.

According to the Lagrangian configuration, they always have their centres of mass at the three points of an equilateral triangle and rotate around that triangle at a constant angular velocity. The author also examined the non-linear stability with respect to Lyapunov of the elliptic equilibrium for the particular values the primaries, that is, all the primaries have unequal masses.

In order to learn more about the six-body problem and its periodic solutions in a fresh way, Alsaedi et al. [73] employed a combination of variational approaches and a computer algorithm. All the equilibrium points are located on the concentric circles denoted as C_1, C_2, and C_3 with the centre at the origin, as demonstrated by Idrisi and Shahbaz Ullah [74]. Some liberation points on circle C_2 are stable, but those on C_1 and C_3 are unstable.

Idrisi and Shahbaz Ullah [75], in the square CC of the restricted 6-body problem, studied the stability of equilibrium solutions under minor perturbations of the coriolis as well as centrifugal forces. There were total of twelve equilibrium points, with four being collinear and eight being non-collinear. These equilibrium points are situated on three concentric circles, namely C_1, C_2, and C_3 that all share a common origin. The authors also observed that there are four *off-axes* equilibrium points and eight *on-axes* equilibrium points., i.e., L_1, L_2, L_3, and L_4 are on the x-axis, L_5, L_6, L_7, and L_8 occupy the y-axis, and the remaining four are *off-axes*.

Further, the positions at which each equilibrium point is located were only altered by a minor change to the centrifugal force. Furthermore, it has been discovered that the stability of the equilibrium points located on the circles denoted as C_1 and C_3 remains unaltered by perturbations, and they continue to remain unstable across all values of the mass parameter (μ), however, the impact of perturbations on the stability of equilibrium points situated on the circle C_2 is noteworthy, and and it was found that all of the equilibrium points were stable for μ_c (the critical mass parameter).

1.3 Literature Review Relevant to the Problem Statement

"The restricted rhomboidal five body problem" was coined by Kuleza et al. in 2011 [76], they devised a system which involved four masses, referred to as the primaries, go around in a circle side-by-side in such a way that their configuration is rhombus through out their motion, with the fifth mass being tiny and having no influence on the motion of the four primaries. It was postulated that the fifth mass lies on the same plane as the primary masses, wherein $m_1 = m_2 = m$ and $m_3 = m_4 = \widetilde{m}$. The radius linked to the circular movement of m_1 and m_2 is denoted as λ, which varies in the interval $[1, \sqrt{3}]$, and the radius is unity for $\widetilde{m}$.

The Hamiltonian structure was utilized to delineate the feasible motion regions and establish the existence of equilibrium solutions, both on and off the coordinate axes. It was demonstrated that the number of equilibrium solutions is dependent on λ and that there may be 11, 13, or 15 unstable equilibrium solutions.

In 2012, Waldvogel [77] investigated "The rhomboidal symmetric four-body problem" and demonstrated binary collision, periodic solutions, chaos, and 4-body collision and escape manifolds, and discovered that a key role is played by resonance activities between interacting rectilinear binaries.

Also in 2012, Shoaib et al. [47] investigated a CC for the N-body problem in

which each particle's position vector with relation to the center of mass follows the condition for CC, and the authors identified specific areas within the phase space wherein the selection of positive masses would result in a CC. They also demonstrated that no central arrangements are viable in the complement of those regions.

Vidal and Marchesin in 2013, [78] studied "Stability in a rhomboidal 5-body problem with generalized central forces" and they demonstrated that three unique relative rhomboidal solutions exist, with the following CC:

1. The rhombus is a square in which all of the primaries have the same mass;
2. There is no transformation from rhombus to square with equal masses for all primaries;
3. There is no transformation from rhombus to square with different masses for the pairs of primaries.

Marchesin in 2017 [79], took into account a planar 5-body system with masses of m_0, $m_1 = m_2 = m$, and $m_3 = m_4 = \widetilde{m}$ moving in a plane and correspondingly positioned at r_0, r_1, r_2, r_3, and r_4. m_0 is placed at the configuration's centre, which is taken to represent the coordinate system's origin. The four additional bodies, known as the primaries, are always arranged in a rhombus configuration. The existence of multiple rhomboidal CCs with a central body was exhibited by the author under the assumption that all of the bodies had Newtonian-type mutual attraction. One of the semi-diagonals was normalised to one, whereas the second semi-diagonal varied over the interval $[1, \sqrt{3}]$. The author has shown that the parameter value as well as the central mass have an impact on the masses of the primaries.

Additionally, the square configuration case and the situation with no mass at the centre were both analysed by the author. In these specific circumstances, the values of the parameters were determined to be $\lambda = 1$ and $m_0 = 0$, correspondingly. The value of $\lambda = \sqrt{3}$ represents the degenerate case where the masses of two primary bodies and the central body become negligible, resulting in the configuration

of a limited 5-body problem with three bodies having null masses. This research targets the rhombidal CC with five masses to find the equilibrium solutions and their stability, which have not been targeted since Kuleza et al [76].

The study of CCs and liberation points is a very important topic and it was identified by Smale [80] as the problem for 21^{st} century. This research of restricted rhomboidal six body problem illustrated that the CCs depend upon μ, which is the mass parameter and assumed that the collinear masses along the horizontal axis, m_0, m_1 and m_2 are equal to m, where the remaining two masses, m_3 and m_4 are equal to $\widetilde{m}$. The change in the value of μ, considerable changes in equilibrium point locations and numbers have been seen, resulting in 12 equilibrium points in all cases. The value of the Jacobian constant has also been found for the possible motion region for the infinitesimal body. The stability analysis showed that all the equilibrium points are unstable.

Idrisi and Shabaz Ullah in 2020, presented "Central-Body Square Configuration of Restricted Six-Body Problem" and they discovered a total of twelve equilibrium points, four of which are collinear and the remaining eight of which are not collinear. Concentric circles C_1, C_2, C_3 centred at the origin consist of all the equilibrium points. For all μ, the equilibrium points on C_1 and C_3 are unstable, but the equilibrium points on C_2 are stable for $\mu_c = 0.00910065$. This research also shows that when taking the masses relation $m_0 = 1 - 2(m + \widetilde{m})$, where $m_1 = m_2 = m$ and $m_3 = m_4 = \widetilde{m}$ the mass parameter are now a and b and both vary in the interval $(0.5, 1)$. This changes the gravitational field of the primaries, which makes a significant change in the dynamics of the infinitesimal body and leads to some stable points, which has become a remarkable contribution to the literature for future research. The Jacobian constant has been determined for the infinitesimal body's motion, which could represent a future satellite or space mission.

1.4 Dissertation Contribution

The rhomboidal six-body problem comprises five heavenly bodies (primaries), and a restricted test particle that is very small as compared to the five primaries

has been modelled in this dissertation. The four primary bodies are commonly perceived to be situated at the vertices of a rhombus, while the fifth primary body is located at the intersection point of the rhombus' diagonals. This intersection point is also regarded as the origin of the coordinate system. The primaries have the property of CC, and no matter how they move, they always stay in a rhombus shape. The CC of primaries in relation to their masses is looked at in two different ways: In the first case, the primaries along the horizontal axis, including the one placed on the origin of the coordinated axis, are considered to have the same mass, while the primaries placed on the vertical axis have the same mass; in the second case, the primaries along the horizontal axis are assumed to have the same mass, while the primaries along the vertical axis are of the same mass, where the primary placed at the origin of the coordinated axis is neither equal to the primaries that are along the horizontal axis nor equal to the primaries that are along the vertical axis. The equations of motion of the primaries are obtained using Newtonian mechanics, and after setting the values of angular velocity and gravitational constant unity according to the natural units, the bounds for the mass parameters for which the families of rhomboidal CC hold are discovered. In the first case, among the families of CCs, some special cases are presented, among which, when the mass parameters become equal, a square CC is observed, and the values for which the CC degenerates are also shown. The second case of CCs shows that families of CC hold in the same interval for both mass parameters. Four special cases of CC are shown in which one mass parameter is kept fixed while the variation of masses is observed when the other parameter varies in the specific interval. The sixth, very small mass moves under the gravitational influence of the primaries, and due to its very small mass, its gravitational force has no influence on the primaries. The equation of motion of the sixth body is also found using Newtonian mechanics, and after transforming the coordinate system into a co-rotating coordinate system, the equilibrium points of the sixth body for both cases of CC are found, and only those are shown where either the positions or the number of equilibrium points change significantly. The qualitative analysis is carried out using contour plots, in which red dots represent the equilibrium points while black dots are for the primaries of the system that maintain a rhomboidal CC. The behaviour of the sixth mass in

the presence of a changing gravitational field is explored, and equilibrium points are tested for their stability by linearizing the system around each equilibrium point. The first case of CC doesn't show any stable equilibrium point but the second case of CC shows some stable equilibrium points. The Hill sphere and the permissible and non-permissible regions of motion of the small mass with respect to the Jacobian constant have also been discussed.

1.5 Organization of Dissertation

Here is how the rest of the dissertation is laid out:

- Chapter 2 is dedicated to the fundamental concepts, definitions, and proofs presented. This chapter begins with Newtonian mechanics and progresses to proofs of Kepler's Laws of Planetary Motion and all other fundamental and advanced concepts upon which subsequent chapters are built.

- In Chapter 3, the focus is on the study of CCs within the context of the rhomboidal restricted six-body problem in Newtonian gravity. This particular problem involves four primary masses, denoted as m_i where i ranges from 1 to 4, located at the vertices of a rhombus with coordinates $(a, 0), (-a, 0), (0, b)$, and $(0, -b)$, respectively. Additionally, a fifth mass denoted as m_0 is situated at the intersection point of the diagonals of the rhombus, which is placed at the centre of the coordinate system (i.e., in the first case, the masses of primaries are $m_1 = m_2 = m_0 = m$ and $m_3 = m_4 = \widetilde{m}$, while in the second case, $m_1 = m_2 = m$, $m_3 = m_4 = \widetilde{m}$, and $m_0 = 1 - 2(m + \widetilde{m})$. We find the CCs equations in both cases and transform the masses m and $\widetilde{m}$ as a function of a and b as algebraic equations. The CC hold in the interval b belongs to $(1/\sqrt{3}, 1.1394282249562009)$ and $a = 1$ in the first case, and CC hold in interval $(0.5, 1)$ for both a and b in the second case.

- Chapter 4 is dedicated to the sixth-body motion and its equilibrium points in connection to the two models of rhomboidal CC represented in Chapter 3.

The existence and stability of equilibrium solutions, along with the effective potential, zero-velocity surface, and Jacobian constant based regions of motion, have been given in this chapter.

The findings prescribed in Chapter 3 and Chapter 4 have been published in the following journal articles:

- **M. A. R. Siddique**, A. R. Kashif, "The Restricted Six-Body Problem with Stable Equilibrium Points and a Rhomboidal Configuration", Advances in Astronomy, vol. 2022, Article ID 8100523, 17 pages, 2022. https://doi.org/10.1155/2022/8100523

- **M. A. R. Siddique**, A. R. Kashif, M. Shoaib, S. Hussain, "Stability Analysis of the Rhomboidal Restricted Six-Body Problem", Advances in Astronomy, vol. 2021, Article ID 5575826, 15 pages, 2021. https://doi.org/10.1155/2021/5575826

- Chapter 5 is dedicated to the conclusions and the future work.

Chapter 2

Preliminaries

The essential definitions, concepts, and Celestial models on which the other chapters of the dissertation are built, are covered in this chapter. We begin our first section with the basic definitions of Celestial Mechanics, center of mass, point mass, frame of references, etc., and then go through the two and three body problems in depth in the second section.

2.1 Definitions

In this section, some definitions are provided to help understand certain concepts related to the work presented in this dissertation.

2.1.1 Newtonian Mechanics

Newtonian mechanics is a mathematical framework that attempts to explain how various objects in the universe move. Sir Isaac Newton initially stated the main ideas of this approach in his work **Philosophiae Naturalis Principia Mathematica (Mathematical Principles of Natural Philosophy)**. The Principia is the modern name for this book, which was first published in 1687.

2.1.2 Newton's Laws of Motion

The Newton's three laws of motion served as the cornerstone for the study of dynamics. Although some, if not all, of these laws which, at the time, were taken for granted in the scientific paradigm, his concise elaboration of these laws and exploration of their implications, coupled with the law of universal gravitation, contributed more than any of his contemporaries' work to the modern scientific era. They can be expressed as follows [81]:

i. "Every body continues in its state of rest or of uniform motion in a straight line except in so far as it is compelled to change that state by an external impressed force.

ii. The rate of change of momentum of the body is proportional to the impressed force and takes place in the direction in which the force acts.

iii. To every action there is an equal and opposite reaction."

2.1.3 Newton's Law of Gravitation

Astrodynamics and Celestial Mechanics are both based on Newton's law of universal gravitation. In order to have the solution of the a set of complex equations resulting from the formulation of problems related to systems of masses that attract one another mutually, several beautiful mathematical techniques were developed. The law states that "Every particle of matter in the universe attracts every other particle of matter with a force directly proportional to the product of the masses and inversely proportional to the square of the distance between them" [81]. Thus, we obtain the relationship between two particles separated by distance r.

$$F = G\frac{m_1\, m_2}{r^2}, \tag{2.1}$$

where G is the constant of universal gravitation, F represents gravitational force, m_1 and m_2 represent the masses of the particles.

The relation 2.1 in vector form can be written as

$$\mathbf{F} = -G\frac{m_1\, m_2}{r^3}\mathbf{r}, \tag{2.2}$$

where at a distance r from a particle of mass m_1 a second particle of mass m_2 experiences an attractive force. Here the minus sign ensures that the force is attractive, i.e., $m_1(< m_2)$ is attracted towards m_2. According to Newton, the gravitational force operating on mass 'i' due to presence of other masses in the system is

$$\mathbf{F}_i = m_i\, \ddot{\mathbf{r}}_i = \sum_{\substack{j=1 \\ j\neq i}}^{N} G m_i\, m_j \frac{(\mathbf{r}_j - \mathbf{r}_i)}{|\mathbf{r}_j - \mathbf{r}_i|^3}, \tag{2.3}$$

where $\mathbf{F}_i$ is the force applied on the i^{th} mass, the value of G, the universal gravitational constant, is 6.67×10^{-11} $\mathtt{Nm}^2\, \mathtt{Kg}^{-2}$, $\ddot{\mathbf{r}}$ is acceleration of the masses, $\mathbf{r}_i$ and $\mathbf{r}_j$ are the position vectors, 'i' is from 1 to N and N is number of masses, m_i and m_j are the masses, $(\mathbf{r}_j – \mathbf{r}_i) = \mathbf{r}_{ij}$ is the distance of j^{th} mass from i^{th} mass.

2.1.4 Celestial Mechanics

Celestial Mechanics, a notion that Laplace first proposed in 1799, is the field of astronomy associated with the movements of celestial objects under the effect of gravity, particularly objects comprising the solar system. The objective of Celestial Mechanics is to explain these movements based on Newtonian physics. Modern analytic Celestial Mechanics began in 1687 with the appearance of Newton's famous Principia.

2.1.5 Kepler's Laws

After Tycho Brahe passed away on October 24, 1601, Johannes Kepler, a German astronomer, was named Tycho's successor as the imperial mathematician and given the task of finishing his unfinished work. Kepler was an assistant to Tycho Brahe while the two worked together in Prague. Kepler analysed Tycho

Brahe's great number of observational data on the movements of the planets, and then formulated the three laws that govern the motion of planets and carry his name. The three laws are:

Kepler's First Law (The Law of Orbits)

The geometry of the orbits of the planets and the Sun's location inside them are revealed by Kepler's first law which is stated as:
"The orbit of each planet is an ellipse with the sun at one focus." [81]

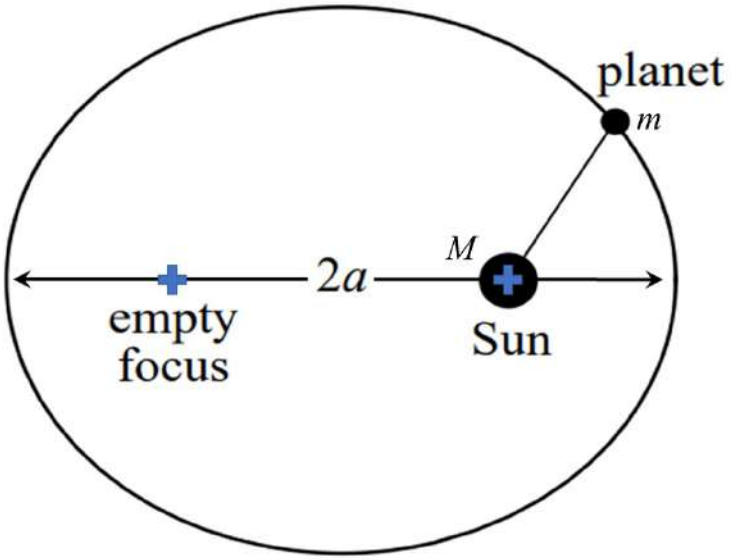

FIGURE 2.1: In the geometry for Kepler's first law, the Sun is at one of the two focal points of the planet's elliptical path. The other focal point is empty.

The proof of Kepler's First Law can be seen in the solution of Two Body Problem in Section 2.1.16

Kepler's Second Law (The Law of Areas)

The second law of Kepler claims that regardless of whether a planet is close to its perihelion or aphelion, an equivalent amount of area is spanned by the radial vector that extends from the Sun to the planet in an equal amount of time, which

can be seen in Figure 2.2. According to the law:

"*For any planet the rate of description of area by the radius vector joining planet to Sun is constant.*" [81]

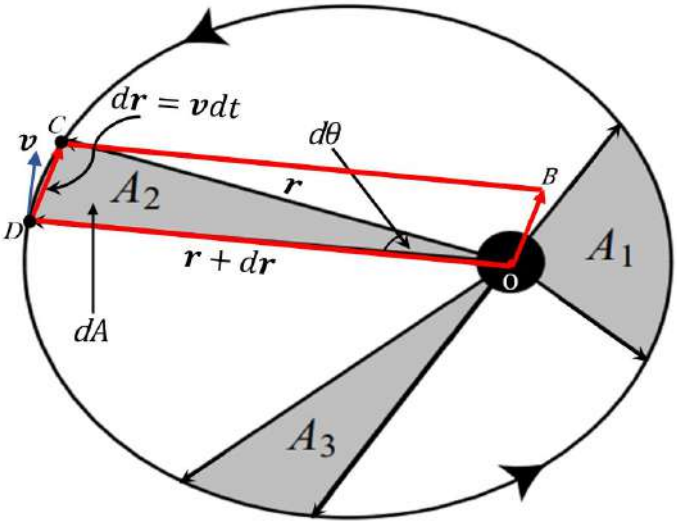

FIGURE 2.2: The regions A_1, A_2, and A_3 in the geometry for Kepler's second law of planetary motion stand for equal areas swept out in equal periods by the radius vector.

Consider a planet of mass m that is rotating at a velocity $\boldsymbol{v}$ under the gravitational pull of the Sun, which has mass M. The radius vector $\mathbf{r}$ displays planet-Sun distance at time t_1 and position C. The radius vector is now represented by $\mathbf{r}+d\mathbf{r}$ when the planet sweeps out the region A_2 in Figure 2.2 after time dt planet travels to position D and time at this place time is indicated by t_2. $d\theta$ is the small angle moved in small time dt and dA is the area that the radius vector $\mathbf{r}$ covers that is A_2 (see Figure 2.2).Consider the parallelogram $OBCD$, the area for the shaded region in Figure 2.2 dA is

$$dA = \frac{1}{2}\left|\mathbf{r} \times d\mathbf{r}\right|, \tag{2.4}$$

since $d\mathbf{r} = \boldsymbol{v}dt$, then Equation (2.4) becomes

$$dA = \frac{1}{2}\left|\mathbf{r} \times \boldsymbol{v}dt\right|,$$

$$\frac{dA}{dt} = \frac{1}{2}\left|\mathbf{r} \times \boldsymbol{v}\right|. \tag{2.5}$$

The angular momentum $\mathbf{L}$ is given by

$$\mathbf{L} = \mathbf{r} \times \mathbf{p}, \tag{2.6}$$

where the linear momentum ($\mathbf{p}$)is equal to m$\mathbf{v}$, then the Equation (2.6) can be expressed as

$$\begin{aligned} \mathbf{L} &= \mathbf{r} \times m\boldsymbol{v}, \\ &= m(\mathbf{r} \times \boldsymbol{v}), \\ \frac{\mathbf{L}}{m} &= \mathbf{r} \times \boldsymbol{v}. \end{aligned} \tag{2.7}$$

Using Equation (2.7) in Equation (2.5)

$$\frac{dA}{dt} = \frac{L}{2m} = constant, \tag{2.8}$$

since angular momentum is conserved and mass is constant therefore the rate of change in area is constant which means that the areas in Figure 2.2 are equal provided that intervals of time are equal that is

$$A_1 = A_2 = A_3. \tag{2.9}$$

Kepler's Third Law (The Law of Periods)

Kepler's third law of planetary motion claims that the time required to complete one revolution around the orbit of any planet is proportional to the semi-major axis cube of the elliptic orbit, implying that as the length of the semi-major axis increases, so does the time period. This is why that at perihelion the the planet's speed increases and the planet's speed reduces at aphelion. The Kepler's third law of planetary motion can be stated as:

"*The cubes of the semimajor axes of the planetary orbits are proportional to the squares of the planets periods of revolution.*"[81]

The revolution's time period T is provided by

$$T = \frac{Area\ of\ ellipse}{Areal\ velocity} \tag{2.10}$$

πab is the area of ellipse and the areal velocity is $\frac{L}{2m}$, where a is semi-major axis, b is semi-minor axis which can be seen in Figure 2.3,
$\boldsymbol{L}$ is angular momentum and m represents the mass of the planet.

The Equation (2.10) takes the form

$$T = \frac{\pi ab}{|\mathbf{L}/2m|} \tag{2.11}$$

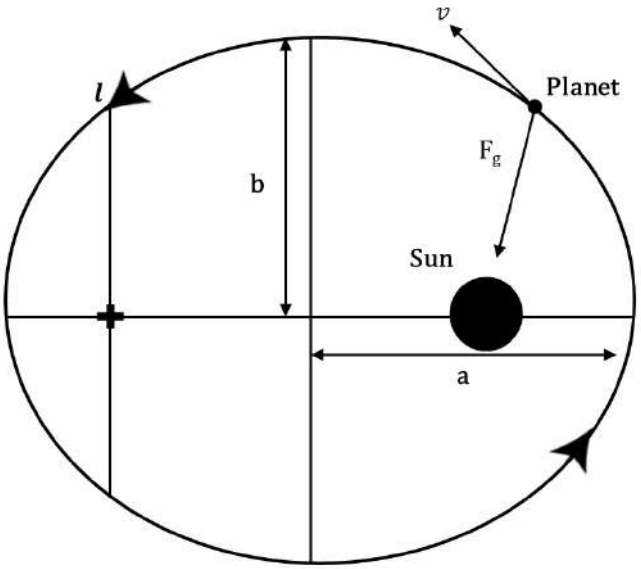

FIGURE 2.3: The geometry for Kepler's third law: a is semi-major axis, b is the semi-minor axis.

$$T^2 = \frac{4m^2\pi^2a^2b^2}{L^2}. \tag{2.12}$$

The latus rectum l is

$$l = \frac{b^2}{a},$$

and also it is given by

$$l = \frac{L^2}{GMm^2}.$$

Comparing the last two equations, we get

$$\begin{aligned} \frac{b^2}{a} &= \frac{L^2}{GMm^2}, \\ b^2 &= \frac{L^2 a}{GMm^2}. \end{aligned} \tag{2.13}$$

Substituting the value of b^2 from Equation (2.13) into the Equation (2.12), we have

$$\begin{aligned} T^2 &= \frac{4m^2\pi^2a^2}{L^2} \times \frac{L^2 a}{GMm^2}, \\ T^2 &= \frac{4\pi^2}{GM}a^3, \\ T^2 &\propto a^3, \end{aligned} \tag{2.14}$$

as $\frac{4\pi^2}{GM}$ is the constant term therefore we can write that square of time period is proportional to the semi-major axis cube.

In reality, Kepler's laws are a depiction of a unique approach to the N-Body Gravitational Problems in which: all of the bodies thought of as the point masses and all but one of the masses are so tiny that they are only attracted by the larger mass.

Planetary bodies in our solar system and the Sun, as well as each system of satellite groups orbiting their mother planet, precisely meet these requirements. It was Sir Isaac Newton who first understood this and used a systematic approach to the problem.

Kepler's rules were precise in terms of observational precision at the time they were developed. They still serve as highly accurate representations of reality today. They apply to both the system of planets around the Sun and the different satellite systems orbiting their primaries. They only fail to accurately represent the behaviour of such entities when the Solar System's farthest retrograde satellites or nearby satellites orbiting a planet that is not spherical in shape are taken into account. They may still be utilized as a first estimate even then.

2.1.6 Gravitational Potential

Gravitational potential is defined as

"The potential energy per unit mass placed in the gravitational field is called gravitaional potential. Thus if, at a certain point in a gravitational field, a mass m' has a potential energy E_p, the gravitational potential at that point is $V = \frac{E_p}{m'}$. The gravitational potential is thus expressed in the units Jkg^{-1} or m^2s^{-2}" [82].

If $E_p = -G\frac{mm'}{r}$ then potential V becomes

$$V = -G\frac{m}{r}, \tag{2.15}$$

where G is the universal gravitational constant.

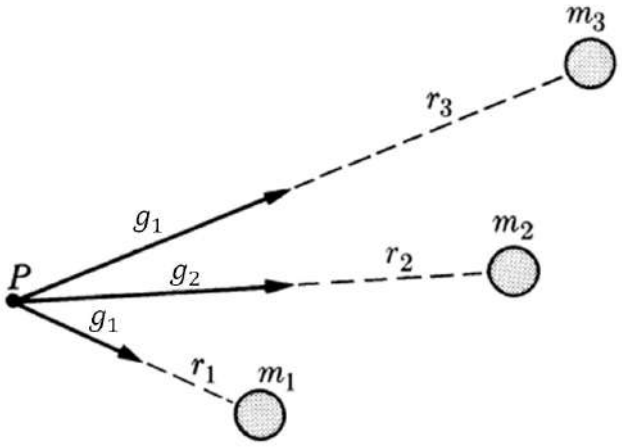

FIGURE 2.4: The Gravitational potential the point P due to the three masses, where g_1, g_2 and g_3 are the gravitational fields at P due to each mass.

For the three masses as shown in Figure 2.4, the potential at P will be the scalar sum of all the potential with respect to the masses, which is

$$V = V_1 + V_2 + V_3. \tag{2.16}$$

From the Equation (2.15) above equation takes the form

$$V = -G\left(\frac{m_1}{r_1} + \frac{m_2}{r_2} + \frac{m_3}{r_3}\right), \tag{2.17}$$

for N several masses the gravitational potential can be written as follows

$$V = -G\sum_{i}^{N}\frac{m_i}{r_i}. \tag{2.18}$$

2.1.7 Central Force

If a force acts on a particle in such way that it is always directed towards or away from a fixed center and its magnitude depends only upon the distance 'r' from the center, then this force is called central force. Mathematically

$$\boldsymbol{F} = f(r)\hat{r}, \tag{2.19}$$

where $f(r)$ is the magnitude of the force and $\hat{r}$ is the unit vector directed along the position vector $\mathbf{r}$.

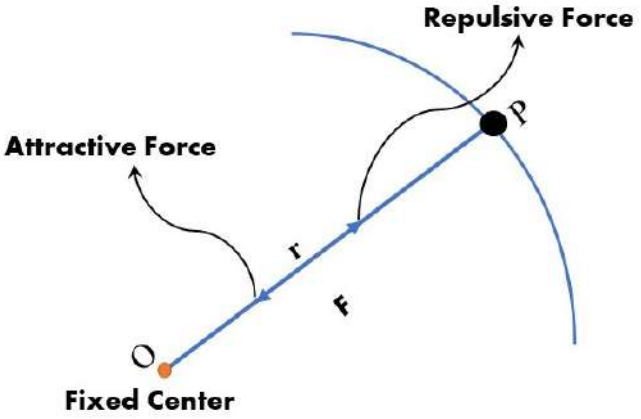

FIGURE 2.5: Central Force of particle 'P': attractive and repulsive forces directed towards and away from a fixed center 'O'.

Following are the examples of central force:

i. **Gravitational Force**: There is an attractive central force between Sun and Earth which is directed towards the Sun (see Figure 2.6).

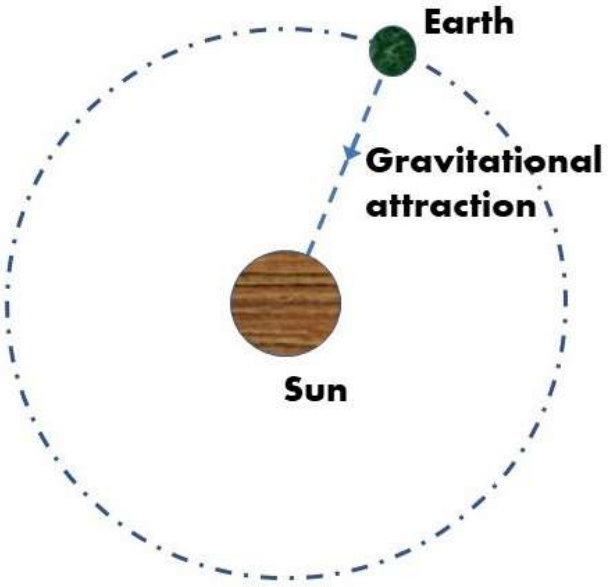

FIGURE 2.6: The gavitaional force between the Sun and the Earth.

$$\boldsymbol{F} = -G\frac{Mm}{r^3}\boldsymbol{r}, \tag{2.20}$$

where G is universal gravitation constant, M is the mass of Sun, m is the mass of Earth, $\boldsymbol{r}$ is the position vector, r is the distance between the Sun and Earth.

ii. **Electrostatic Force**: The force of attraction or repulsion between two point charges is also a central force (see Figure 2.7).

$$F_e = k\frac{q_1 q_2}{r^2},$$

where F_e is electrostatic force, q_1 and q_2 are the charged particles, k is coulomb constant and has the value $9 \times 10^9 Nm^2C^{-2}$, and r is the distance between the charges.

iii. **Magnetostatic Force**: The magnetostatic force between two magnetic charges is also an example of central force.

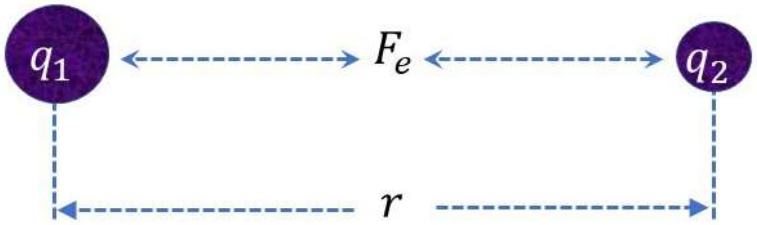

FIGURE 2.7: The electrostatic force between two point charges.

Characteristics of Central Force

The characteristics of central force are as follows:

i. Central force is attractive if $f(r) < 0$ and repulsive if $f(r) > 0$.

ii. Central force is always conservative force, i.e.,

$$f(r) = -\frac{\partial V}{\partial r}.$$

iii. The angular momentum about the force center is constant. Angular momentum is given mathematically as

$$\mathbf{L} = \mathbf{r} \times \mathbf{p},$$

where $\mathbf{p}$ is linear momentum.

Now, taking dot product with $\mathbf{r}$ on both side of the above equation, gives

$$\mathbf{r} \cdot \mathbf{L} = \mathbf{r} \cdot (\mathbf{r} \times \mathbf{p}).$$

Since 'dot' and 'cross' are interchangeable according to vector algebra therefore the above equation can be written as

$$\mathbf{r} \cdot \mathbf{L} = (\mathbf{r} \times \mathbf{r}) \cdot \mathbf{p},$$

as $\mathbf{r} \times \mathbf{r} = 0$, therefore

$$\mathbf{r} \cdot \mathbf{L} = 0. \tag{2.21}$$

This implies that $\mathbf{r}$ is perpendicular to $\mathbf{L}$, indicating that the motion of the particle is in the plane.

iv. The Equation (2.21) indicates that the motion of a particle under central force always takes place in a plane.

2.1.8 Center of Mass

The centre of mass (commonly referred to as the barycenter) plays an important role in Celestial Mechanics. The barycenter is the point where the centres of two celestial objects meet and balance each other and this is the point where two heavenly bodies orbit each other.

When two celestial bodies interact (for example, a moon and a planet or a planet and a star), the smaller body (sometimes called the secondary) does not orbit the exact centre of the primary but a point on the line between the centres of the primary and secondary.

For example, in the case of the Moon and Earth, the centre of mass lie approximately 1710 km below the surface of the Earth, where the masses of both the Earth and the Moon balance each other. If the masses are similar to Pluto and Charon, the centre of mass lies outside the bodies.

The point whose distance from any particle in the plane is equal to the average distances of all the particles in that plane is known as the centre of mass of the particles. If we denote center of mass by $\mathbf{c}$, see Figure 2.8, then

$$\boldsymbol{c} = \frac{\sum_{i=1}^{N} m_i \boldsymbol{r}_i}{\sum_{i=1}^{N} m_i}, \tag{2.22}$$

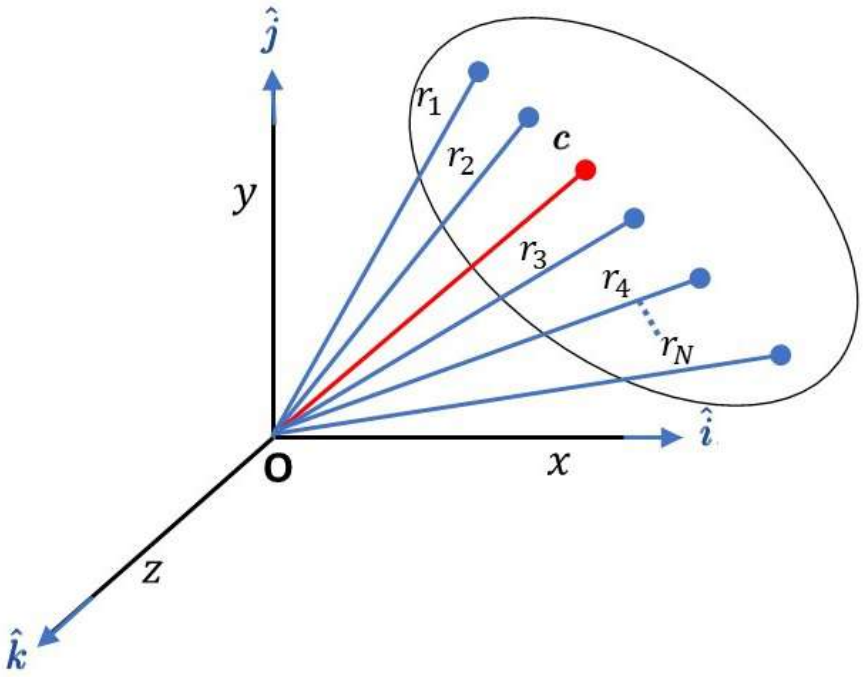

FIGURE 2.8: Location of the center of mass for N particles

is the center of mass, and the position vector of the N bodies is $\boldsymbol{r}_i$, $(i = 1,...,N)$.

Coordinate Components of the Position Vector Representing the Centre of Mass

Consider a system of N-point particles with masses m_1, m_2,... m_N and position vectors $\boldsymbol{r_1}$, $\boldsymbol{r_2}$,... $\boldsymbol{r_N}$ with respect to the origin, as shown in Figure 2.8, and then let (x_1, y_1, z_1), (x_2, y_2, z_2),...,(x_N, y_N, z_N) represent the rectangular coordinates for the N-point particles, i.e.,

$$\begin{aligned}
\boldsymbol{r_1} &= x_1\hat{i} + y_1\hat{j} + z_1\hat{k}, \\
\boldsymbol{r_2} &= x_2\hat{i} + y_2\hat{j} + z_2\hat{k}, \\
\boldsymbol{r_3} &= x_3\hat{i} + y_3\hat{j} + z_3\hat{k}, \\
&\cdot \quad \cdot \quad \cdot \quad \cdot \quad \cdot \quad \cdot \\
&\cdot \quad \cdot \quad \cdot \quad \cdot \quad \cdot \quad \cdot \\
&\cdot \quad \cdot \quad \cdot \quad \cdot \quad \cdot \quad \cdot \\
\boldsymbol{r_N} &= x_N\hat{i} + y_N\hat{j} + z_N\hat{k},
\end{aligned}$$

and $\mathring{x}$, $\mathring{y}$, $\mathring{z}$ are the rectangular coordinates for their center of mass

$$\boldsymbol{c} = \mathring{x}\hat{i} + \mathring{y}\hat{j} + \mathring{z}\hat{k} \tag{2.23}$$

then $\mathring{x}$, $\mathring{y}$, $\mathring{z}$ may be expressed as

$$\left.\begin{aligned} \mathring{x} &= \frac{\sum_{i=1}^{N} m_i x_i}{M}, \\ \mathring{y} &= \frac{\sum_{i=1}^{N} m_i y_i}{M}, \\ \mathring{z} &= \frac{\sum_{i=1}^{N} m_i z_i}{M}, \end{aligned}\right\} \tag{2.24}$$

where m_i ; $i = 1, 2, ..., N$ is mass of each particle and the system's entire mass is M and is given by $M = m_1 + m_2 + ... + m_N$ [83].

2.1.9 Degree of Freedom

The total number of coordinates necessary to fully characterise the location and configuration of the system, or the number of dimensions in which a particle may move freely, is the degree of freedom of a dynamic system. f is used to express it. It goes without saying that a system of N point particles with no constraints whatsoever has three degrees of freedom. The motion of such a system can be fully characterised by knowing how the relevant degrees of freedom change over time.

The equation $f = Nd$, where f is the number of degrees of freedom for the system of N point particles, represents the degrees of freedom in d-dimensional space. The total number of degrees of freedom is given by $f = Nd - k$ if there are k constraints on the dynamical system of N particles in d-dimensions. In the situation of three particles moving in three dimensions, the system has nine degrees of freedom.

2.1.10 Angular Velocity

A vector quantity, angular velocity is the rate at which an angle changes over time and has a direction perpendicular to the plane of motion. Whenever the

rotation is anticlockwise, the direction of angular velocity will be outwards of the plane of motion; that is, direction will be along the positive side of the rotational axis; and if the rotation is clockwise, the direction will be inwards of the plane of motion; that is, direction will be along the negative side of the axis of rotation. It is denoted by $\boldsymbol{\omega}$ and is expressed in radians per second, $rad\ s^{-1}$. If ϕ is angular displacement then

$$\boldsymbol{\omega} = \frac{d\phi}{dt}. \tag{2.25}$$

2.1.11 Zero Velocity Surface

Zero velocity surfaces or curves are the constraints that a satellite or any other item travelling under the gravitational attraction of other large particles cannot pass. These areas divide the satellite's motion into permitted and forbidden areas. Consider the well-known "Restricted Three-Body Problem", which consists of two large particles (referred to as the "primaries") and a third, much smaller particle that acts independently of the two "primaries" yet travels under their gravitational influence. A centrifugal force is introduced by switching to a rotating coordinate system with stationary masses. In this coordinate system, energy and momentum are not conserved separately, but the Jacobi integral remains constant, then

$$\boldsymbol{v^2} = 2U - C, \tag{2.26}$$

where $\boldsymbol{v}$ represents the velocity of the third small particle, U is the effective potential and the Jacobi constant is the name given to the constant C by Carl Jacobi $(1804 - 1851)$, a German mathematician who made the Jacobian constant discovery in 1836. C is also called the constant of motion of the small particle.

The zero velocity surfaces are given by $2U - C = 0$ and the permissible regions of motion for the particle can be found by setting $2U - C > 0$ as we can not have $\boldsymbol{v^2}$ negative.

2.1.12 Hill's Sphere

Hills Spheres, as they were named after the American astronomer and mathematician George William Hill, are the regions surrounding a celestial object where the greatest attraction is felt by other celestial objects and may turn into a satellite of the large celestial object. The radius of the Hill's sphere is defined approximately by

$$r_H \approx a(1-e)\sqrt[3]{\frac{m}{3M}}, \tag{2.27}$$

where r_H is the Hill's radius, M and m are the masses of two celestial bodies, a is the length of the semi-major axis and e gives the eccentricity of the orbit of the mass m.

For the Sun-Earth-Moon system, the radius of the Hill's spheres is shown in Figure 2.9. The Earths gravity dominates in this radius of Hill's region and the moon orbits the earth in a stable way only if it stays in the Hill's sphere [84]. The red circle in Figure 2.9 depicts the Hill's sphere of Earth in the Earth-Sun-and-moon system, and the moon in this zone is tidally locked and revolves around Earth in a stable orbit.

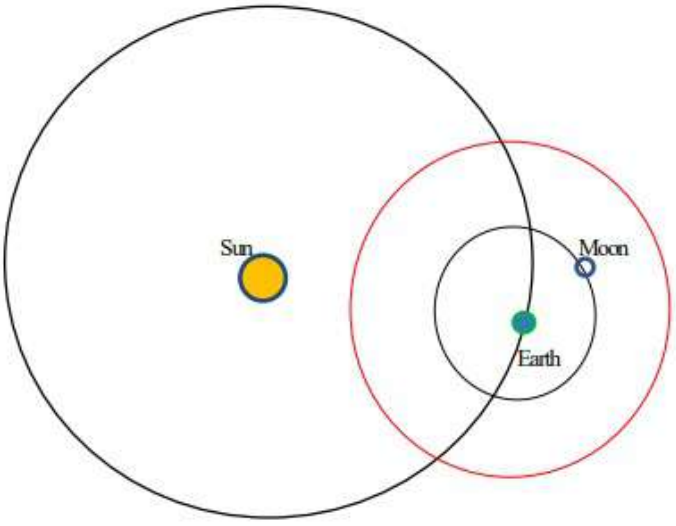

FIGURE 2.9: The Hill sphere is the red circle. The Earth-Moon system moves as a single gravitational unit in its orbit around the Sun.

2.1.13 Inertial Frame of Reference

As the name implies, an inertial reference frame is one in which no acceleration is taking place, therefore all forces are considered to be real and Newton's equations are simplified to their lowest possible forms. All inertial reference frames share the same form of the physical laws.

It must be remembered that Newton's Laws are predicated on the premise that all measurements or observations are made in relation to a frame of reference or coordinate system that is fixed in an absolutely stationary space. This alleged presumption that motion or space are absolute. But it's obvious that a particle can be at rest or moving in a uniform straight path with respect to a one reference frame while moving in a curve and accelerating relative to another. Newton's laws may be demonstrated to hold in any other frame of reference that is travelling relative to the first frame of reference at a constant speed.

2.1.14 Non-Inertial Frame of Reference

A non-inertial frame of reference is a reference frame that is not progressively moving or accelerating. It is possible to create the appropriate equations of motion using either Newtonian mechanics, Lagrangian mechanics, or Hamiltonian mechanics when using inertial frames of reference. In some circumstances, treating the motion in a non-inertial reference frame is more practical.

This type of reference frame experiences acceleration due to translation, rotation of the reference frame, or simultaneous rotation and translation motion [85]. The study of motion in the non inertial reference frame is carried out by using Newtonian mechanics, as well as Lagrangian and Hamiltonian approaches with the introduction of an extra inertial force that is often called fictitious force.

Translating Frame of Reference

A non-inertial system (x', y', z') is moving in a direction relative to the inertial frame so as to preserve constant orientations of the axes with respect to the inertial

frame, as shown in Figure 2.10. Take an inertial system (x, y, z) into consideration that is fixed in space. The relative position vector to the inertial reference frame is

$$\mathbf{r} = \mathbf{R} + \boldsymbol{r'}, \tag{2.28}$$

where "$\mathbf{R}$" is a position vector from the inertial reference frame to the non-inertial frame, "$\mathbf{r}$" is the vector relative to the inertial frame of reference, and "$\boldsymbol{r'}$" is the vector related to the frame of reference that is translating.

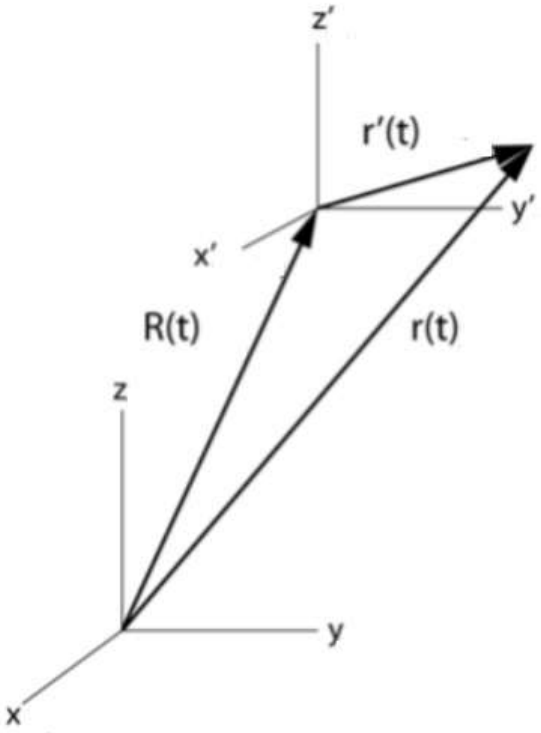

FIGURE 2.10: Inertial frame xyz relative to the non-inertial frame $x'y'z'$.

Differentiating Equation (2.28) two times with respect to time yields

$$\begin{aligned} \mathbf{a} &= \boldsymbol{A} + \boldsymbol{a'}, \\ m\boldsymbol{a} &= m\boldsymbol{A} + m\boldsymbol{a'}, \\ m\boldsymbol{a'} &= m\boldsymbol{a} - m\boldsymbol{A}, \end{aligned} \tag{2.29}$$

since $\mathbf{F} = m\mathbf{a}$ the Equation (2.29) becomes

$$m\boldsymbol{a'} = \boldsymbol{F} - m\boldsymbol{A}, \tag{2.30}$$

$$\boldsymbol{F'} = \boldsymbol{F} - m\boldsymbol{A}. \tag{2.31}$$

The additional term '$-m\boldsymbol{A}$' in Equation (2.31) is the fictitious force and is observer's frame of reference dependent.

Rotating Frame of Reference

Consider a Cartesian system of inertial frame containing $[x, y, z]$ coordinates and a non-inertial rotating frame coordinate system of $[x^*, y^*, z^*]$. The rotational axis is chosen to be aligned parallel to the z-axis of both the systems (i.e., z and z^* axes overlap each other) and only z-axis is shown in the Figure (2.11) to track the rotation.

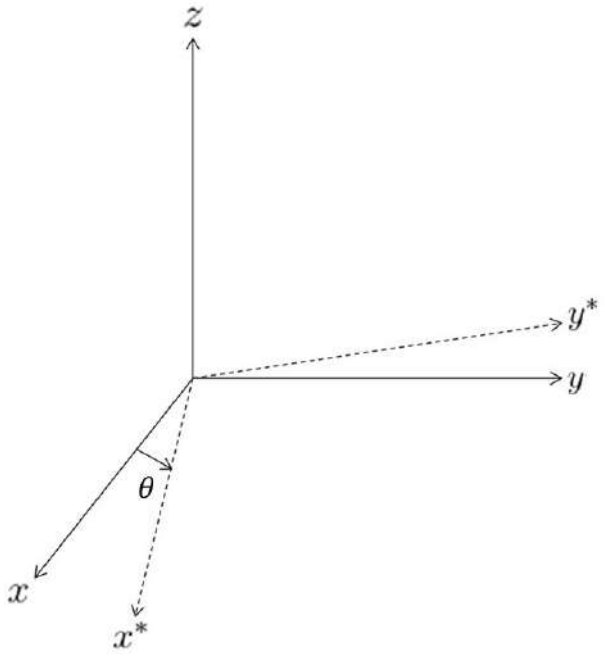

FIGURE 2.11: The rotation of θ angle about the z-axis and $[x^*, y^*, z^*]$ represent the rotating coordinates axes relative to the inertial reference frame that has coordinate axes $[x, y, z]$.

Let $\theta(t)$ be the angle that is spanned by the x or y axes during their rotation with relation to the inertial reference frame then angular velocity $\boldsymbol{\omega}$ is given by

$$\boldsymbol{\omega} = \frac{d\theta}{dt}. \tag{2.32}$$

Let's assume that a rigid body denoted by B has an inscribed time-dependent vector $\boldsymbol{\Upsilon}$ of a fixed magnitude. The body B rotates slightly relative to a inertial reference frame xyz as seen in Figure (2.12)

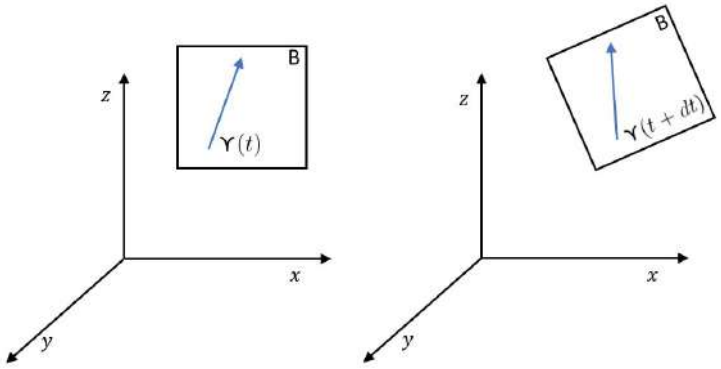

FIGURE 2.12: The infinitesimal rotation of vector $\boldsymbol{\Upsilon}$ that is inscribed in the rigid body 'B'.

According to Leonhard Euler, all across the differential time interval dt, B and hence, $\boldsymbol{\Upsilon}$ rotates along a particular axis of rotation. The $\boldsymbol{\Upsilon}$ at time t and time $t + dt$ are moved to a common point that is tail to tail at a unique axis of rotation to determine the infinitesimal rotation as seen in Figure (2.13).

At some differential time dt the vector $\boldsymbol{\Upsilon}(t)$ rotates and sweeps a very infinitesimal angle $d\theta$ where α is the angle of $\boldsymbol{\Upsilon}(t)$ with the axis of rotation. In Figure (2.13) the vector $\boldsymbol{\Upsilon}$ at time t is shown with solid line while the $\boldsymbol{\Upsilon}$ at time $t + dt$ is shown with the doted line.

If d$\boldsymbol{\theta}$ is a vector pointing along the rotational axis then the infinitesimal rotational change is supplied by

$$d\boldsymbol{\Upsilon} \quad = \quad \Upsilon \sin\alpha \; d\theta \; \hat{\boldsymbol{n}}, \tag{2.33}$$

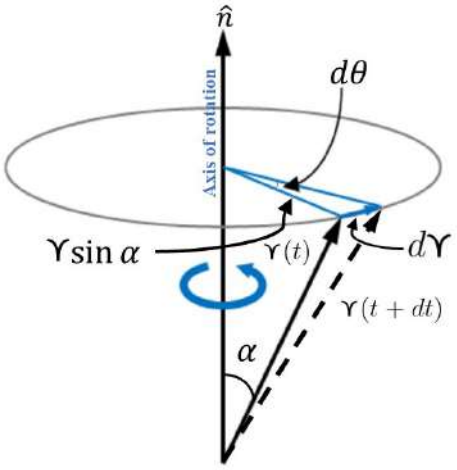

FIGURE 2.13: The vector $\boldsymbol{\Upsilon}$ at time t and after time interval $t+dt$ on a unique axis of rotation.

where $\hat{\boldsymbol{n}}$ is the unit vector normal to the plane of rotation, defined by the vector $\boldsymbol{\Upsilon}$ and from Equation (2.32) the Equation (2.33) becomes

$$\begin{aligned} d\boldsymbol{\Upsilon} &= \| \boldsymbol{\omega} \| \| \boldsymbol{\Upsilon} \| \sin\alpha \; dt \; \hat{\boldsymbol{n}}, \\ &= \boldsymbol{\omega} \times \boldsymbol{\Upsilon} \; dt, \end{aligned}$$

finally we divide by dt to obtain

$$\frac{d\boldsymbol{\Upsilon}}{dt} = \boldsymbol{\omega} \times \boldsymbol{\Upsilon} \tag{2.34}$$

The Equation (2.34) is the relation that can be used for the determination of time derivative of any constant vector.

Rotating and Translating Frame of Reference

Consider the reference frame that is moving as well as translating with respect to some other fixed inertial frame. Let xyz represent the inertial frame of reference and $x^*y^*z^*$ represent the moving reference frame that is rotating as well as translating freely, both the frame are supposed to be rigid. The quantities measured

relative to the inertial frame will be given a suffix 'in' and the quantities that will be measured relative to the moving frame will be given a suffix of "mov". The unit vectors along the inertial fame will be given by $\hat{\boldsymbol{i}}$, $\hat{\boldsymbol{j}}$ and $\hat{\boldsymbol{k}}$ while $\hat{\boldsymbol{i}}^*$, $\hat{\boldsymbol{j}}^*$ and $\hat{\boldsymbol{k}}^*$ will be the unit vectors with respect to the moving frame. The angular velocity of the moving frame is ω, and its motion is arbitrary.

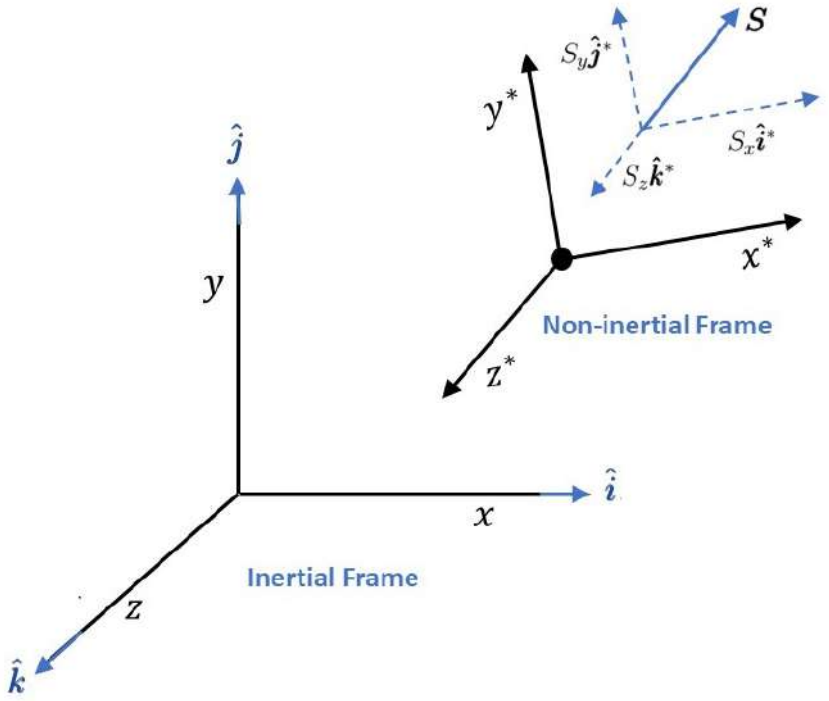

FIGURE 2.14: The vector $\boldsymbol{S}$ along with its components with respect to the non-inertial moving frame.

Let us define a vector S which is time dependent, see Figure 2.14 and its components regarding the inertial frame of reference are

$$\boldsymbol{S} = S_x\hat{\boldsymbol{i}} + S_y\hat{\boldsymbol{j}} + S_z\hat{\boldsymbol{k}},$$

and the time derivative is given by

$$\frac{d\boldsymbol{S}}{dt} = \frac{dS_x}{dt}\hat{\boldsymbol{i}} + \frac{dS_y}{dt}\hat{\boldsymbol{j}} + \frac{dS_z}{dt}\hat{\boldsymbol{k}}. \tag{2.35}$$

The vector **S** in a moving reference frame will be

$$\boldsymbol{S} = S_x\hat{\boldsymbol{i}}^* + S_y\hat{\boldsymbol{j}}^* + S_z\hat{\boldsymbol{k}}^*.$$

The derivatives of the unit vectors with respect to time $\hat{\boldsymbol{i}}^*$, $\hat{\boldsymbol{j}}^*$ and $\hat{\boldsymbol{k}}^*$ are not zero as they are not stationary in space but instead are changing direction constantly. They all have unit magnitude and due to their attachment to the $x^*y^*z^*$ frame they all have the same angular velocity ω, and the time derivative is

$$\frac{d\boldsymbol{S}}{dt} = \frac{dS_x}{dt}\hat{\boldsymbol{i}}^* + \frac{S_y}{dt}\hat{\boldsymbol{j}}^* + \frac{dS_z}{dt}\hat{\boldsymbol{k}}^* + S_x\frac{d\hat{\boldsymbol{i}}^*}{dt} + S_y\frac{d\hat{\boldsymbol{j}}^*}{dt} + S_z\frac{d\hat{\boldsymbol{k}}^*}{dt}. \tag{2.36}$$

Using Equation (2.34) in Equation (2.36), we obtain

$$\frac{d\boldsymbol{S}}{dt} = \frac{dS_x}{dt}\hat{\boldsymbol{i}}^* + \frac{S_y}{dt}\hat{\boldsymbol{j}}^* + \frac{dS_z}{dt}\hat{\boldsymbol{k}}^* + S_x(\boldsymbol{\omega}\times\hat{\boldsymbol{i}}^*) + S_y(\boldsymbol{\omega}\times\hat{\boldsymbol{j}}^*) + S_z(\boldsymbol{\omega}\times\hat{\boldsymbol{k}}^*). \tag{2.37}$$

The unit vectors $\hat{\boldsymbol{i}}^*$, $\hat{\boldsymbol{j}}^*$ and $\hat{\boldsymbol{k}}^*$ will not vary in direction with respect to the moving frame, but they will have a constant magnitude of unity, therefore the time derivative of $\boldsymbol{S}$ relative to the moving frame will be

$$\left.\frac{d\boldsymbol{S}}{dt}\right]_{mov} = \frac{dS_x}{dt}\hat{\boldsymbol{i}}^* + \frac{S_y}{dt}\hat{\boldsymbol{j}}^* + \frac{dS_z}{dt}\hat{\boldsymbol{k}}^*. \tag{2.38}$$

The Equation (2.37) then takes the form

$$\begin{aligned}
\frac{d\boldsymbol{S}}{dt} &= \left.\frac{d\boldsymbol{S}}{dt}\right]_{mov} + S_x(\boldsymbol{\omega}\times\hat{\boldsymbol{i}}^*) + S_y(\boldsymbol{\omega}\times\hat{\boldsymbol{j}}^*) + S_z(\boldsymbol{\omega}\times\hat{\boldsymbol{k}}^*),\\
&= \left.\frac{d\boldsymbol{S}}{dt}\right]_{mov} + (\boldsymbol{\omega}\times S_x\hat{\boldsymbol{i}}^*) + (\boldsymbol{\omega}\times S_y\hat{\boldsymbol{j}}^*) + (\boldsymbol{\omega}\times S_z\hat{\boldsymbol{k}}^*),\\
&= \left.\frac{d\boldsymbol{S}}{dt}\right]_{mov} + \boldsymbol{\omega}\times(S_x\hat{\boldsymbol{i}}^* + S_y\hat{\boldsymbol{j}}^* + (S_z\hat{\boldsymbol{k}}^*),\\
\frac{d\boldsymbol{S}}{dt} &= \left.\frac{d\boldsymbol{S}}{dt}\right]_{mov} + \boldsymbol{\omega}\times\boldsymbol{S}
\end{aligned} \tag{2.39}$$

The Equation (2.39) can also be written as

$$\boldsymbol{V} = \boldsymbol{V}_{mov} + \boldsymbol{\omega} \times \boldsymbol{S}; \quad \text{where} \quad \frac{d\boldsymbol{S}}{dt}\bigg|_{mov} = \boldsymbol{V}_{mov}. \tag{2.40}$$

The Equation (2.40) represents the velocity in terms of the velocity of the moving frame, if ω is zero then there will be no rotational motion of the particle. The Equation (2.39) can be differentiated further with respect to t to have the acceleration vector, thus

$$\frac{d^2\boldsymbol{S}}{dt^2} = \frac{d}{dt}\frac{d\boldsymbol{S}}{dt}\bigg|_{mov} + \frac{d\boldsymbol{\omega}}{dt} \times \boldsymbol{S} + \boldsymbol{\omega} \times \frac{d\boldsymbol{S}}{dt} \tag{2.41}$$

The non-inertial frame has a constant angular velocity ω then the time derivative of the Equation (2.39) relative to the moving frame is

$$\frac{d}{dt}\frac{d\boldsymbol{S}}{dt} = \frac{d^2\boldsymbol{S}}{dt^2}\bigg|_{mov} + \boldsymbol{\omega} \times \frac{d\boldsymbol{S}}{dt}\bigg|_{mov}. \tag{2.42}$$

Using Equation (2.40) and (2.42) in Equation (2.41) we obtain

$$\frac{d^2\boldsymbol{S}}{dt^2} = \frac{d^2\boldsymbol{S}}{dt^2}\bigg|_{mov} + \boldsymbol{\omega} \times \frac{d\boldsymbol{S}}{dt}\bigg|_{mov} + \frac{d\boldsymbol{\omega}}{dt} \times \boldsymbol{S} + \boldsymbol{\omega} \times \left(\frac{d\boldsymbol{S}}{dt}\bigg|_{mov} + \boldsymbol{\omega} \times \boldsymbol{S}\right), \tag{2.43}$$

and it can be written after as

$$\frac{d^2\boldsymbol{S}}{dt^2} = \frac{d^2\boldsymbol{S}}{dt^2}\bigg|_{mov} + \dot{\boldsymbol{\omega}} \times \boldsymbol{S} + 2\boldsymbol{\omega} \times \frac{d\boldsymbol{S}}{dt}\bigg|_{mov} + \boldsymbol{\omega} \times (\boldsymbol{\omega} \times \boldsymbol{S}), \tag{2.44}$$

where the it can also be written as

$$\boldsymbol{a} = \boldsymbol{a}_{mov} + \dot{\boldsymbol{\omega}} \times \boldsymbol{S} + 2\boldsymbol{\omega} \times \boldsymbol{V}_{mov} + \boldsymbol{\omega} \times (\boldsymbol{\omega} \times \boldsymbol{S}). \tag{2.45}$$

For the acceleration formula for a point mass Q that is in random motion and its position vector $\boldsymbol{r} = x\hat{\boldsymbol{i}} + y\hat{\boldsymbol{j}} + z\hat{\boldsymbol{k}}$ relative to the inertial frame can be given as

$$\boldsymbol{r} = \boldsymbol{R} + \boldsymbol{r}_{mov}, \tag{2.46}$$

where $\boldsymbol{R}$ is the relative location of the moving reference frame's origin and the vector $\boldsymbol{r}_{mov} = x^*\hat{\boldsymbol{i}}^* + y^*\hat{\boldsymbol{j}}^* + z^*\hat{\boldsymbol{k}}^*$ is the position vector of the point Q in the moving frame, this can be seen in Figure 2.15.

Taking derivative of Equation (2.46) with respect to t, gives

$$\frac{d\boldsymbol{r}}{dt} = \frac{d\boldsymbol{R}}{dt} + \frac{d\boldsymbol{r}_{mov}}{dt}, \tag{2.47}$$

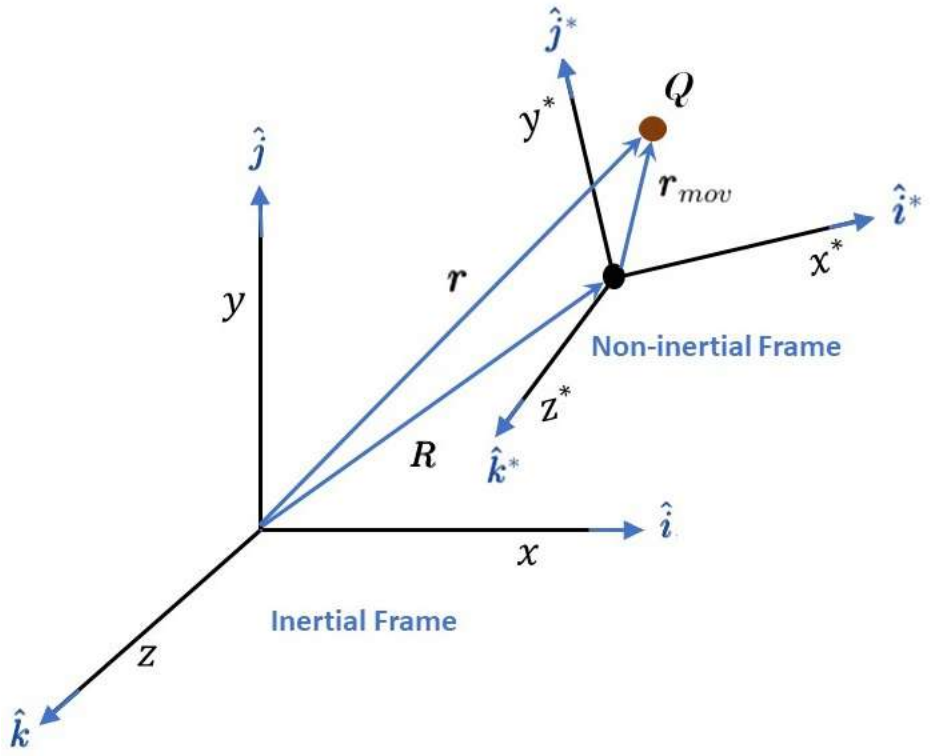

FIGURE 2.15: Position vectors of the point mass Q with respect to both the inertial and non-inertial reference frames.

as $\frac{d\boldsymbol{r}}{dt} = \boldsymbol{V}$ (velocity of Q with relative to the inertial frame), $\frac{d\boldsymbol{R}}{dt} = \boldsymbol{V_R}$ (moving frame's origin velocity) and $\frac{d\boldsymbol{r}_{mov}}{dt} = \boldsymbol{V}_{mov}$ (velocity of the Q relative to the moving

frame of reference) then the above equation takes the form

$$\boldsymbol{V} = \boldsymbol{V_R} + \boldsymbol{V}_{mov}. \tag{2.48}$$

From Equation (2.40), the relative velocity of point Q in the moving frame is

$$\boldsymbol{V}_{mov} = \boldsymbol{V}_{mov} + \boldsymbol{\omega} \times \boldsymbol{r}_{mov}. \tag{2.49}$$

The Equation (2.48) can be given as

$$\boldsymbol{V} = \boldsymbol{V_R} + \boldsymbol{V}_{mov} + \boldsymbol{\omega} \times \boldsymbol{r}_{mov}. \tag{2.50}$$

From Equation (2.48) the acceleration of the moving frame's origin is

$$\boldsymbol{a} = \boldsymbol{a_R} + \boldsymbol{a}_{mov}. \tag{2.51}$$

using Equation (2.45) we can write

$$\boldsymbol{a}_{mov} = \boldsymbol{a}_{mov} + \dot{\boldsymbol{\omega}} \times \boldsymbol{r}_{mov} + 2\boldsymbol{\omega} \times \boldsymbol{V}_{mov} + \boldsymbol{\omega} \times (\boldsymbol{\omega} \times \boldsymbol{r}_{mov}). \tag{2.52}$$

Substutuing Equation (2.52 into Equation (2.51)), we obtain

$$\boldsymbol{a} = \boldsymbol{a_R} + \boldsymbol{a}_{mov} + \dot{\boldsymbol{\omega}} \times \boldsymbol{r}_{mov} + 2\boldsymbol{\omega} \times \boldsymbol{V}_{mov} + \boldsymbol{\omega} \times (\boldsymbol{\omega} \times \boldsymbol{r}_{mov}). \tag{2.53}$$

The Equation (2.53) represents the relation for the acceration of the point Q which is moving randomly. The term $2\boldsymbol{\omega} \times \boldsymbol{V}_{mov}$ represents the Coriolis acceleration and $\boldsymbol{\omega} \times (\boldsymbol{\omega} \times \boldsymbol{r}_{mov})$ is the centrifugal acceleration.

2.1.15 Solar System and Eight Two Body System

The solar system is the set of all objects that are gravitationally attached to the star, the Sun. *Mercury, Venus, Earth, Mars, Jupiter, Saturn, Uranus, and Neptune* are the planets that constitute our Solar System. The Solar System contains numerous dwarf planets such as Pluto, a multitude of moons, and millions of asteroids, comets, and meteoroids.

A star is an object that gives off its own light. The planets, on the other hand, do not give off their own light but can reflect it. There could also be things moving around the planets. The name for these is "satellites". In the solar system, the moon is a satellite of the planet Earth, which orbits around the Sun. There are also satellites that were made by humans and can move around planets or their moons.

The trajectory followed by a planet or satellite is denoted as its orbit.The aphelion and perihelion represent the maximum and minimum distance of a planet from the Sun, respectively. The farthest point from the planet that a satellite orbits is called the apogee and the closest point to the planet is called the perigee.

The duration of one full revolution of a celestial body in its orbit is referred to as its period. The term "sidereal period" is occasionally utilised to distinguish it from other periods, like the time it takes for the earth to move around its axis, etc.

Since most of the mass is in the sun, it will be supposed that each of the planets move independently of the other and is acted on only by the sun. Then we have eight independent two body systems each consisting of the sun and one planet.

2.1.16 Two Body Problem

The 2-body problem, Newton initially investigated and solved, says that if the locations and the velocities of two celestial objects moving under the influence of their shared gravitational field is known at any given time t, then what would be the locations and the velocities at any other time t? Examples include a satellite revolving around a planet, two stars orbiting each other, and a planet orbiting a star e.g., Earth-Sun, Earth-Moon. The following details highlight the significance of the two-body problem:

- Aside from rather limited answers to the $N \geq 3$ body problems, it is the sole gravitational problem of Celestial Mechanics for which we know a complete solution.

- Numerous real-world orbital motion problems may be handled as approximations of two body problems.
- The two-body solution can be used as a foundation for the development of analytical solutions that are accurate to higher degrees of precision or to offer approximations of orbital parameters and estimations.

Solution of Two Body Problem

Let us take two point masses M and m that are moving under their mutual gravitational influence and are $\boldsymbol{r}$ distance away from each other then their equation of motion as given in can be given as

$$\mathbf{F} = G\frac{mM}{r^3}\boldsymbol{r},$$

where G denotes the Newtonian universal gravitational constant.

Given the particles' initial positions and velocities, the aim of this particular situation is to determine the particles' positions and velocities at any given time t. Figure (2.16) depicts the forces of attraction F_1 and F_2 of masses M and m acting in opposite directions along r.

As per the Newton's third law of motion,

$$\mathbf{F}_1 = -\mathbf{F}_2, \tag{2.54}$$

where

$$\mathbf{F}_1 = G\frac{mM}{r^3}\boldsymbol{r}, \tag{2.55}$$

and

$$\mathbf{F}_2 = -G\frac{mM}{r^3}\boldsymbol{r}. \tag{2.56}$$

Using Newton's second law, we get $\mathbf{F}_1 = M\,\ddot{\boldsymbol{r}}_1$ and $\mathbf{F}_2 = m\,\ddot{\boldsymbol{r}}_2$, therefore

$$M\ddot{\boldsymbol{r}}_1 = G\frac{mM}{r^3}\boldsymbol{r}, \tag{2.57}$$

and

$$m\ddot{\boldsymbol{r}}_2 = -G\frac{mM}{r^3}\boldsymbol{r}. \tag{2.58}$$

where $\mathbf{r}_1$ and $\mathbf{r}_2$ are the position vectors from 'O', the origin of the reference frame, $\boldsymbol{r}$ is the position vector of m relative to M and $\hat{r}$ is a unit vector that points from M to m as depicted in Figure 2.16 the Equations (2.57) and (2.58) are added to give

$$M\,\ddot{\boldsymbol{r}}_1 + m\,\ddot{\boldsymbol{r}}_2 = \mathbf{0}. \tag{2.59}$$

Integrating the above equation to obtain

$$M\,\dot{\boldsymbol{r}}_1 + m\,\dot{\boldsymbol{r}}_2 = \boldsymbol{c}_1, \tag{2.60}$$

as

$$\dot{\boldsymbol{r}}_1 = \boldsymbol{v}_M,$$

and

$$\dot{\boldsymbol{r}}_2 = \boldsymbol{v}_m.$$

Then the Equation (2.60) will become

$$M\boldsymbol{v}_M + m\boldsymbol{v}_m = \boldsymbol{c}_1, \tag{2.61}$$

where, vector $\boldsymbol{c}_1$ is constant of integration.
Equation (2.61) implies that the system of bodies has constant linear momentum, the integration of Equation (2.61) gives

$$M\boldsymbol{r}_1 + m\boldsymbol{r}_2 = \boldsymbol{c}_1 t + \boldsymbol{c}_2, \tag{2.62}$$

where $\boldsymbol{c}_2$ (constant of integration) represent the constant vectors.

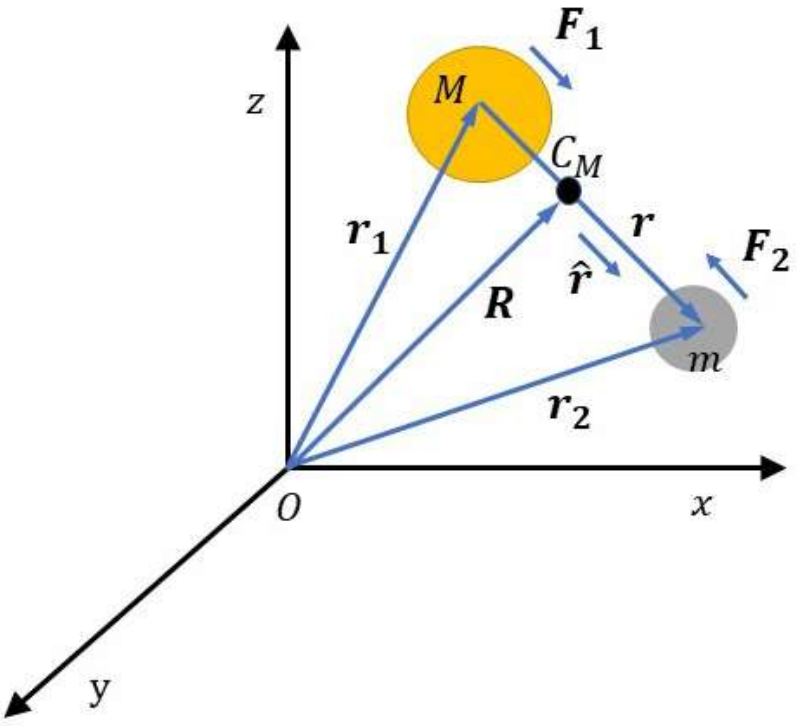

FIGURE 2.16: The Two Body System

Let $\boldsymbol{R}$ be the coordinate of center of mass (C_M) then by the definition of C_M we can wrtie the center of mass for two bodies M and m as

$$\begin{aligned}(M+m)\boldsymbol{R} &= M\boldsymbol{r}_1 + m\boldsymbol{r}_2,\\ \mathbb{M}\boldsymbol{R} &= M\boldsymbol{r}_1 + m\boldsymbol{r}_2,\end{aligned} \tag{2.63}$$

where

$$\mathbb{M} = M + m.$$

Differentiate Equation (2.63) with respect to 'time' and after using Equation (2.60), we have

$$\mathbb{M}\dot{\boldsymbol{R}} = \boldsymbol{c}_1.$$

It can be seen that it is constant, that is

$$\dot{\boldsymbol{R}} = \frac{\boldsymbol{c}_1}{\mathbb{M}} = \text{constant}, \tag{2.64}$$

which shows that $\dot{\boldsymbol{R}} = \boldsymbol{v}_c$; where the velocity of the center of mass, denoted by $\boldsymbol{v}_c$, is constant. The Equations (2.57) and (2.58) are subtracted to obtain

$$\begin{aligned} \ddot{\boldsymbol{r}}_1 - \ddot{\boldsymbol{r}}_2 &= \frac{GM}{r^3}\boldsymbol{r} + \frac{Gm}{r^3}\boldsymbol{r}, \\ \ddot{\mathbf{r}}_1 - \ddot{\mathbf{r}}_2 &= G(m+M)\frac{\mathbf{r}}{r^3}. \end{aligned}$$

It can also be written as

$$\ddot{\boldsymbol{r}} = -\mu\frac{\boldsymbol{r}}{r^3},$$

and

$$\ddot{\boldsymbol{r}} + \mu\frac{\boldsymbol{r}}{r^3} = \mathbf{0}, \tag{2.65}$$

where μ is the some dimensional constant and is equal to $G(m+M)$, also $\boldsymbol{r}_1 - \boldsymbol{r}_2 = -\boldsymbol{r}$.

The Equation (2.65) is differential equation of second order that controls how m moves in relation to M. It has two vector integration constants with three scalar components each. Equation (2.65) thus includes six integration constants. Note that multiplying Equation (2.65) through by -1 when M and m are switched in all of the aforementioned derivation results in no change. As a result, when viewed from M, the motion of m is exactly the same as when viewed from M.

Taking cross product of $\boldsymbol{r}$ with Equation (2.65), we get

$$\begin{aligned} \boldsymbol{r} \times \ddot{\boldsymbol{r}} + \frac{\mu}{r^3}\boldsymbol{r} \times \boldsymbol{r} &= \mathbf{0} \\ \Rightarrow \mathbf{r} \times \ddot{\mathbf{r}} &= \mathbf{0}. \end{aligned} \tag{2.66}$$

Integrate the above equation, gives

$$\boldsymbol{r} \times \mu\dot{\boldsymbol{r}} = \boldsymbol{L}, \tag{2.67}$$

here $\boldsymbol{L}$ is a constant vector and the Equation (2.66) can be written as

$$\boldsymbol{r} \times \mu \ddot{\boldsymbol{r}} \;=\; \boldsymbol{0}. \tag{2.68}$$

Because we know that

$$\boldsymbol{F} = \mu \ddot{\boldsymbol{r}} = \mu \boldsymbol{a},$$

the Equation (2.68) with the above expression becomes

$$\boldsymbol{r} \times \boldsymbol{F} \;=\; \boldsymbol{0}. \tag{2.69}$$

It can be inferred from the definitions of torque and angular momentum

$$\boldsymbol{\tau} = \frac{d\boldsymbol{L}}{dt} = \boldsymbol{r} \times \boldsymbol{F}. \tag{2.70}$$

The Equations (2.69) and (2.70), together give

$$\boldsymbol{\tau} = \frac{d\boldsymbol{L}}{dt} = \boldsymbol{r} \times \boldsymbol{F} = \boldsymbol{0},$$

$$\frac{d\boldsymbol{L}}{dt} = \boldsymbol{0}$$

which implies that

$$\boldsymbol{L} = constant,$$

and this suggests that the angular momentum of the system consisting of two bodies remains constant.

Transverse and Radial Components of Velocity and Acceleration

Consider r and θ, the polar coordinates in the plane as depicted in Figure 2.17. The $\dot{r}$ and $r\dot{\theta}$ represent the velocity components that are parallel and perpendicular

to the radius vector connecting m and M, respectively. Then the velocity vector in polar coordinates is

$$\dot{\boldsymbol{r}} = \frac{d\boldsymbol{r}}{dt} = \dot{r}\,\hat{\boldsymbol{r}} + r\dot{\theta}\,\hat{\boldsymbol{\theta}}, \tag{2.71}$$

where, $\hat{\boldsymbol{r}}$ and $\hat{\boldsymbol{\theta}}$ represent the unit vectors along and perpendicular to the radius vector. Taking the cross product of above equation with $\boldsymbol{r}$, implies

$$\boldsymbol{r} \times (\dot{r}\,\hat{\boldsymbol{r}} + r\dot{\theta}\,\hat{\boldsymbol{\theta}}) = \mu\, r^2\dot{\theta}\,\hat{\boldsymbol{k}} = L\,\hat{\boldsymbol{k}}, \tag{2.72}$$

where $\hat{\boldsymbol{k}}$ is a unit vector that is perpendicular to the plane of the orbit and also

$$\mu\, r^2\dot{\theta} = L, \tag{2.73}$$

where the radius vector's area description is found to be twice as fast as the constant 'L'. which represents the second law of Kepler's mathematical form.

Taking the dot product of $\dot{\boldsymbol{r}}$ with Equation (2.65), gives

$$\dot{\boldsymbol{r}}.\frac{d^2\boldsymbol{r}}{dt^2} + \mu\frac{\dot{\boldsymbol{r}}.\boldsymbol{r}}{r^3} = 0,$$

the integration of above equation gives

$$\frac{1}{2}\dot{\boldsymbol{r}}.\dot{\boldsymbol{r}} - \frac{\mu}{r} = c,$$

$$\frac{1}{2}v^2 - \frac{\mu}{r} = c, \tag{2.74}$$

where, c is a constant of integration.

Equation (2.74) implies that the total energy of the system is conserved, with $\frac{1}{2}v^2$ representing the kinetic energy while $\frac{-\mu}{r}$ the potential energy of the system. Consider the radial and transverse components of acceleration vector

$$\boldsymbol{a} = \ddot{\boldsymbol{r}} = (\ddot{r} - r\dot{\theta}^2)\hat{\boldsymbol{r}} + \frac{1}{r}\frac{d}{dt}(r^2\dot{\theta})\hat{\boldsymbol{\theta}},$$

substituting the $\ddot{\boldsymbol{r}}$ into expression (2.65), gives

$$(\ddot{r} - r\dot{\theta}^2)\hat{\boldsymbol{r}} + \frac{1}{r}\frac{d}{dt}(r^2\dot{\theta})\hat{\boldsymbol{\theta}} = -\frac{\mu}{r^3}r\hat{\boldsymbol{r}}. \tag{2.75}$$

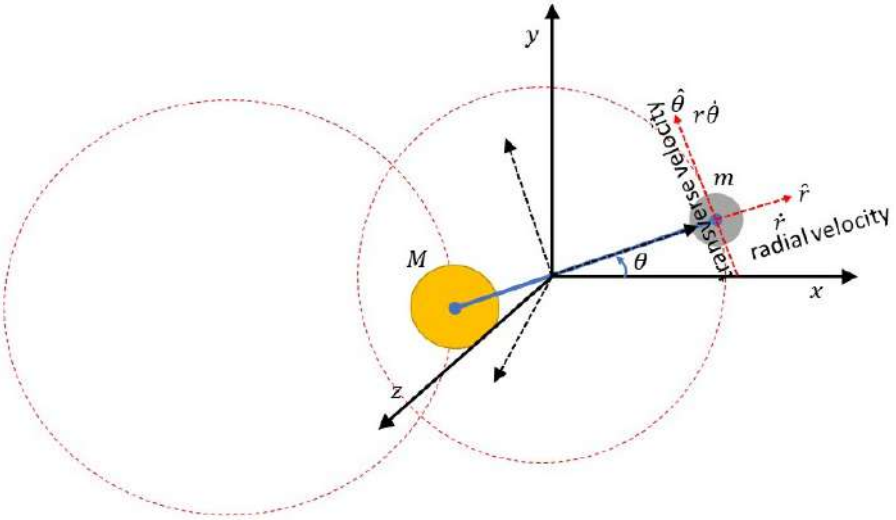

FIGURE 2.17: The radial as well as transverse components of velocity

The above equation on comparing the coefficients of unit vectors $\hat{\boldsymbol{r}}$ and $\hat{\boldsymbol{\theta}}$, implies

$$\ddot{r} - r\dot{\theta}^2 = -\frac{\mu}{r^2}, \tag{2.76}$$

and

$$\frac{1}{r}\frac{d}{dt}(r^2\dot{\theta}) = 0. \tag{2.77}$$

Let

$$u = \frac{1}{r}, \tag{2.78}$$

and the Equations (2.76) and (2.77), yield

$$\frac{d^2u}{d\theta^2} + u = \frac{\mu}{L^2}. \tag{2.79}$$

The general solution to the above Equation is

$$u = \frac{\mu}{L^2} + \mathcal{A}\cos(\theta - \theta^*), \tag{2.80}$$

where $\mathcal{A}$ and θ^* are two constants of integration. Replace u with $\frac{1}{r}$ in the above equation, to get

$$\frac{1}{r} = \frac{\mu}{L^2} + A\cos(\theta - \theta^*)$$

which implies

$$r = \frac{\frac{\boldsymbol{L}^2}{\mu}}{1 + \frac{\boldsymbol{L}^2 A}{\mu}\cos(\theta - \theta^*)},$$

gives the polar form of the conic equation, the above equation can be expressed as

$$r = \frac{p}{1 + e\cos(\theta - \theta^*)}, \tag{2.81}$$

where $p = \dfrac{L^2}{\mu}$, and $e = \dfrac{AL^2}{\mu}$.

Trajectories in the two body system around one another may be categorised according to their eccentricity, denoted by e. From the Equation (2.81) there rise three different possibilities of the orbits of two body system:

(i) If $0 < e < 1$ then the orbital shape will be elliptical;

(ii) If $e = 1$ then the orbital shape will be parabolic;

(iii) If $e > 1$ then the orbital shape will be hyperbolic.

Thus, Kepler's first law is a special case of the conic section that represents the solution to the two-body problem.

2.1.17 Equilibrium Solutions and their Stability

It is often beneficial to examine the behaviour of solutions to differential equation systems rather than trying to deduce their algebraic form. In order to do this, solutions near equilibrium solutions and those at equilibrium are investigated. These methods will be beneficial for investigating non-linear systems locally. Without really solving the problem, the Equilibrium solution can help us understand how the equation that represents the problem works. We can only find these solutions if all rates are equal to zero, which is a sufficient condition.

If we have a system of equations in two variables, then

$$\dot{x} = \ddot{x} = \dot{y} = \ddot{y} = ... = x^{(n)} = y^{(n)} = 0.$$

These solutions could be either stable or unstable. The finding of stable solutions in Celestial Mechanics facilitates the determination of locations suitable for indefinite parking of a satellite or any other object. Along Jupiter's orbital route, these kinds of locations can also be observed where bodies known as Trojans and Greeks asteroids are present at L_4 and L_5. In honour of the French mathematician and astronomer Joseph-Louis Lagrange, these equilibrium points with regard to Celestial Mechanics are sometimes known as Lagrange points. He was the first to identify equilibrium points mathematically. Three of these five spots L_1, L_2, and L_3 were discovered to be collinear, according to his discovery. To verify the stability of equilibrium points, we must take subsequent actions:

i. Put all the rates in the differential equation equal to zero to get the equilibrium solutions, i.e., $(x_1, y_1), (x_2, y_2), ..., (x_n, y_n)$.

ii. Let $(\breve{x}, \breve{y})$; be the small perturbation from the equilibrium points, then the for the linear stability analysis new location of equilibrium points will be $(x_1 + \breve{x}_1, y_1 + \breve{y}_1), (x_2 + \breve{x}_2, y_2 + \breve{y}_2), ..., (x_n + \breve{x}_n, y_n + \breve{y}_n)$.

iii. Use Taylor series expansion to linearise around the equilibrium point and write the relations in matrix form, that is, $\dot{X} = \mathcal{A}X$.

iv. Use the equilibrium points one by one to evaluate $\mathcal{A}$ and $|\mathcal{A} - \lambda I| = 0$ to determine the eigenvalues;

v. Based on the eigenvalues, stability analysis is carried out, that is, if the eigenvalues are:

   a. complex having positive real part then the equilibrium point will be *unstable*;

   b. complex having negative real part then the equilibrium point will be *stable*;

   c. both real and positive then the equilibrium point will be *unstable*;

   d. both real and negative as well then the equilibrium point will be *stable*; and if

   e. one eigenvalue is negative and other is positive then the equilibrium point will be a *saddle point*.

Equilibrium Solutions of a non-linear System of First Order Ordinary Differential Equations

Let us consider a non linear system of ordinary differential equations

$$\begin{aligned} \dot{\xi} &= \xi(3 - \xi - 2\eta), \\ \dot{\eta} &= \eta(2 - \xi - \eta). \end{aligned} \tag{2.82}$$

For equilibrium solutions all rates should be equal to zero therefore system in (2.82) becomes

$$\xi(3 - \xi - 2\eta) = 0, \tag{2.83}$$

$$\eta(2 - \xi - \eta) = 0. \tag{2.84}$$

Solving the Equations (2.83) and (2.84) we obtain the following equilibrium solutions

$$(0, 0), \quad (0, 2), \quad (3, 0) \quad \textit{and} \quad (1, 1). \tag{2.85}$$

Stability Analysis of the Equilibrium Solutions

The equilibrium solutions are analysed by using eigenvalues for the Equations (2.82). The conventional linearization approach is used to investigate the equilibrium solution stability. Now let the Equations (2.83) and (2.84) can be written as

$$f(\xi,\eta) = \xi(3-\xi-2\eta), \tag{2.86}$$

$$g(\xi,\eta) = \eta(2-\xi-\eta). \tag{2.87}$$

By the Taylor series expansion we have the following for both in (2.86) and (2.87)

$$f(\xi,\eta) \approx f(a,b) + (\xi-a)\frac{\partial f}{\partial \xi}(a,b) + (\eta-b)\frac{\partial f}{\partial \eta}(a,b), \tag{2.88}$$

$$g(\xi,\eta) \approx g(a,b) + (\xi-a)\frac{\partial g}{\partial \xi}(a,b) + (\eta-b)\frac{\partial g}{\partial \eta}(a,b), \tag{2.89}$$

and in matrix form Equations (2.88) and (2.89) are

$$\begin{bmatrix} f(\xi,\eta) \\ g(\xi,\eta) \end{bmatrix} = \begin{bmatrix} \frac{\partial f}{\partial \xi}(a,b) & \frac{\partial f}{\partial \eta}(a,b) \\ \frac{\partial g}{\partial \xi}(a,b) & \frac{\partial g}{\partial \eta}(a,b) \end{bmatrix} \begin{bmatrix} \xi-a \\ \eta-b \end{bmatrix}, \tag{2.90}$$

Now using Expression (2.90) in (2.82), we get

$$\begin{bmatrix} \dot{\xi} \\ \dot{\eta} \end{bmatrix} = \begin{bmatrix} 3-2a-2b & -2a \\ -b & 2-a-2b \end{bmatrix} \begin{bmatrix} \xi-a \\ \eta-b \end{bmatrix}, \tag{2.91}$$

and the Equation (2.91) can be written as

$$\dot{X} = \mathcal{A}X, \tag{2.92}$$

where

$$\dot{X} = \begin{bmatrix} \dot{\xi} \\ \dot{\eta} \end{bmatrix}, \quad X = \begin{bmatrix} \xi - a \\ \eta - b \end{bmatrix}, \quad A = \begin{bmatrix} 3 - 2a - 2b & -2a \\ -b & 2 - a - 2b \end{bmatrix}. \tag{2.93}$$

The critical points in (2.85) are replaced one by one for the eigenvalues in the $|\mathcal{A} - \lambda I| = 0$ and if the resulting eigenvalue values are both negative, then the critical point (equilibrium point) is said to be stable; otherwise, it will be unstable. The state of equilibrium points stability, and the subsequent collection of eigenvalues corresponding to the equilibrium points are given in the table 2.1

TABLE 2.1: Stability analysis of equilibrium points

Equilibrium Point	Eigenvalues	Stability
$(0, 0)$	$\lambda_1 = 3, \quad \lambda_2 = 2$	unstable
$(0, 2)$	$\lambda_1 = -1, \ \lambda_2 = -2$	Stable
$(3, 0)$	$\lambda_1 = -3, \ \lambda_2 = -1$	Stable
$(1, 1)$	$\lambda_1 = -1 - \sqrt{2}, \ \lambda_2 = -1 + \sqrt{2}$	Unstable

2.2 N-Body Problem

The N-body issue is a challenge in the field of Celestial Mechanics that involves attempting to forecast the individual motions of a collection of astronomical objects that are gravitationally interacting with one another. The desire to understand the motions of the Sun, Moon, planets and visible stars has been a driving force behind the effort to find a solution to this problem. Throughout the 20^{th} century, one of the most important N-body problems to solve was trying to understand how the dynamics of globular cluster star systems worked.

The Dynamics of the N-Body Problem

The two-body problem (2BP) handles a large portion of the crucial astrodynamics job, but occasionally additional bodies are needed to represent the real Universe.

The next step is to develop formulae for $N \geq 3$ body problems, and it might be said that the N-body problem is an extension of the 3-body problem, i.e., $N > 3$. In general, a specified number of constants of integration are needed to solve generic the N-body problem differential equation of motion.

Consider a simple gravity problem in which the acceleration is constant with respect to time, i.e., $\boldsymbol{a}(t) = \boldsymbol{a}_0$. The velocity is obtained by integrating this equation, $\boldsymbol{v}(t) = \boldsymbol{a}_0 t + \boldsymbol{v}_0$. Integrating again provides, $r(t) = r_0 + \boldsymbol{v}_0 t + \frac{1}{2}\boldsymbol{a}_0 t^2$. We need to know the initial conditions in order to finish the solution. This example has a simple analytical solution that makes use of the initial conditions, a function of the time, and integration constants (also known as integrals of the motion). Sadly, this isn't always the straight forward situation and Integrals of the motion can lower the order of differential equations when initial conditions alone are unable to produce a solution. Ideally, we can reduce the differential equations to order zero if the number of integrals equals the order of the equations. The name "constants of the motion" refers to the fact that these integrals are constant functions of the initial conditions as well as the location and speed of the object at any given moment.

We require $6N$ integrals of motion to fully solve the N-body problem, which is a set of $3N$ second order differential equations. Six are obtained from the conservation of linear momentum, one from the energy conservation, and three from the conservation of total angular momentum, for a total of ten. A system of order $6N-10$ for $N \geq 3$ is obtained as there are no laws analogous to Kepler's first two laws that create further constants. Closed-form solutions to these equations for N-bodies, $N \geq 3$, are impossible.

In 1887, H. Brun demonstrated that there were no additional algebraic integrals. We only have the 10 known integrals even if Poincaré subsequently generalised Brun's work. They help us understand how the three body and N-body problems evolve. Total linear momentum conservation presupposes that there are no outside forces acting on the system.

The equations of motion of N massive particles with masses $m_i (i = 1, 2, ...N)$, whose radius vectors from an un-accelerated point O is $\mathbf{r}_i$ and mutual distances

are given by $\mathbf{r}_{ij}$, i.e.,

$$\boldsymbol{r}_{ij} = \boldsymbol{r}_j - \boldsymbol{r}_i \tag{2.94}$$

Based on Newton's laws of motion and gravity,

$$m_i \ddot{\boldsymbol{r}}_i = G \sum_{j=1 j \neq i}^{N} \frac{m_i m_j}{r_{ij}^3} \boldsymbol{r}_{ij} \quad , \qquad (i = 1, ...N), \tag{2.95}$$

Here, we see that $\boldsymbol{r}_{ij}$ suggests that the vector between m_i and m_j is directed from m_i to m_j, hence.

$$\boldsymbol{r}_{ij} = -\boldsymbol{r}_{ji} \tag{2.96}$$

The necessary equations of motion for an N-body problem are represented by the set of Equations (2.95) and G represents the gravitational constant.

2.2.1 Three Body Problem (3BP)

The three body problem can be divided into two parts for understanding and solution purposes:

- General Three Body Problem (G3BP).
- Restricted Three Body Problem (R3BP).

General Three Body Problem

Three celestial bodies moving in space, such as the Sun, Earth, and Moon, can be taken as an example of the "three body problem." Generally, in space, there are no constraints on masses or initial conditions and this is referred as the ***General Three Body Problem***.

Restricted three body problem

If two bodies are positioned to have the central configuration and the third body with very little mass whose motion is subject to the gravitational pull of the two massive bodies, then this is called a ***Restricted Three Body Problem***.

Circular Restricted Three Body Problem (CR3BP)

If the motion of the objects in the R3BP is considered to be in a circular orbit then this is called ***Circular Restricted Three Body Problem***. For space mission study, such as spacecraft moving from Earth to the Moon, we can use the model called the R3BP, in which the gravitational forces of two bodies affect the mass of a small spacecraft, but the massive bodies do not feel the spacecraft's impact.

2.2.2 Solution of CR3BP

The "Circular Restricted Three Body Problem" contains three masses, m_1, m_2, and m_3, of which m_1 and m_2 are massive while the third mass, m_3 is very small as compared to the other two masses. m_3 moves under the gravitational influence of other massive bodies (see Figure 2.18(i)).

Let us assume:

- m_1 and m_2 represent the masses of the primaries,
- the sum of masses m_1 and m_2 be unit, i.e., $m_1 + m_2 = 1$,
- $\mu = Gm_2$, $(1-\mu) = Gm_1$, where μ is some dimensional constant, while from the natural units $G = 1$ and the coordinates of masses are (ξ_2, η_2, ζ_2) and (ξ_1, η_1, ζ_1) respectively,
- m_3 is the mass of the third smaller particle; its coordinates are (ξ, η, ζ).
- $\mathbf{r_i} = (\xi_\mathbf{i}, \eta_\mathbf{i}, \zeta_\mathbf{i})$ represents the vector positions of the primaries.

Using the universal gravitational law, we get the equations of motion in the gravitational field of primaries for m_3

$$m_3\ddot{\boldsymbol{r}}_3 = m_3 \sum_{j=1, j\neq i}^{2} m_j \frac{\boldsymbol{r}_2 - \boldsymbol{r}_3}{|\boldsymbol{r}_2 - \boldsymbol{r}_3|^3}, \tag{2.97}$$

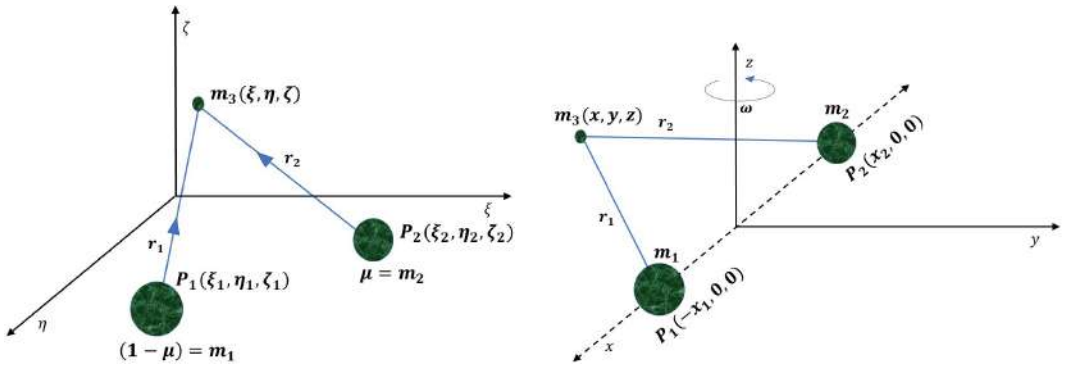

(i) (ii)

FIGURE 2.18: Circular restricted three body problem.

$$\cancel{m_3}\ddot{\mathbf{r}}_3 = \cancel{m_3}\left(m_1\frac{\mathbf{r}_1-\mathbf{r}_3}{|\mathbf{r}_1-\mathbf{r}_3|^3}+m_2\frac{\mathbf{r}_2-\mathbf{r}_3}{|\mathbf{r}_2-\mathbf{r}_3|^3}\right), \tag{2.98}$$

$$\begin{bmatrix}\ddot{\xi}\\ \ddot{\eta}\\ \ddot{\zeta}\end{bmatrix} = \frac{m_1}{{r_1}^3}\begin{bmatrix}\xi_1-\xi\\ \eta_1-\eta\\ \zeta_1-\zeta\end{bmatrix}+\frac{m_2}{{r_2}^3}\begin{bmatrix}\xi_2-\xi\\ \eta_2-\eta\\ \zeta_2-\zeta\end{bmatrix}, \tag{2.99}$$

where

$$\ddot{\boldsymbol{r}}_3 = \begin{bmatrix}\ddot{\xi}\\ \ddot{\eta}\\ \ddot{\zeta}\end{bmatrix}, \quad \boldsymbol{r}_1-\boldsymbol{r}_3 = \begin{bmatrix}\xi_1-\xi\\ \eta_1-\eta\\ \zeta_1-\zeta\end{bmatrix}, \quad \boldsymbol{r}_2-\boldsymbol{r}_3 = \begin{bmatrix}\xi_2-\xi\\ \eta_2-\eta\\ \zeta_2-\zeta\end{bmatrix}, \tag{2.100}$$

$$\left.\begin{aligned}{r_1}^2 &= (\xi_1-\xi)^2+(\eta_1-\eta)^2+(\zeta_1-\zeta)^2,\\ {r_2}^2 &= (\xi_2-\xi)^2+(\eta_2-\eta)^2+(\zeta_2-\zeta)^2.\end{aligned}\right\} \tag{2.101}$$

From Equation (2.99), we have

$$\left.\begin{aligned}\ddot{\xi} &= \frac{1-\mu}{{r_1}^3}(\xi_1-\xi)+\frac{\mu}{{r_2}^3}(\xi_2-\xi),\\ \ddot{\eta} &= \frac{1-\mu}{{r_1}^3}(\eta_1-\eta)+\frac{\mu}{{r_2}^3}(\eta_2-\eta),\\ \ddot{\zeta} &= \frac{1-\mu}{{r_1}^3}(\zeta_1-\zeta)+\frac{\mu}{{r_2}^3}(\zeta_2-\zeta).\end{aligned}\right\} \tag{2.102}$$

Consider the same origin of coordinate axes $(x,\ y,\ z)$ as before, but this time the x and y axes rotate about the z-axis with an angular velocity of unity, such that they are perpendicular to the plane of rotation. It is possible to choose the configuration of the x-axis so that the primaries at P_1 and P_2 always lie on it, then we may write: $(-x_1, 0, 0)$ and $(x_2, 0, 0)$ (see Figure 2.18(ii)).

Using the rotation matrix we obtained the ξ and η in terms of the coordinates of rotating axes, i.e.,

$$\begin{bmatrix} \xi \\ \eta \end{bmatrix} = \begin{bmatrix} \cos t & -\sin t \\ \sin t & \cos t \end{bmatrix} \begin{bmatrix} x \\ y \end{bmatrix}, \zeta = z, \tag{2.103}$$

which follows that $\xi = x\cos t - y\sin t,\ \eta = x\sin t + y\cos t,\ \zeta = z$ and yields

$$\begin{aligned} \xi_1 &= x_1\cos t - y_1\sin t, \quad \eta_1 = x_1\sin t + y_1\cos t, \\ \xi_2 &= x_2\cos t - y_2\sin t, \quad \eta_2 = x_2\sin t + y_2\cos t. \end{aligned}$$

Using the transformation in (2.103), one can easily transform the equation (2.102) in rotating frame as follows:

$$\left.\begin{aligned} \ddot{x} - 2\dot{y} - x &= \left(\frac{1-\mu}{{r_1}^3}\right)(x_1 - x) + \frac{\mu}{{r_2}^3}(x_2 - x), \\ \ddot{y} + 2\dot{x} - y &= -\left(\frac{1-\mu}{{r_1}^3}\right)(y_1 - y) + \frac{\mu}{{r_2}^3}(y_2 - y), \\ \ddot{z} &= \left(\frac{1-\mu}{{r_1}^3} + \frac{\mu}{{r_2}^3}\right) z. \end{aligned}\right\} \tag{2.104}$$

The distances r_1 and r_2 of m_3 in rotating frame are

$$\left.\begin{aligned} {r_1}^2 &= (x_1 - x)^2 + (y_1 - y)^2 + z^2, \\ {r_2}^2 &= (x_2 - x)^2 + (y_2 - y)^2 + z^2. \end{aligned}\right\} \tag{2.105}$$

Since from the Figure 2.18 (ii)) $y_1 = y_2 = 0$ therefore the systems (2.104) and (2.105) respectively become

$$\left.\begin{aligned} \ddot{x} - 2\dot{y} - x &= \left(\frac{1-\mu}{{r_1}^3}\right)(x_1 - x) + \frac{\mu}{{r_2}^3}(x_2 - x), \\ \ddot{y} + 2\dot{x} - y &= -\left[\left(\frac{1-\mu}{{r_1}^3}\right) + \frac{\mu}{{r_2}^3}\right] y, \\ \ddot{z} &= \left(\frac{1-\mu}{{r_1}^3} + \frac{\mu}{{r_2}^3}\right) z, \end{aligned}\right\} \tag{2.106}$$

and

$$\left.\begin{aligned} {r_1}^2 &= (x_1 - x)^2 + y^2 + z^2, \\ {r_2}^2 &= (x_2 - x)^2 + y^2 + z^2. \end{aligned}\right\} \tag{2.107}$$

The set of Equations in (2.106) can also be written as

$$\ddot{x} - 2\dot{y} = \frac{\partial U}{\partial x}, \tag{2.108}$$

$$\ddot{y} + 2\dot{x} = \frac{\partial U}{\partial y}, \tag{2.109}$$

$$\ddot{z} = \frac{\partial U}{\partial z}, \tag{2.110}$$

where

$$U = \frac{1}{2}(x^2 + y^2) + \frac{1-\mu}{r_1} + \frac{\mu}{r_2}, \tag{2.111}$$

is the effective potential of m_3 in the gravitational field of primaries and $x_1 = -\mu$ and $x_2 = 1 - \mu$.

Jacobian Constant

By multiply Equations (2.108), (2.109) and (2.110) by $\dot{x}$, $\dot{y}$ and $\dot{z}$ respectively, and when the resultant equations are added, we get

$$\dot{x}\ddot{x} + \dot{y}\ddot{y} + \dot{z}\ddot{z} = \frac{\partial U}{\partial x}\dot{x} + \frac{\partial U}{\partial y}\dot{y} + \frac{\partial U}{\partial z}\dot{z}. \tag{2.112}$$

U depends on three variables (x, y, and z), then the equation obtained by integrating the previous equation is

$$\dot{x}^2 + \dot{y}^2 + \dot{z}^2 = 2U + C, \tag{2.113}$$

where C represents the constant of integration and is also called *Jacobian constant*. The L.H.S. of above equation is square of velocity (v^2), so above equation can be written as

$$v^2 = 2U + C. \tag{2.114}$$

Equilibrium Solutions in the CR3BP

The equations of motion in (2.106) for m_3 are non-linear and instead of solving these equations we will do the qualitative analysis of these equations and find the equilibrium points. For this we follow the procedure given in Section 2.1.17.To find the equilibrium solution all rates should be zero, i.e., $\dot{x} = \dot{y} = \ddot{x} = \ddot{y} = 0$, then equilibrium solutions are given by the following equations:

$$x + \left(\frac{1-\mu}{{r_1}^3}\right)(x_1 - x) - \frac{\mu}{{r_2}^3}(x_2 - x) = 0, \tag{2.115}$$

$$\left[1 + \left(\frac{1-\mu}{{r_1}^3}\right) + \frac{\mu}{{r_2}^3}\right] y = 0, \tag{2.116}$$

$$\left(\frac{1-\mu}{{r_1}^3} + \frac{\mu}{{r_2}^3}\right) z = 0. \tag{2.117}$$

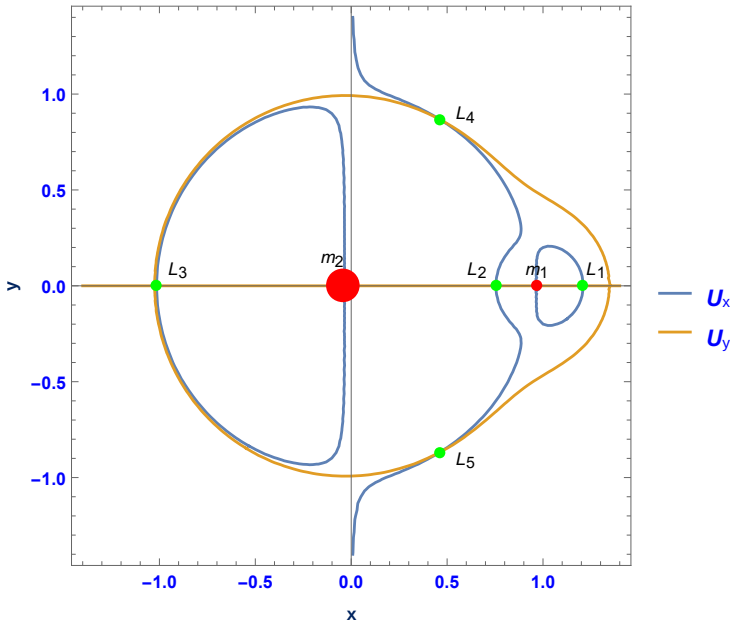

FIGURE 2.19: Red dots represent masses while the green dots represent equilibrium points

From Equation (2.117), $z = 0$ indicates that the motion of the bodies is in xy-plane. The equilibrium points of m_3 are shown with green dots by choosing the value of $\mu = 0.0350$ in the Figure 2.19.

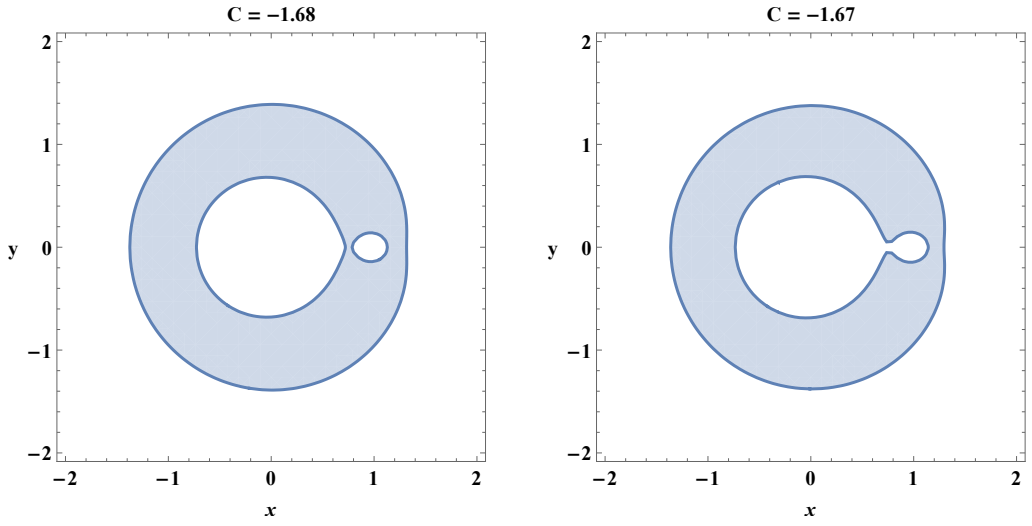

(i) (ii)

FIGURE 2.20: The permissible regions of motion of m_3 (white regions) and prohibited regions (shaded) when, (i) $C = -1.68$, (ii) $C = -1.67$

Regions of Possible Motion of the Restricted Body in the Sun-Earth System

The regions of possible motion of m_3, called the permissible regions, are given in white in the Figures 2.20−2.23. The boundaries between the permissible and prohibited regions (shaded) are given by setting the $v^2 = 0$ in Equation (2.114) for the Sun-Earth system. Secondary body, m_3 cannot cross these boundaries while moving inside the permissible region. Smaller C values suggest that the m_3 is distant from the centre of mass, while larger C values indicate that the m_3 is near one of the primaries. It has been observed that by increasing the value of the Jacobian constant, the permissible region increases (see Figures 2.20−2.23).

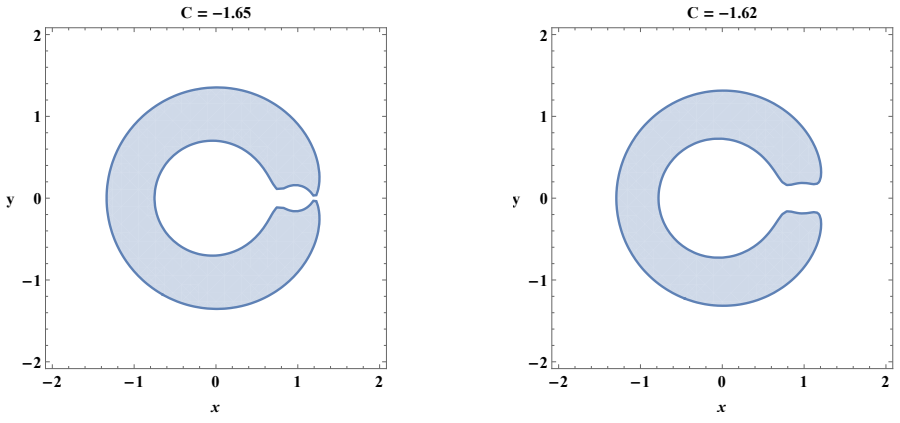

(i) (ii)

FIGURE 2.21: The permissible regions of motion of m_3 (white) and prohibited regions (shaded) when, (i) $C = -1.65$, (ii) $C = -1.62$

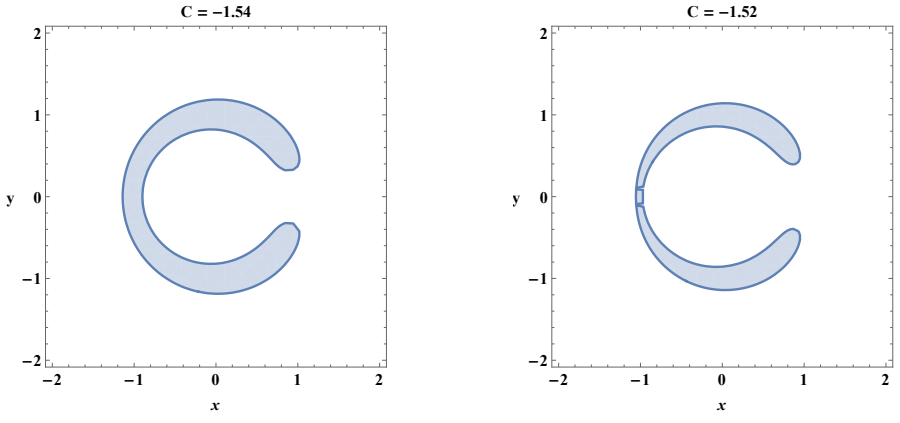

(i) (ii)

FIGURE 2.22: The permissible regions of motion of m_3 (white) and prohibited regions (shaded) when, (i) $C = -1.54$, (ii) $C = -1.52$

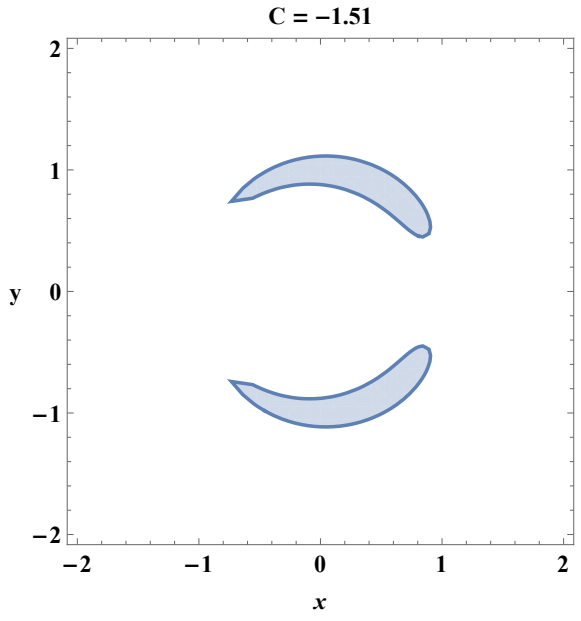

(i)

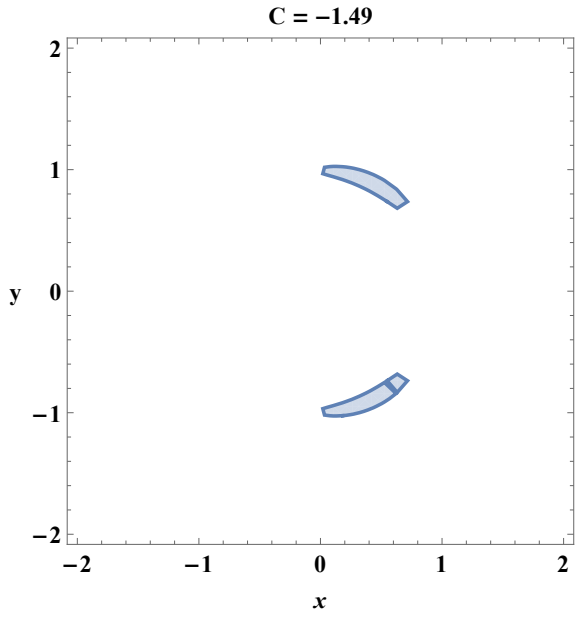

(ii)

FIGURE 2.23: The permissible regions of motion of m_3 (white) and prohibited regions (shaded) when, (i) $C = -1.51$, (ii) $C = -1.49$

Stability of Equilibrium Solutions of the Sun-Earth System

The stability analysis of equilibrium solutions/Lagrange points is performed by applying the eigenvalue test to each Lagrange point by following the procedure as mentioned in the Section 2.1.17, the results are gathered in the Table 2.2:

TABLE 2.2: Equilibrium points and stability analysis for $CR3BP$

Equilibrium Point	Eigenvalues	stability
$L_1 = (+0.836892919, 0)$	$\pm 5.87637, \pm -4.29283i$	unstable
$L_2 = (+1.155699520, 0)$	$\pm 3.08895, \pm -2.43375i$	unstable
$L_3 = (-1.005064520, 0)$	$\pm 0.319644, \pm 0.870371i$	unstable
$L_4 = (+0.487844901, +0.866025404)$	$\pm 0.59297i, \pm 0.805225i$	stable
$L_5 = (+0.487844901, -0.866025404)$	$\pm 0.59297i, \pm 0.805225i$	stable

2.2.3 The Restricted Three-Body Problem Equilibrium Solutions and their Stability

The restricted three-body problem has solutions that follow a consistent pattern, and these are called Lagrange points. For instance, if there are two heavenly bodies already in orbit around their common barycenter, there are five different locations in space where a third body with a comparably small mass may be placed in order to keep its position in relation to the two massive ones. This occurs due to the fact that the combined gravitational pulls of the two huge bodies produce the precise centripetal force that is necessary to maintain the circular motion that matches their orbital motion.

Alternately, when viewed in a rotating reference frame that is in synchronize with the angular velocity of the two bodies that are co-orbiting, the combined gravitational fields of the two massive bodies at the Lagrange points to balance the centrifugal pseudo-force, which allows the smaller third body to remain stationary (with respect to the first two bodies) in this frame.

Leonhard Euler made the discovery of the three collinear Lagrange points around the year 1750, a decade before Joseph-Louis Lagrange made the discovery of the remaining two. These points are denoted by the letters L_1, L_2, L_3, L_4 and L_5.

Lagrange wrote an "Essay on the Three-Body Problem" that came out in 1772. In the first chapter, he thought about the three-body problem in general. From this, in the second chapter, he showed that there are two special constant-pattern solutions with circular orbits for any three masses: the collinear and the equilateral.

Lagrange points may be stable or unstable. For a stable Lagrange point, the object at the stable equilibrium will frequently move itself back where it started if pushed out of position and oscillate about the equilibrium point in small orbits called *halo orbits*. The objects in these halo orbits need a very less amount of energy to stay around the equilibrium point. An object in an unstable equilibrium point is the same as an object on a hill: the slightest disturbance will shift its position and it will not return to the unstable equilibrium point by itself.

The $L_{1,2,3}$ are collinear, unstable equilibrium points and are positioned on the connecting line of the large bodies, while points $L_{4,5}$ are stable equilibrium points. The points L_4 and L_5 make an equilateral triangle of length equal to 1 AU (AU stands for Astronomical Unit, and 1 AU equals 150 million kilometers, which represents the mean distance to Earth from the Sun.) with the C_S (the center of Sun) and the C_E (the center of Earth) which can be seen in Figure (2.24).These five Lagrange points can be found in the case of any planet and the Sun but we will only discuss here the Lagrange points of the Earth-Sun System. Some of the solar system's natural objects at Lagrange points, such as asteroids, meteoroids, and dust, are illustrated here.

- At the L_4 and L_5 points between the Sun and Earth, there is dust from other planets and at least two asteroids, 2010 TK_7, and 2020 XL_5 [86–88], the Sun's gravitational pull makes it very hard for these points to stay stable. [89]
- The Neptune trojans are a group of about a dozen known objects that are at the Sun-Neptune L_4 and L_5 points. [90]
- Mars has four accepted trojans: 5261 Eureka [91], 1999 UJ_7 [92], 1998 VF_{31} [93], and 2007 NS_2 [94].

- In its L_4 and L_5 points, the moon Tethys of Saturn has two smaller moons of Saturn named Telesto and Calypso. Dione, another moon of Saturn, has two Lagrange co-orbitals, Helene at L_4 and Polydeuces at L_5. The moons move in all directions around the Lagrange points. Polydeuces is the moon that moves the most, up to 32° from the Saturn Dione L_5 point [95].

- One version of the giant impact theory says that the Moon was made when an object called Theia formed at the L_4 or L_5 point between the Sun and the Earth and then crashed into Earth when its orbit became unstable [96].

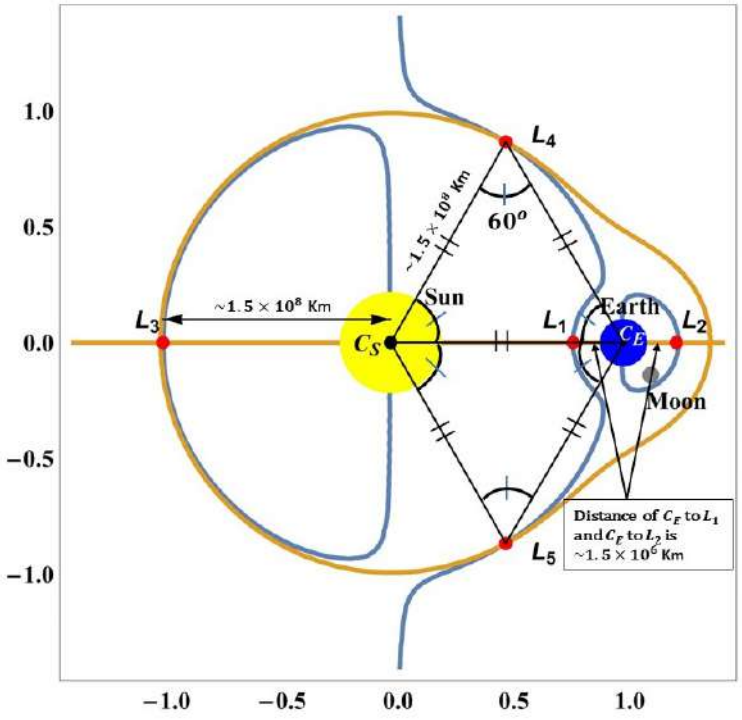

FIGURE 2.24: The five Lagrange points, L_1, L_2, L_3, L_4, L_5 and there corresponding distances are given in Kilometers.

2.2.4 Different Space Missions sent to the Lagrange Points of Sun-Earth System

Since the discovery of the Lagrange points, scientists have continued their endeavour to seek the knowledge and benefits of these places in space. In this regard, the following is the detail of some space missions sent to the Sun-Earth Lagrange points:

Lagrange Point: L_1

The Lagrange point L_1 lies inside the Earth and the Sun, about 1% (1.5 million Km) of distance to Earth from the Sun. The objects that are closer to Sun have smaller orbit than the farther objects so they move faster than the farther objects. L_1 is an unstable equilibrium point, but at this point the gravitational pull of the Earth reduces the gravitational attraction of the Sun, requiring less energy to maintain its orbit around L_1. According to the European Space Agency the solar wind, the continuous stream of the solar particles, passes L_1 approximately an hour before it reaches Earth, making it an ideal location from which the Sun can be observed. L_1 is also very important for a clear and lucid view of our planet Earth.

The present space missions as per the National Aeronautics and Space Administration (NASA) at L_1 are the **Solar and Heliosphere Observatory (SOHO)**, launched in 2^{nd} December, 1995, its a combined mission of both European Space Agency (ESA) and NASA. In addition to keeping an eye on how space weather affects our world, SOHO is essential for predicting solar storms that might be deadly; the NASA's **Advanced Composition Explorer (ACE)** gathers and examines particles from solar, interplanetary, interstellar, and cosmological origins. This data helps us understand the Sun, its interaction with Earth, as well as the Solar System's evolution; ACE was launched in August 25, 1997 by NASA.

NASA's **Wind**, a spin-stabilized spacecraft that was launched on November 1^{st}, 1994, is now in a halo orbit around the Sun-Earth L_1 Lagrange point. As the solar wind reaches the magnetosphere of Earth and becomes close enough to interfere, the satellite keeps watch on it.

Deep Space Climate Observatory (DSCOVR) is an American space weather station that keeps track of variations in the solar wind and issues warnings and predictions for geomagnetic storms that might interfere with GPS, satellites, power grids, telecommunications, and aviation. and was launched on February 11, 2015. **Interstellar Mapping and Acceleration Probe (IMAP)**, a space mission that NASA is planning to launch in 2024 at L_1, will collect, analyse, and map the

particles that are flowing to Earth from the borders of interstellar space. Additionally, the IMAP will aid scientists improve their understanding of the heliosphere's edge, a magnetic bubble that surrounds and guards our solar system.

L_1 is the future home of **NEO Surveyor**, **SWFO-L1** and **Advanced Telescope for High Energy Astrophysics (ATHENA)**.

Lagrange Point: L_2

The Earth-Sun Lagrange point L_2 lies outside the Earth, about 1% (1.5 million Km) of Earth's distance from the Sun. As L_2 is an unstable equilibrium point so any orbit around it is dynamically unstable, and because of its location, it is an excellent place to explore the space and L_2 offers a considerably more steady perspective since it is unrestricted and distant from the heat that the Earth emits. The space missions positioned at L_2 include **Gaia**, an ESA space project that was launched on December 19, 2013, is now mapping the stars at L_2, its aim is to construct a 3D map of the Milky Way galaxy that will show how the galaxy formed, evolved, and is composed; **Spektr-RG** was launched On July 13, 2019, the Aerospace Center of Germany ("Deutsches Zentrum fr Luft- und Raumfahrt; DLR") and the Russian space agency Roscosmos collaborated on the Spektrum-Rntgen-Gamma mission, commonly known as Spektr-RG. According to Roscosmos, the spacecraft is likely to find thousands of; galaxy clusters, super-massive black holes, star-forming galaxies, plasma, and a variety of other phenomena.

James Webb Space Telescope (JWST) is a joint mission of NASA, ESA and Space Agency of Canada ("CSA") which began its journey on the 25^{th} of December, 2021. JWST is expected to explore the whole history of the solar system, starting with the first sparks of light after the big bang to the creation of solar systems able to sustain life on Planets like Earth. L_2 is the future home of **Euclid**, **WFIRST**, **LiteBIRD**.

Lagrange Point: L_3

L_3 is located opposite Earth, behind the Sun, slightly outside of our planet's orbit. The Earth cannot see anything in L_3, but it gives the opportunity to view the Sun's

far side, and it is also an unstable equilibrium point. This position doesn't contain any known objects.

Lagrange Points: L_4 & L_5

L_4 & L_5 are both stable equilibrium points that lie about 1 AU from Earth as well as from Sun that is any object would remain stationary from the Earth's perspective because of the combined gravitational forces of the Earth and the Sun. Figure (2.24) shows an equilateral triangle formed by L_4 & L_5 and both are at 60° from C_S & C_E). According to EAS dust and asteroids tend to accumulate in L_4 & L_5 regions. The asteroids at L_4 & L_5 of the Jupiter-Sun system were initially discovered and named *Trojans* by the Greeks.

2.2.5 Central Configuration

The special arrangement of celestial objects is known as central configuration; the objects may vary in distance from each other during this configuration, but the special arrangement remains the same; for example, if the special arrangement is a triangular shape, the objects will maintain this shape throughout their motion, regardless of the triangle size. To put it another way, the triangle will only vary in scale, translation, and rotation at any time. Central configuration can lead us to the special homo-graphic solutions and the first homo-graphic solution for $N = 3$ bodies was found by Euler [3] in 1767, Lagrange [4] established the existence of the well-known equilateral-triangle central configuration in 1772.

The N-bodies are said to be in central configuration if and only if they meet the following mathematical relationship:

$$-\omega^2 m_i(\mathbf{r}_i - \mathbf{c}) = \sum_{j=0, j\neq i}^{N} m_i m_j \frac{\mathbf{r}_j - \mathbf{r}_i}{\left|\mathbf{r}_j - \mathbf{r}_i\right|^3}, \tag{2.118}$$

where ω is angular velocity and

$$\mathbf{c} = \frac{\sum_{i=1}^{N} m_i \mathbf{r}_i}{\sum_{i=1}^{N} m_i}, \tag{2.119}$$

represents the center of mass for the N-bodies and the expression $(\mathbf{r_i} - \mathbf{c})$ denotes the configuration in relation to the central configuration.

2.3 Role of Central Configuration

Central configuration refers to configurations that are constant with reference to translation, rotation, and scaling about a fixed point known as the center of mass (CM). We can discover homo-graphic solutions by considering central configurations that are constant in rotation and scaling. Objects can orbit in elliptic or circular orbits at about the center of mass; for example, particles move in a circle around Saturn, producing a ring (see Figure 2.25).

FIGURE 2.25: The rings of Saturn.

Saari [97] demonstrated this configuration by symmetrically putting equal masses on a circle, the configuration of this type can also be seen around Neptune and Uranus. Yan-ning and Yi-sui [98] investigated the homographic solutions for the N body problem in the context of general attraction; they established the existence of homographic solutions and demonstrated that if the homographic solutions are not planar, they are homothetic.

The central configuration also allows us to get homothetic solutions, in which, given some initial conditions, point masses with some CC translate and dilate down a line towards the center of mass, and the configuration collapses to a collision

singularity. In homothetic solutions, the bodies remain in the CC throughout their motion prior to the collision. For more detail about the role of CC and special properties see [80, 99–106].

Chapter 3

Characterization of Rhomboidal Central Configuration with Five Primary Masses

3.1 Introduction

Lots of attention has been paid to the problems regarding central configuration of $N \geq 3$ for the past many years. The central configuration is seen to exist with some special arrangements, and the rhombus is one of such arrangements. This chapter discusses this special arrangement in two different ways and finds the range of mass parameters in which the families of rhombus central configurations can be held. The gravitational field of the model changes but the shape of the configuration remains the same through out the motion.

3.2 Rhomboidal Central Configuration

In the general four body problem in plane for which, four point masses are positioned at the vertices of a quadrilateral, so far, particular configurations such as square, rhombus, trapezium, and kite have been discussed. Kulesza et al. [76]

demonstrated the presence of a square central configuration for the $\lambda = 1$ semi-diagonal ratio, $\kappa = 1$ mass ratio, and all masses should be equal to 1.04482, and the same has been proved by Marchesin [107] by placing a possibly null mass at the center of the configuration. Albouy in 1996 [108] demonstrated that there are three types of symmetric central configurations for the four body problem: square CC, equilateral triangular CC with the forth mass placed at the center of the triangle, and isosceles triangular configuration with the forth mass positioned anywhere in the triangle. Simo [109] explored for relative equilibrium solutions in the four body problem, that is, the solutions in which the collection of bodies acts like a rigid body and their mutual distances stay constant throughout time, while their motion (planar) is made up of circular orbits around the center of mass.

The rhomboidal four body central configuration is defined as the central configuration in which all of the system's point masses preserve a rhombus geometry. This is the particular case of planer four body problem in which the four point masses are put on a plane at the vertices of a rhombus in this arrangement, and the masses maintain the rhombus shape throughout their two by two motion. The four point masses are supposed to move in circular orbits around a center of mass, with their acceleration vectors always pointing in the same direction, towards the barycentre of the rhomboidal configuration. J. Waldvogel [77] investigated the rhomboidal symmetric four-body problem, which is the planar symmetric four-body problem with two equal masses $m_1 = m_3$ at locations $(x_1(t), 0)$ and two equal masses $m_2 = m_4$ at positions $(0, x_2(t))$ at all times t. They found that as the equations of motion are simple, this problem is a good to study the regularisation of binary collisions, periodic solutions, chaotic motion, the collision and escape manifolds for four bodies, and resonance effects between the two rectilinear binaries that interact with each other also play an important role.

Marchesin and Claudio Vidal [48] investigated the spatially restricted rhomboidal five-body problem, which entails describing the motion of an infinitesimal mass, m_5, under the gravitational attraction of four other bodies, known as the primaries, m_1, m_2, m_3, and m_4, which move two by two in coplanar circular periodic orbits around their centre of mass fixed at the coordinate system's origin, they assumed in

the spatially restricted rhomboidal five-body problem model that $m_1 = m_2 = m$, $m_3 = m_4 = \tilde{m}$, and that the radius of $m_1 = m_2$ circular motion is a and that of $m_3 = m_4$ circular motion is b. They have also showed a family of spatial rectilinear restricted rhomboidal five-body problems with a single parameter that starts and ends with the Sitnikov circular five-body problem.

A non-collinear rhomboidal four- and five-body problem with four masses situated at the vertices of an isosceles rhombus and a stationary fifth mass at the system's centre of mass was analysed by Shoaib et al [47]. The central configurations in the rhomboidal four- and five-body problems are given by the formulae for m and M that the authors formed as functions of x_1, x_2, and m_0. Regions in the x_1x_2-plane where no central configurations are feasible if we consider all four masses to be positive were discovered in the $m_0 = 0$ case of this five-body problem, i.e. the rhomboidal four-body problem. Similar to this, the areas of the centre configurations were obtained both analytically and numerically in the $m_0 \neq 0$ case, where numerous examples of the rhomboidal five-body problem are presented.

Marchesin and Claudio Vidal [78] took into account a system of five mass points with masses $m_1 = m_2 = m$ and $m_3 = m_4 = \widetilde{m}$ that revolve around a single massive body with mass m_0 at its centre, which is taken to represent the origin of the coordinate system, designated as r_0. On the one hand, they suppose that the attraction between the bodies is Newtonian in character and that the central body exerts a generalised force on the four mass points that is produced by a potential of the Manev's type, or a potential of the kind $\frac{1}{r} + \frac{\epsilon}{r^2}$. The model illustrates a variety of situations, such as when the core body is a spheroid or a radiating source. In the beginning, the authors establish the existence of three distinct relative rhomboidal solutions, each of which has the following (central) configuration: first, the rhombus is a square with equal masses for all primaries; second, the rhombus is not a square with equal masses for all primaries; and third, the rhombus is not a square with different masses for all primaries. The radiation or the oblateness coefficient, ϵ and m $=\mu$, which is the common mass of the primaries, are the two parameters presented in the first two cases. It can be shown that in the third case, both m and $\tilde{m}$ dependent on ϵ; thus, that is the

only parameter to take into account. In the other two cases, authors show that the rhomboidal solutions are unstable in the Lyapunov sense, and they calculated the values of the parameters (ϵ, μ) that allow the square solution to be spectrally stable.

Marchesin [79] also took into account a planar system of five bodies with masses of m_0, m_1, m_2, and m_3 moving in a plane and correspondingly positioned at r_0, r_1, r_2, r_3, and r_4. m_0 is placed at the configuration's centre, which is taken to represent the origin of the coordinate system. The four additional bodies, known as the primaries, are always arranged in a rhombus configuration. The author demonstrated the existence of several rhomboidal configurations with a body at their centre under the assumption that all of the bodies had Newtonian-type mutual attraction. One of the semi-diagonals was normalised to equal one, whereas the other semi-diagonal varied over the region $[1, \sqrt{3}]$. The author has shown that the parameter value as well as the central mass have an impact on the masses of the primaries. Additionally, the square configuration case and the situation with no mass at the centre were both analysed by the author. In these specific circumstances, the parameters were $\lambda = 1$ and $m_0 = 0$, respectively. The limit case of $\lambda = \sqrt{3}$ corresponds to the degenerate scenario in which the masses of two of the primaries and the mass of the central body disappear, resulting in the configuration of a limited five-body problem with three bodies having null masses.

Three unequal collinear masses were put on the axis of symmetry in the symmetric five-body problem that Shoaib et al. [110] studied, while the other two masses were symmetrically positioned on each side. For the four and five-body problems, regions of potential central configurations are generated analytically and investigated numerically. The Levi-Civita transformations are used to regularise the equations of motion, and the Poincaré surface of sections is used to analyse the phase space for chaotic and periodic orbits. By placing two pairs of masses at a vertices of rhombus and the fifth mass any place on the axis of symmetry other than the origin, they demonstrated that no center configurations were possible. For all other circumstances, such as isosceles and equilateral triangular five-body problems, rhomboidal four and five-body problems, regions of central

configurations were obtained using analytical methods. For more recent work on the rhomboidal central configuration see [60, 111–113].

3.2.1 Central Configuration for Five Masses: when the three masses along the horizontal axis, m_0, m_1, m_2, and the two remaining masses along the vertical axis m_3 and m_4 are equal.

In the rhomboidal five-body central configuration, four point masses are placed at the vertices of the rhombus, while a fifth point mass is placed in the middle of the rhombus. The five point masses preserve rhombus geometry throughout their motion. In this section, we prove the existence and uniqueness of central configuration of a rhomboidal 5-body problem for positive masses when m_0, m_1, and m_2 along the horizontal axis, are equal. The mass ratio is written as a function of 'a' and 'b' which can be used to find regions of central configuration for the rhomboidal 5-body problem.

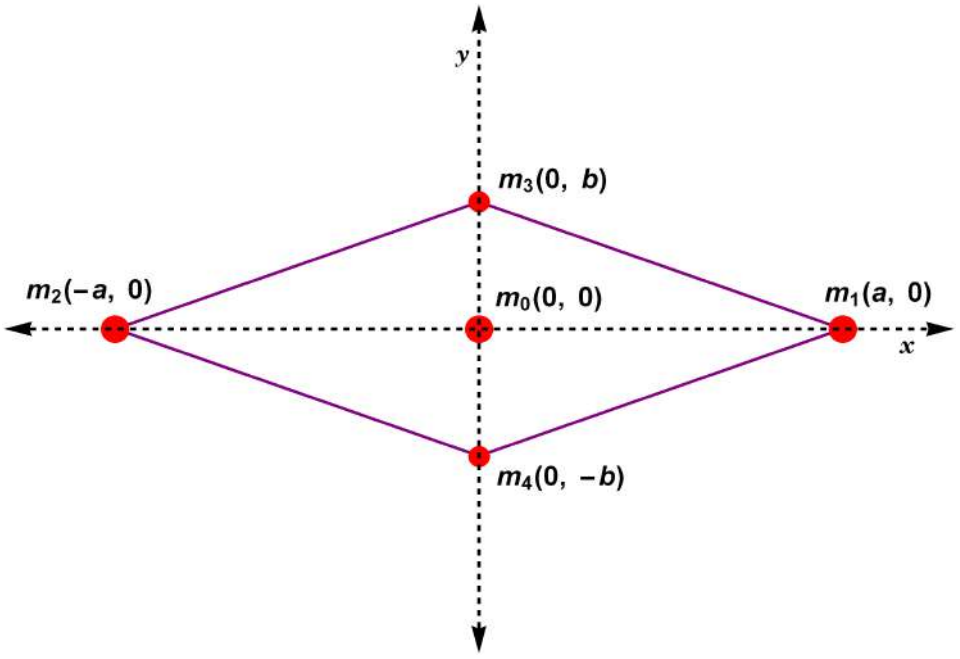

FIGURE 3.1: The rhomboidal central configuration of five bodies, when $m_0 = m_1 = m_2$ and $m_3 = m_4$.

The locations of the point masses on the vertices of a rhombus are shown in the Figure 3.1, m_1 and m_2 lie along the x-axis and are symmetric along the y-axis, whereas m_3 and m_4 lie along the y-axis and are symmetric along the x-axis. The mass m_0 lies on the point of intersection of the two diagonals of the rhombus. The masses m_0, m_1, and m_2 are assumed to be identical, whereas the masses m_3 and m_4 are assumed to be different than the other three masses but are identical to each other. Therefore the primaries along the horizontal axis, including m_0 have the same mass, i.e., m, while the primaries along the vertical axis have the same mass, i.e., $\widetilde{m}$.

The classical equation of motion for the N-body problem has the form

$$m_i\ddot{\mathbf{r}}_i = G\sum_{j=0,j\neq i}^{N} m_i m_j \frac{\mathbf{r}_j - \mathbf{r}_i}{\left|\mathbf{r}_j - \mathbf{r}_i\right|^3}, \tag{3.1}$$

where the natural units are chosen so that the gravitational constant is equal to one. A central configuration is a particular configuration of the N bodies where the acceleration vector of each body is proportional to its position vector, and the constant of proportionality is the same for the N-bodies. Therefore, a CC is a configuration that satisfies the Equation (2.118).

We take the position vector (see Figure 3.1) of the five primaries m_j, where $j = 0, 1, ..., 4$ as

$$\mathbf{r}_0 = (0,0), \quad \mathbf{r}_1 = (a,0), \quad \mathbf{r}_2 = (-a,0), \quad \mathbf{r}_3 = (0,b), \quad \mathbf{r}_4 = (0,-b). \tag{3.2}$$

Using the Equation (3.2) into Equation (2.118), the equation for m_0 is identically zero and the CC equations for m_1, m_2, m_3 and m_4 respectively, are

$$-\omega^2(a,0) = \frac{m_0(-a,0)}{a^3} + \frac{m_2(-2a,0)}{8a^3} + \frac{m_3(-a,b)}{(a^2+b^2)^{3/2}} + \frac{m_4(-a,-b)}{(a^2+b^2)^{3/2}} \tag{3.3}$$

$$-\omega^2(-a,0) = \frac{m_0(a,0)}{a^3} + \frac{m_1(2a,0)}{8a^3} + \frac{m_3(a,b)}{(a^2+b^2)^{3/2}} + \frac{m_4(a,-b)}{(a^2+b^2)^{3/2}} \tag{3.4}$$

$$-\omega^2(0,b) = \frac{m_0(0,-b)}{b^3} + \frac{m_1(a,-b)}{(a^2+b^2)^{3/2}} + \frac{m_2(-a,-b)}{(a^2+b^2)^{3/2}} + \frac{m_4(0,-2b)}{8b^3} \tag{3.5}$$

$$-\omega^2(0,-b) = \frac{m_0(0,b)}{b^3} + \frac{m_1(a,b)}{(a^2+b^2)^{3/2}} + \frac{m_2(-a,b)}{(a^2+b^2)^{3/2}} + \frac{m_3(0,2b)}{8b^3} \tag{3.6}$$

where $m_1 = m_2 = m_0 = m$ and $m_3 = m_4 = \tilde{m}$.

$$-\omega^2(a,0) = \frac{m(-a,0)}{a^3} + \frac{m(-2a,0)}{8a^3} + \frac{\tilde{m}(-a,b)}{(a^2+b^2)^{3/2}} + \frac{\tilde{m}(-a,-b)}{(a^2+b^2)^{3/2}}, \tag{3.7}$$

$$-\omega^2(0,b) = \frac{m(0,-b)}{b^3} + \frac{m(a,-b)}{(a^2+b^2)^{3/2}} + \frac{m(-a,-b)}{(a^2+b^2)^{3/2}} + \frac{\tilde{m}(0,-2b)}{8b^3}, \tag{3.8}$$

Because of the symmetry of the problem the Equation (3.3) is identical to Equation (3.4) and Equation (3.5) is identical to Equation (3.6). Writing Equation (3.7) and (3.8) in components form, we get

$$\omega^2 = \frac{5m}{4a^3} + \frac{2\tilde{m}}{(a^2+b^2)^{3/2}}, \tag{3.9}$$

$$\omega^2 = m\left(\frac{1}{b^3} + \frac{2}{(a^2+b^2)^{3/2}}\right) + \frac{\tilde{m}}{4b^3}. \tag{3.10}$$

We have extended the astrophysical model given in [76] by keeping the mass m_0 at the center. The results of the model given in [76] can be reproduced by taking $m_0 = 0$, in our model. Without loss of generality we take $\omega = 1$ and solve Equations (3.9) and (3.10) simultaneously for $m(a,b)$ and $\widetilde{m}(a,b)$

$$\left.\begin{aligned} m(a,b) &= \frac{N_m(a,b)}{D_m(a,b)}, \\ \widetilde{m}(a,b) &= \frac{N_{\widetilde{m}}(a,b)}{D_m(a,b)}, \end{aligned}\right\} \tag{3.11}$$

where

$$N_m(a,b) = 4a^3(a^2+b^2)^2\left((a^2+b^2)^{3/2}-8b^3\right), \tag{3.12}$$

$$\begin{aligned} N_{\widetilde{m}}(a,b) &= 4\left(a^2+b^2\right)^{3/2}\left(-4a^7-8a^5b^2+5a^4b^3-4a^3b^4+10a^2b^5\right. \\ &\quad \left.-8a^3b^3\sqrt{a^2+b^2}+5b^7\right), \end{aligned} \tag{3.13}$$

and

$$\begin{aligned} D_m(a,b) &= -32a^7-64a^5b^2-32a^3b^4+\left(5a^6+15a^4b^2-64a^3b^3\right. \\ &\quad \left.+15a^2b^4+5b^6\right)\left(\sqrt{a^2+b^2}\right). \end{aligned} \tag{3.14}$$

Taking $\tau = \frac{\tilde{m}}{m}$, and using Equations (3.12) to (3.14) in Equation (3.11) one can easily transform τ as

$$\tau(a,b) = \frac{\left(4-\frac{5b^3}{a^3}\right)\left(1+\frac{b^2}{a^2}\right)^{3/2}+8\frac{b^3}{a^3}}{8\frac{b^3}{a^3}-\left(1+\frac{b^2}{a^2}\right)^{3/2}}. \tag{3.15}$$

Further, let $\mu = \frac{b}{a}$ in Equation (3.15), the following alternate form of Equation (3.15) can be achieved as

$$\tau(\mu) = \frac{8\mu^3+(4-5\mu^3)\left(1+\mu^2\right)^{3/2}}{8\mu^3-\left(1+\mu^2\right)^{3/2}}. \tag{3.16}$$

Lemma 3.1. *The function $\tau(\mu)$ given by (3.16) is continuous, and strictly decreasing positive function in the interval $(1/\sqrt{3}, 1.1394282249562009)$, $\lim_{\mu\to 1/\sqrt{3}}\tau(\mu) = \infty$ and $\tau(1.1394282249562009) = 0$.*

Proof. The continuity of $\tau(\mu)$ can be easily checked, and from Equation (3.16), after putting the denominator equal to zero and solving the resultant equation by Newton's method, we get $\mu = 1/\sqrt{3}$, therefore $\lim_{\mu\to 1/\sqrt{3}}\tau(\mu) = \infty$. Then,

by putting the numerator of the Equation (3.16) equal to zero and solving the resulting equation again by Newton's method, we get $\mu = 1.1394282249562009$, so, $\tau(1.1394282249562009) = 0$. It means the value of $\tau(\mu)$ which is the mass ratio will remain positive i.e., $(\tau \in [0, \infty))$ as the ratio of the distance parameters varies between $(1/\sqrt{3}, 1.1394282249562009]$.

Now we need to prove that the function is decreasing and positive for the given interval. Taking the derivative of $\tau(\mu)$

$$\tau'(\mu) = 5\kappa'(\mu), \tag{3.17}$$

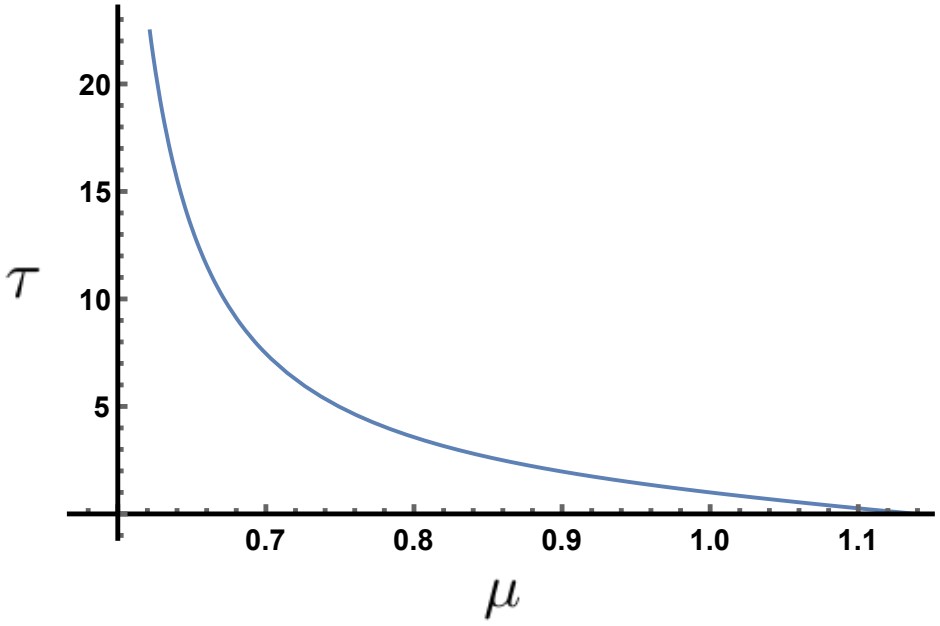

FIGURE 3.2: The plot for τ and μ.

$$\kappa'(\mu) = \frac{15\mu^2\sqrt{\mu^2+1}\left((\mu^2+1)^{5/2} - 8\left(\mu^5+1\right)\right)}{\left((\mu^2+1)^{3/2} - 8\mu^3\right)^2}. \tag{3.18}$$

$\tau'(\mu)$ is a constant multiple of $\kappa'(\lambda)$ given in [76] by Kulesza et. al. Proof will therefore be similar and can be seen in reference [76]. □

Here, we present some particular cases for different values of τ and μ. We show these different shapes of rhombus for different values of τ and μ in 3.3–3.6

- If $\mu = 1$, then $\tau = 1$ from Equation (3.16), we get the shape of true square with $m = \tilde{m} = 1$ and $a = b = 1$ see Figure 3.3.

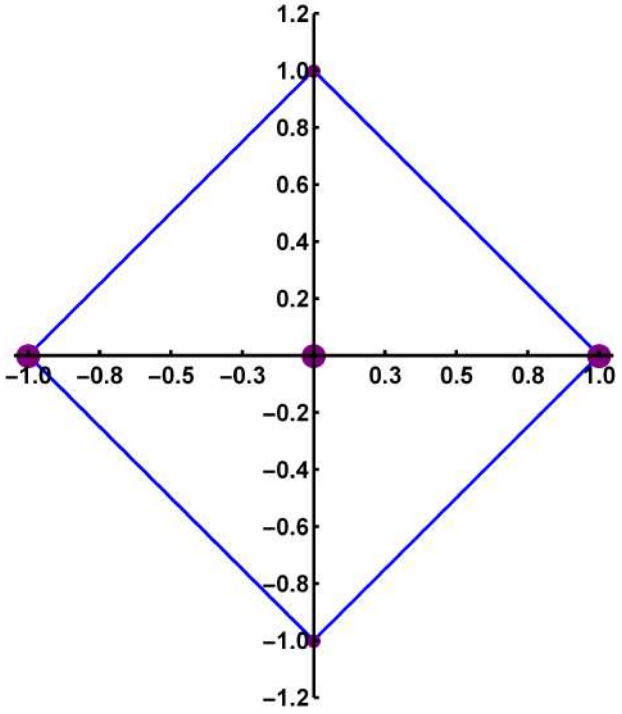

FIGURE 3.3: Shape of true square with $m = \tilde{m} = 1$ when $\mu = 1$ i.e., $a = b = 1$ and $\tau = 1$

- If $\mu = 1.04232$, then $\tau = 0.67$ from Equation (3.16), we get $\tilde{m} = 0.67m$ and $b = 1.04232a$ see Figure 3.4.

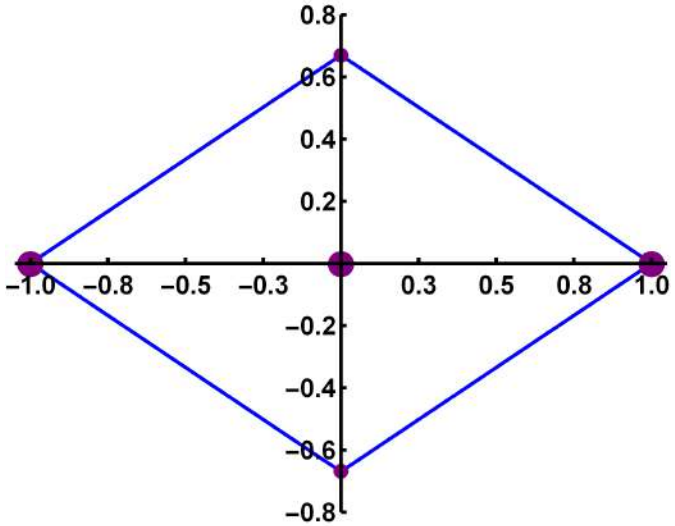

FIGURE 3.4: Shape for the rhombus when $\mu = 1.04232$ and $\tau = 0.67$

- $\mu = 1.00367$, then If $\tau = 0.97$ from Equation (3.16), we get $\tilde{m} = 0.97m$ and $b = 1.00367a$ see Figure 3.5.

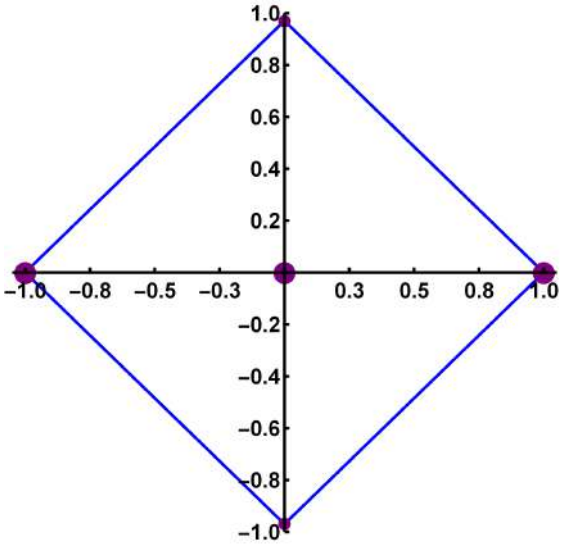

FIGURE 3.5: Shape for the rhombus when $\mu = 1.00367$ and $\tau = 0.97$

- If $\mu = 1.05455$, then $\tau = 0.58$ from Equation (3.16), we get $\tilde{m} = 0.58m$ and $b = 1.05455a$ see Figure 3.6.

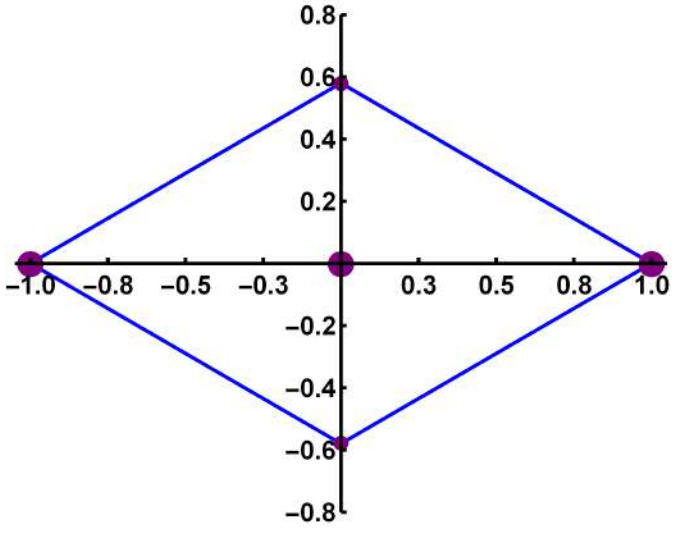

FIGURE 3.6: Shapes for the rhombus when $\mu = 1.05455$ and $\tau = 0.58$

There are two cases in which the central configuration degenerate.

- If $\mu = 1.1394282249562009$ then $\tau = 0$, this implies $\tilde{m} = 0$ and $b = 1.1394282249562009a$.

- If $\mu = 1/\sqrt{3}$ then $\tau = \infty$, this implies $m = 0$ and $b = (1/\sqrt{3})a$.

3.2.2 Central Configuration for Five Masses: when the two masses along the horizontal axis, m_1, m_2, and the two other masses along the vertical axis, m_3, m_4, are equal, and m_0 is not equal to any of the other masses.

Figure 3.7 shows the rhombus shape that has masses m_0, m_1 and m_2 on x-axis while the masses m_3 and m_4 are located at the y-axis. It is assumed that the masses m_1 and m_2 are equal to m, i.e., $m_1 = m_2 = m$ while m_3 and m_4 are equal to $\widetilde{m}$, i.e., $m_3 = m_4 = \widetilde{m}$.

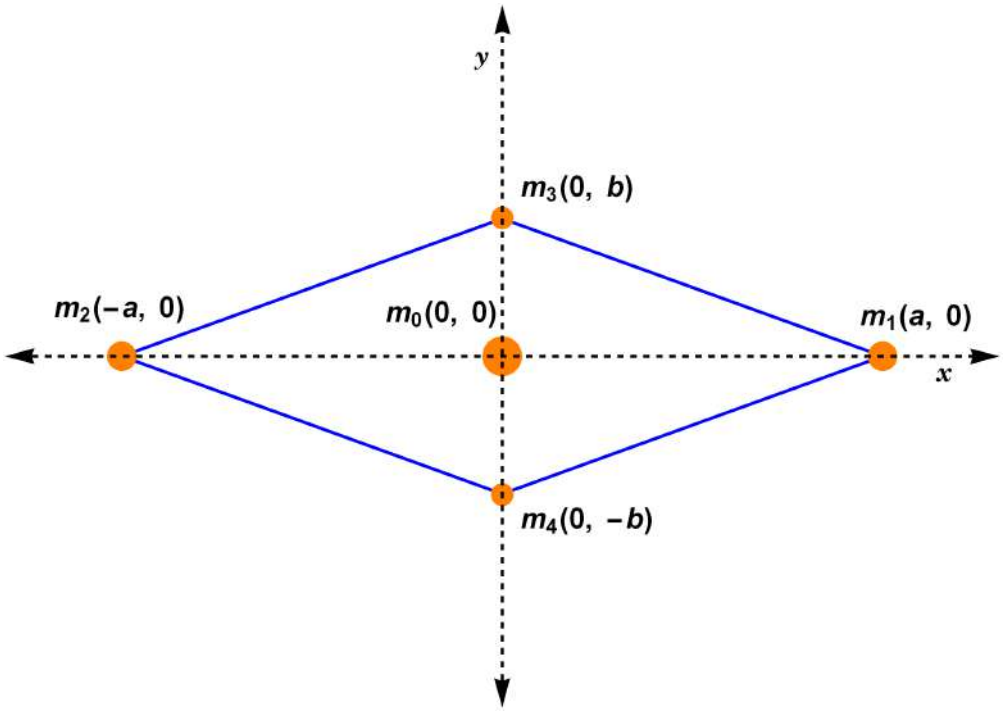

FIGURE 3.7: The rhomboidal central configuration of five bodies, when $m_1 = m_2 = m$, $m_3 = m_4 = \widetilde{m}$ and m_0 is neither equal to m nor equal to $\widetilde{m}$.

Following the same procedure as given in Section 3.2.1, one can easily get the following CC equations (for $m_1 = m_2 = m$ and $m_3 = m_4 = \widetilde{m}$.)

$$\omega^2 = \frac{m_0}{a^3} + \frac{2\widetilde{m}}{(a^2+b^2)^{3/2}} + \frac{m}{4a^3}, \tag{3.19}$$

$$\omega^2 = \frac{m_0}{b^3} + \frac{2m}{(a^2+b^2)^{3/2}} + \frac{\tilde{m}}{4b^3}. \tag{3.20}$$

The mass m_0 is stationery so its equation of motion ends up zero. We take sum of all primaries is equal to unity that is

$$m_0 + 2(m + \widetilde{m}) = 1. \tag{3.21}$$

Taking $\omega = 1$ and solving the Equations (3.19 to 3.21) give

$$m(a,b) = \frac{N_m}{D(a,b)}, \tag{3.22}$$

$$\widetilde{m}(a,b) = \frac{N_{\widetilde{m}}}{D(a,b)}, \tag{3.23}$$

$$D(a,b) \;=\; P_1 - P_2.$$

where

$$N_m \;=\; A(a,b)\left(1 + 7a^3 - 8b^3\right) - (1-b), \tag{3.24}$$

$$N_{\widetilde{m}} \;=\; B(a,b)\left(1 - 8a^3 + 7b^3\right) - (1-a), \tag{3.25}$$

with

$$A(a,b) \;=\; \frac{(a^2+b^2)^{3/2}}{8a^3(1+b+b^2)}, \tag{3.26}$$

and

$$B(a,b) \;=\; \frac{(a^2+b^2)^{3/2}}{8b^3(1+a+a^2)}, \tag{3.27}$$

$$\left.\begin{aligned} P_1 = \;& 15a^6 + 45a^4b^2 + 64a^3b^3 + 45a^2b^4 + 15b^6, \\ P_2 = \;& 64\sqrt{a^2+b^2}\left(a^5 + a^3b^2 + a^2b^3 + b^5\right). \end{aligned}\right\} \tag{3.28}$$

Lemma 3.2. *For any $a > 0$ and $b > 0$, $D(a, b)$ is always negative.*

Proof. Let us define

$$P(\alpha) = \frac{P_1(\alpha)}{P_2(\alpha)} = \frac{15 + 45\alpha^2 + 64\alpha^3 + 45\alpha^4 + 15\alpha^6}{64\sqrt{1+\alpha^2}(1 + \alpha^2 + \alpha^3 + \alpha^5)}, \quad \alpha = \frac{b}{a},$$

$$\frac{dP(\alpha)}{d\alpha} = \frac{2(\alpha - 1)\left(15\alpha^6 + 64\alpha^5 + 109\alpha^4 + 64\alpha^3 + 109\alpha^2 + 64\alpha + 15\right)}{64\left(\alpha^2 + 1\right)^{5/2}\left(\alpha^3 + 1\right)^2}.$$

To prove $D(a, b) < 0$ we need to prove $P(\alpha) < 1$. For this differentiating $P(\alpha)$ with respect to α and finding the critical points of $P(\alpha)$ in $(0, \infty)$. There is only one critical point of $P(\alpha)$ (i.e., $\alpha = 1$) in $(0, \infty)$ and $P(1) = \frac{23}{32\sqrt{2}}$. One can easily see that $P(\alpha)$ is monotonically increasing function because $\frac{dP(\alpha)}{d\alpha} < 0$ in $(0, 1)$ and $P(\alpha)$ is monotonically decreasing function because $\frac{dP(\alpha)}{d\alpha} > 0$ in $(1, \infty)$ (see Figure 3.8). When $\alpha \to 0$ or ∞, then $P(\alpha) \to \frac{15}{64}$. So $P(\alpha) < 1$ for $\alpha \in (0, \infty)$ and hence $D(a, b) < 0$ for $a > 0$ and $b > 0$. □

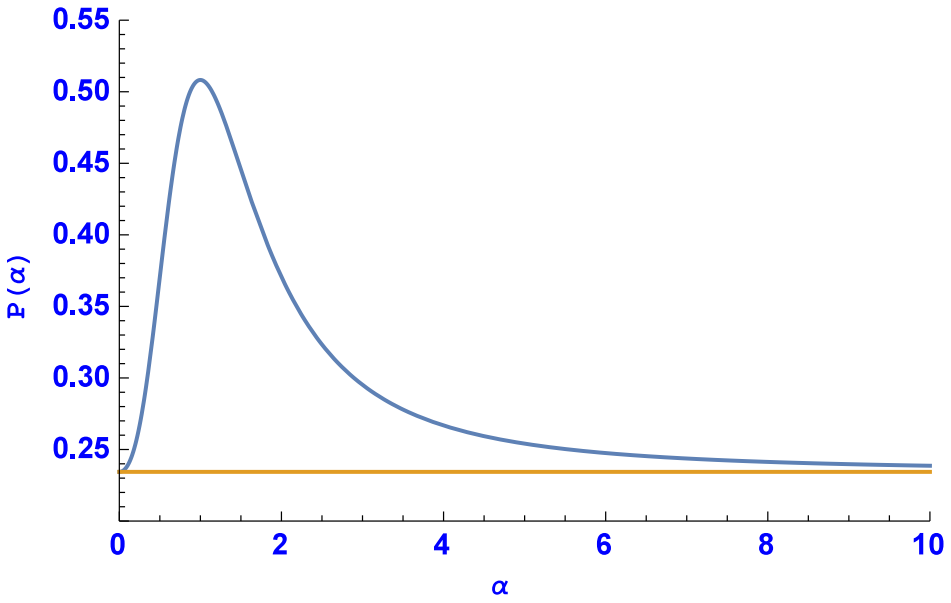

FIGURE 3.8: Graph of $P(\alpha)$ (Blue) and $P(\alpha) = \frac{15}{64}$ (Orange)

To prove $m(a, b)$ and $\widetilde{m}(a, b)$ positive we need to prove N_m and $N_{\widetilde{m}}$ must be negative for $a > 0$ and $b > 0$. Because N_m and $N_{\widetilde{m}}$ are non-linear algebraic functions of a and b, so it is difficult to solve these inequalities. For this we draw the region

(shaded region of Figure 3.9) where both N_m and $N_{\tilde{m}}$ are negative. From the graph we can easily find the approximate bounds for $a > 0$ and $b > 0$ where N_m and $N_{\tilde{m}}$ are negative.

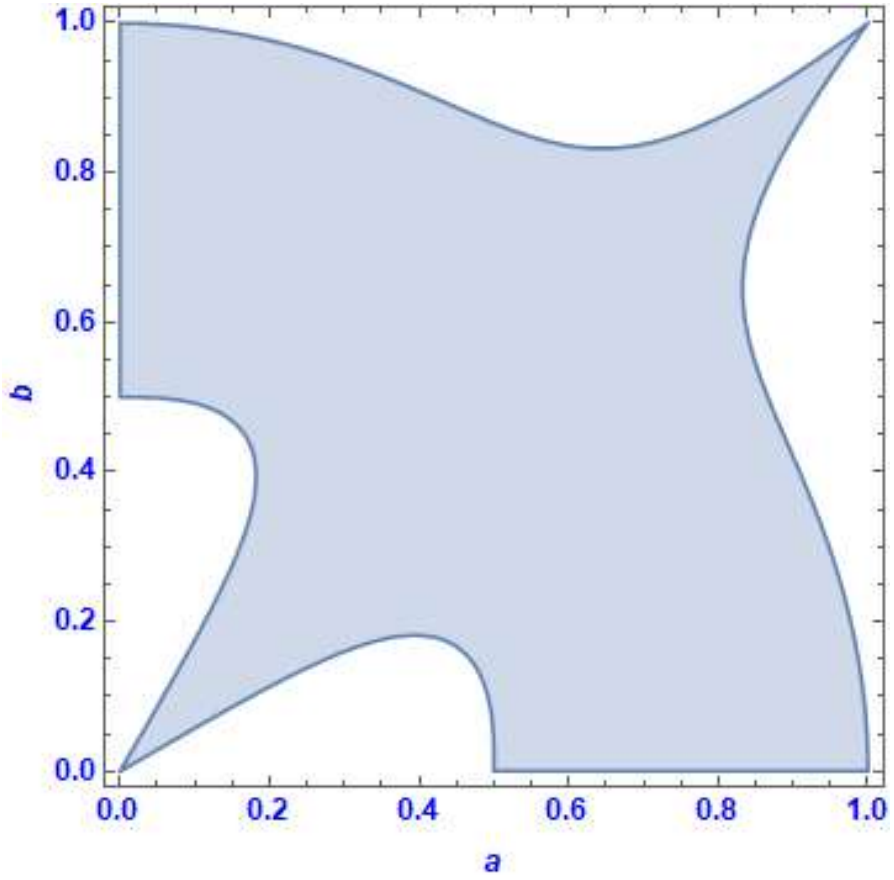

FIGURE 3.9: N_m and $N_{\tilde{m}}$ both are negative (Shaded Region)

Using Equation (3.21) to Equation (3.23) one can easily see that $m(a,b) = \tilde{m}(b,a)$ and $0 < m(a,b) < 0.5$, $0 < m(\tilde{a},b) < 0.5$ and $m_0(a,b) > 0$ for $0.5 < a < 1$ and $0.5 < b < 1$. In Figure 3.10 we show the region of central configuration for which $m, \tilde{m}, m_0 > 0$ are positive.

Because Figure 3.10 is symmetric about the line $b = a$, we divide here Figure 3.10 into two parts upper region (R_u) and lower region (L_u). Here we discuss only the central configuration for the region of R_u. The upper CC region is approximately surrounded by the following three interpolating polynomials as

$$f_1 = a, \tag{3.29}$$

$$f_2 = -220.187a^7 + 1310.43a^6 - 3257.57a^5 + 4399.05a^4 - 3494.37a^3 + 1637.89a^2 - 421.05a + 46.8139, \quad (3.30)$$

$$f_3 = 259.785a^6 - 1127.86a^5 + 2021.17a^4 - 1914.65a^3 + 1013.31a^2 - 284.941a + 34.1992. \quad (3.31)$$

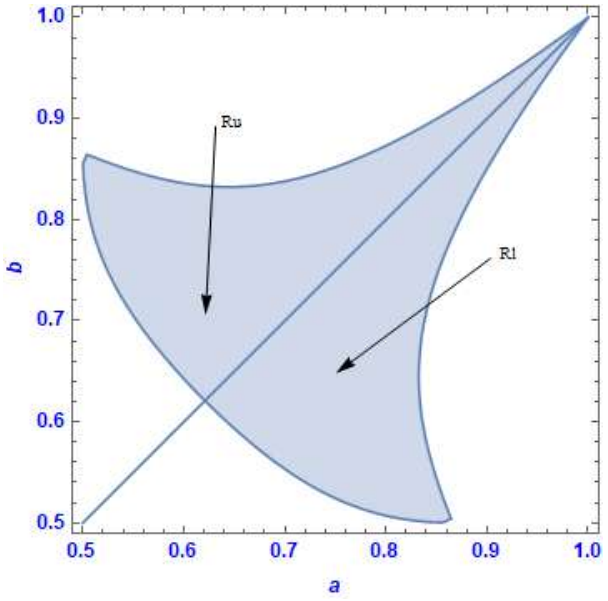

(i)

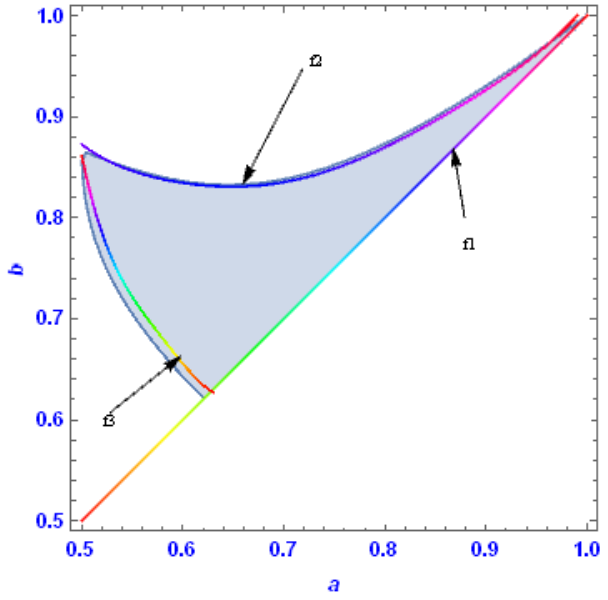

(ii)

FIGURE 3.10: (i): Central configuration region (shaded); (ii) Upper central configuration is surrounded by three interpolating curves (Hue color)

The Figures in 3.11 (i-iv) show the changes of masses m_0, m, and $\tilde{m}$ with variations of parameter b. We can clearly see as b varies in $(0.5, 1)$ the central mass m_0 is increasing and other masses are becoming zeros.

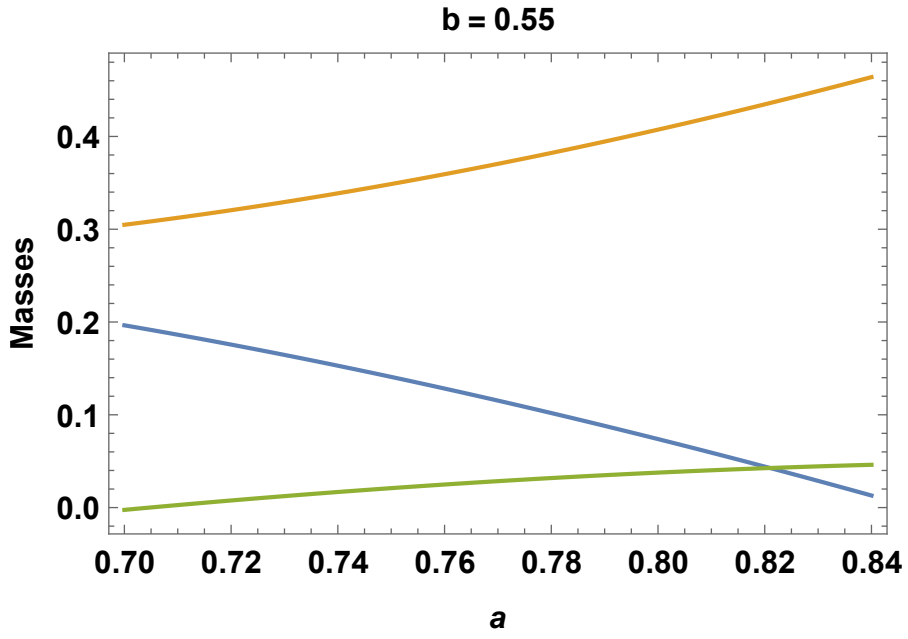

(i)

FIGURE 3.11: Variations of primary masses m_0 (green), $\widetilde{m}$ (orange) and m (blue) for $b = 0.55$

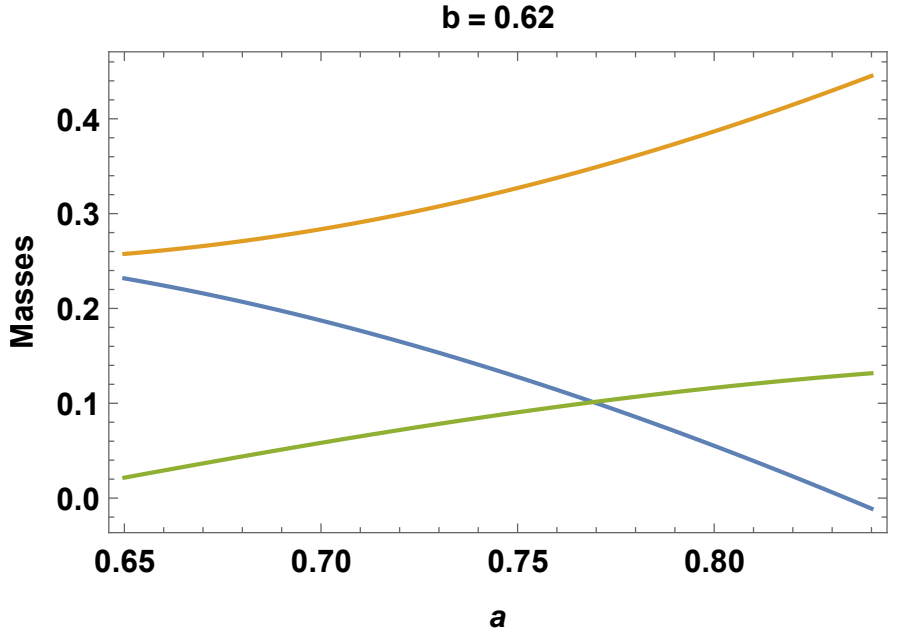

(ii)

FIGURE 3.11: Variations of primary masses m_0 (green), $\widetilde{m}$ (orange) and m (blue) for $b = 0.62$

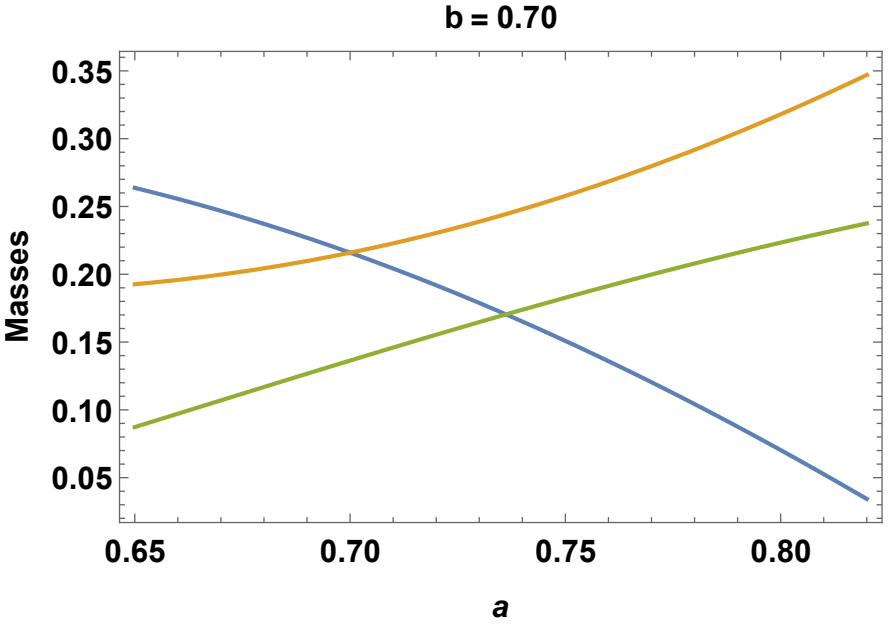

(iii)

FIGURE 3.11: Variations of primary masses m_0 (green), $\widetilde{m}$ (orange) and m (blue) for $b = 0.70$

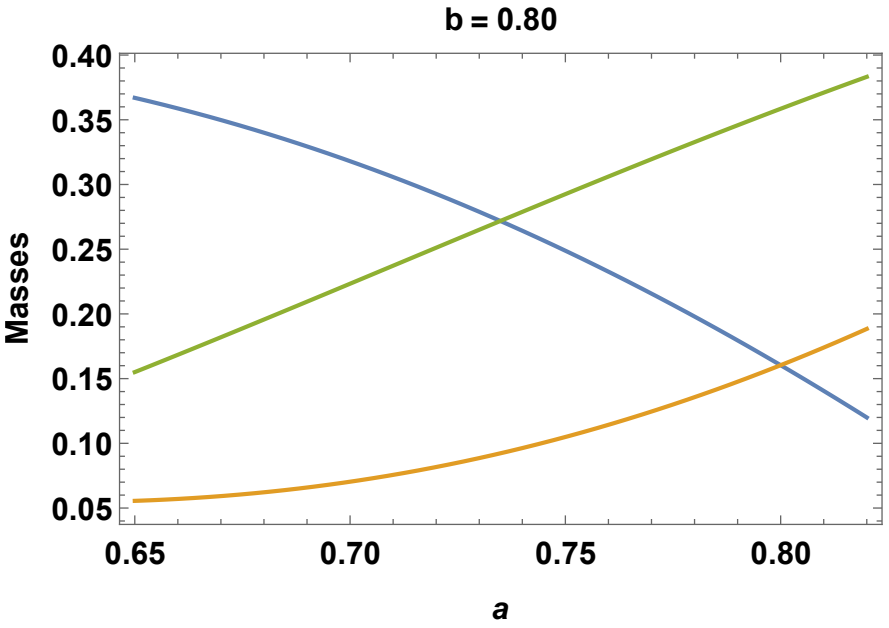

(iv)

FIGURE 3.11: Variations of primary masses m_0 (green), $\widetilde{m}$ (orange) and m (blue) for $b = 0.80$

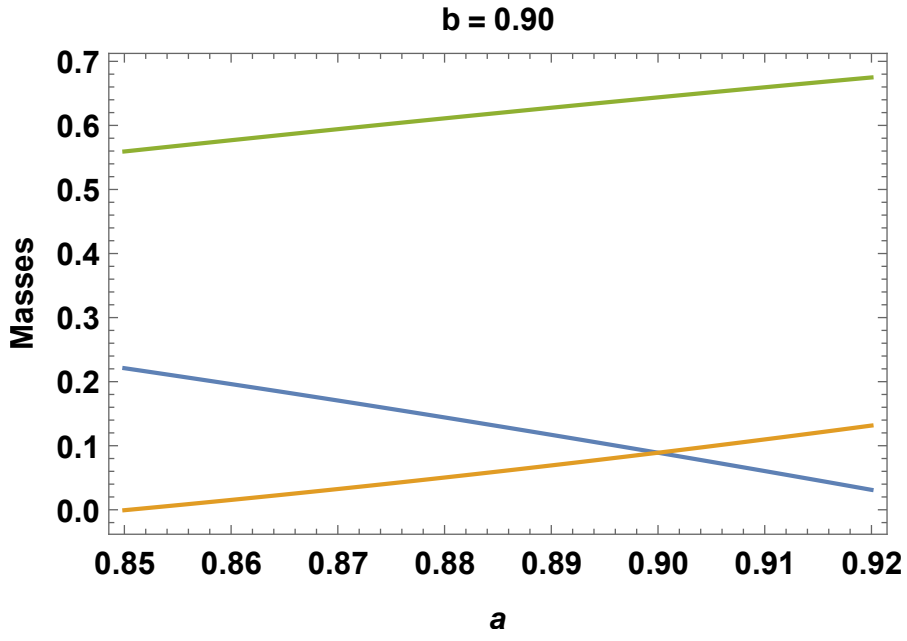

(v)

FIGURE 3.11: Variations of primary masses m_0 (green), $\widetilde{m}$ (orange) and m (blue) for $b = 0.90$

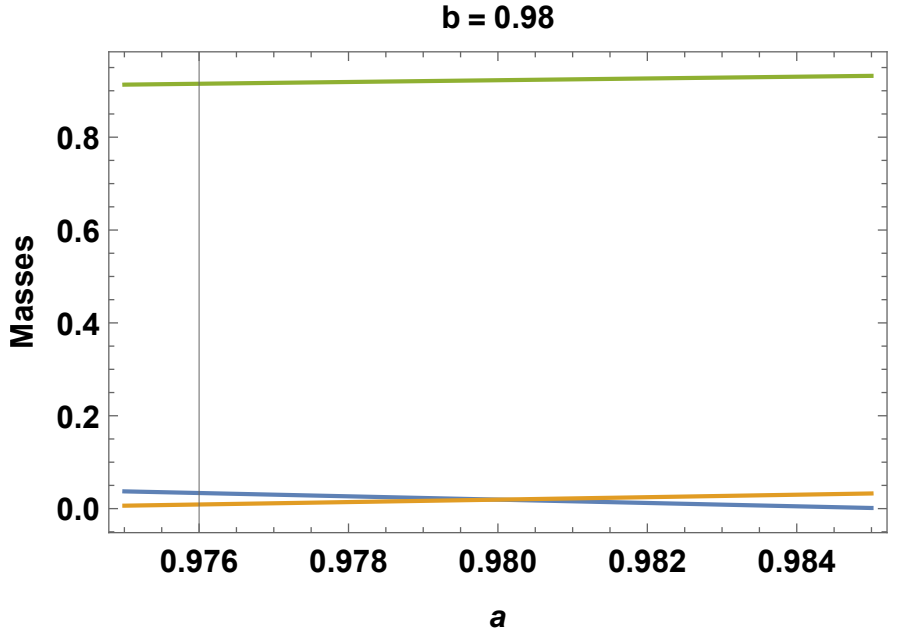

(vi)

FIGURE 3.11: Variations of primary masses m_0 (green), $\widetilde{m}$ (orange) and m (blue) for $b = 0.98$

3.2.3 Summary

The configuration of rhomboidal CC illustrated that the change in the masses of the primaries led to a change in the overall gravitational field of the configuration. This change in the gravitational field gave different bounds for the mass parameters; two cases have been discussed in this capacity. In the first case, the masses along the horizontal axis are considered to be the same, i.e., $m_0 = m_1 = m_2 = m$ while the masses along the vertical axis are equal, i.e., $m_3 = m_4 = \widetilde{m}$.

The equations of motion, after taking $\omega = 1$, without the loss of generality show that masses depend on the values of diagonal lengths a and b, i.e., by changing the values of a and b the values of masses change, which ultimately changes the configuration. The mass parameter μ is taken to be the ratio of diagonal lengths of the rhombus, i.e., $\mu = b/a$. The masses only become subjects of parameter b when we take $a = 1$, and it is found that for the interval $(1/\sqrt{3}, 1.1394282249562009)$ there exist families of CC; the CC degenerates when $b = 1/\sqrt{3}$ or $b = 1.1394282249562009$; there arises a special square configuration when $a = b = 1$.

In the second case, the masses m_1 and m_2 along the horizontal axis are assumed to be the same and taken equal to m, while the masses m_3 and m_4 along the vertical axis are assumed to be the same and taken equal to $\widetilde{m}$. The mass m_0, at the intersection of two diagonals of a rhombus (which is also the origin of the coordinate system), is different from all the other four primaries. This change in the masses of the primaries gave rise to new bound for both a and b, i.e., both vary in the interval $(0.5, 1)$ and families of CCs exist in this interval.

Chapter 4

The Sixth-Body Motion and its Lagrange Points

4.1 Introduction

In this chapter, we discuss the motion of a test particle with a very tiny ignorable mass as compared to the five primaries that move under the gravitational field of the primaries. The test particle cannot impact the gravitational field of primaries but is influenced by their gravitational field. The objective here is to identify the areas for the probable motion of the test mass in the gravitational field of the primaries, as well as the Lagrange points of the test mass in the central configuration of the five primaries.

4.2 Equation of Motion of Sixth-Body

In this section we describe the motion of the infinitesimal sixth-body, m_5, under the gravitational field created by the attraction of the five primaries moving in a planar rhomboidal configuration, as we did in Chapter 3. We assume that the sixth body has a significantly smaller mass compared to the masses of the primary ($m_5 << m_0, m_1, m_2, m_3, m_4$). On this basis, the sixth body acts as an infinitesimal

test particle and therefore it does not influence the motion of the five primaries. In the RR6BP, the equations of motion of m_5, obtained from Equation (2.3) is

$$\begin{aligned}\ddot{\mathbf{r}}_5 &= -m_0\frac{\mathbf{r}_5-\mathbf{r}_0}{|\mathbf{r}_5-\mathbf{r}_0|^3} - m_1\frac{\mathbf{r}_5-\mathbf{r}_1}{|\mathbf{r}_5-\mathbf{r}_1|^3} - m_2\frac{\mathbf{r}_5-\mathbf{r}_2}{|\mathbf{r}_5-\mathbf{r}_2|^3} - m_3\frac{\mathbf{r}_5-\mathbf{r}_3}{|\mathbf{r}_5-\mathbf{r}_3|^3} \\ &\quad -m_4\frac{\mathbf{r}_5-\mathbf{r}_4}{|\mathbf{r}_5-\mathbf{r}_4|^3},\end{aligned} \tag{4.1}$$

where dot represents the derivative with respect to time. We now set up the equation of motion in co-rotating coordinates for m_5 with respect to the two different cases discussed in Chapter 3.

4.2.1 Case-I: $m_0 = m_1 = m_2 = m$, $m_3 = m_4 = \widetilde{m}$

This section discusses the motion of m_5 in the gravitational field set up by the masses in the central configuration of Case-I of Chapter 3. The masses m_0, m_1, m_2 are assumed to be equal to m on the horizontal axis, while the masses m_3 and m_4 on the vertical axis are assumed to be equal to $\widetilde{m}$. From here onward in this section, without loss of generality, we take the value of $a = 1$. The equations of motion of m_5 in the co-rotating coordinates x and y are

$$\begin{aligned}\ddot{x} - 2\dot{y} &= U_x, \\ \ddot{y} + 2\dot{x} &= U_y,\end{aligned} \tag{4.2}$$

where

$$U(x,y) = \frac{(x^2+y^2)}{2} + m\left(\frac{1}{r_{50}} + \frac{1}{r_{51}} + \frac{1}{r_{52}}\right) + \widetilde{m}\left(\frac{1}{r_{53}} + \frac{1}{r_{54}}\right) \tag{4.3}$$

is the effective potential. The mutual distances of m_5 from the primaries in co-rotating frame are

$$\left.\begin{aligned} r_{50} &= \sqrt{x^2+y^2} \quad , \quad r_{51} = \sqrt{(x-1)^2+y^2}, \\ r_{52} &= \sqrt{(x+1)^2+y^2} \quad , \quad r_{53} = \sqrt{x^2+(y-b)^2}, \\ r_{54} &= \sqrt{x^2+(y+b)^2}. \end{aligned}\right\} \tag{4.4}$$

The Jacobian constant is given by [9]

$$C + U = \frac{1}{2}\left(\dot{x}^2 + \dot{y}^2\right) = v^2. \tag{4.5}$$

For a given value of the Jacobi constant, v^2 is only a function of position in the rotating frame. Since v^2 cannot be negative, it must be true that

$$C + U \geq 0. \tag{4.6}$$

The boundaries between forbidden and allowed regions of motion are found by setting $v^2 = 0$, i.e.,

$$C + U = 0. \tag{4.7}$$

It is now trivial to show that $C(x, y)$ is the first integral of motion of system (4.2) by proving that $\dot{C}(x, y) = 0$.

4.2.1.1 The Hill Regions

The region of permitted motion is also known as the Hill region and the curves found by Equation (4.6) for various values of C are known as the zero velocity curves.

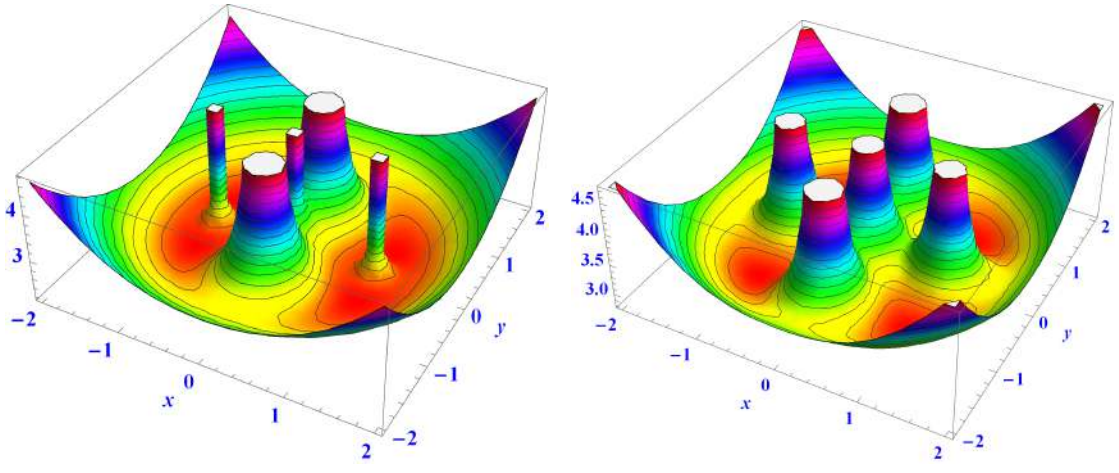

(i) (ii)

FIGURE 4.1: The effective potential (*i*) $b = 0.67$; $m = 0.0778$, $\tilde{m} = 0.7879$. (*ii*) $b = 0.97$; $m = 0.4588$, $\tilde{m} = 0.5766$.

The zero velocity curves when $b = 0.67$, $m = 0.07717$, $\tilde{m} = 0.7879$ and when $b = 0.97$, $m = 0.4588$, $\tilde{m} = 0.5766$ are given in Figure 4.2 and the corresponding Hill regions are given in Figure 4.1.

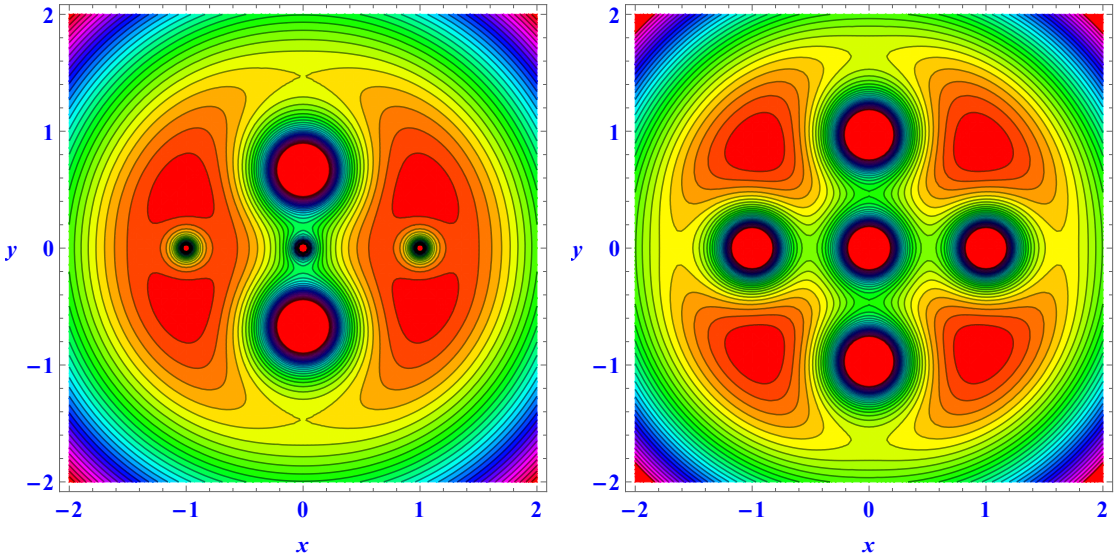

(i) (ii)

FIGURE 4.2: The evolution of zero velocity curves.(i) $b = 0.67$; $m = 0.07717$, $\tilde{m} = 0.7879$. (ii) $b = 0.97$; $m = 0.4588$, $\tilde{m} = 0.5766$.

We also give region of possible motion of m_5 for six different values of Jacobi constants C in Figures 4.3 to 4.5 for mass parameters $b = 0.67, 0.97, 1.13$.

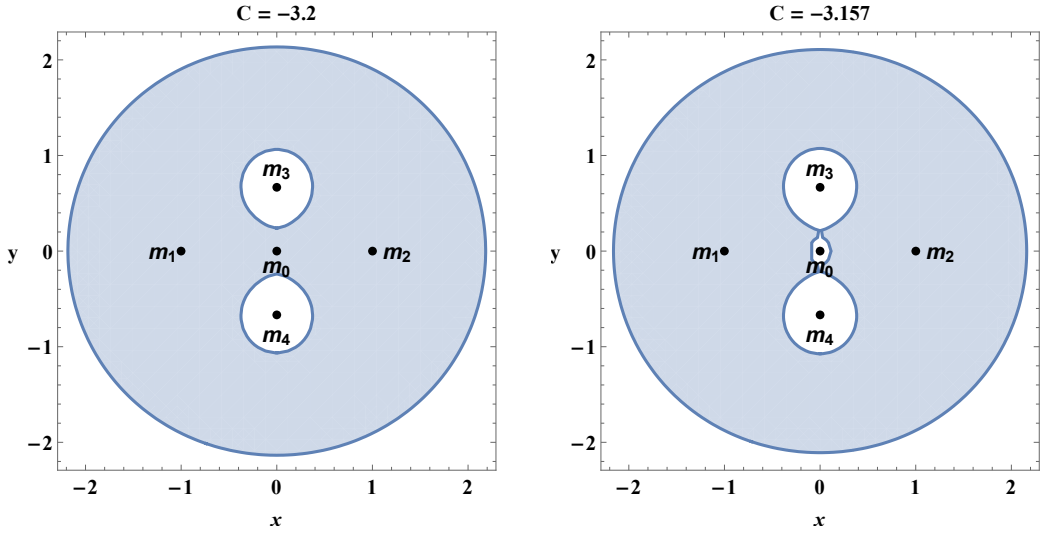

(i) (ii)

FIGURE 4.3: The regions of motion of m_5 (white region) when $b = 0.67$, (i) $C = -3.2$ and (ii) $C = -3.157$.

The shaded regions represent the forbidden regions of motion for the infinitesimal mass m_5. It is numerically confirmed that the permitted regions are completely disconnected for $C \geq -2.20, -2.85, -2.56$ as Figures 4.3 to 4.5 for the above values of b.

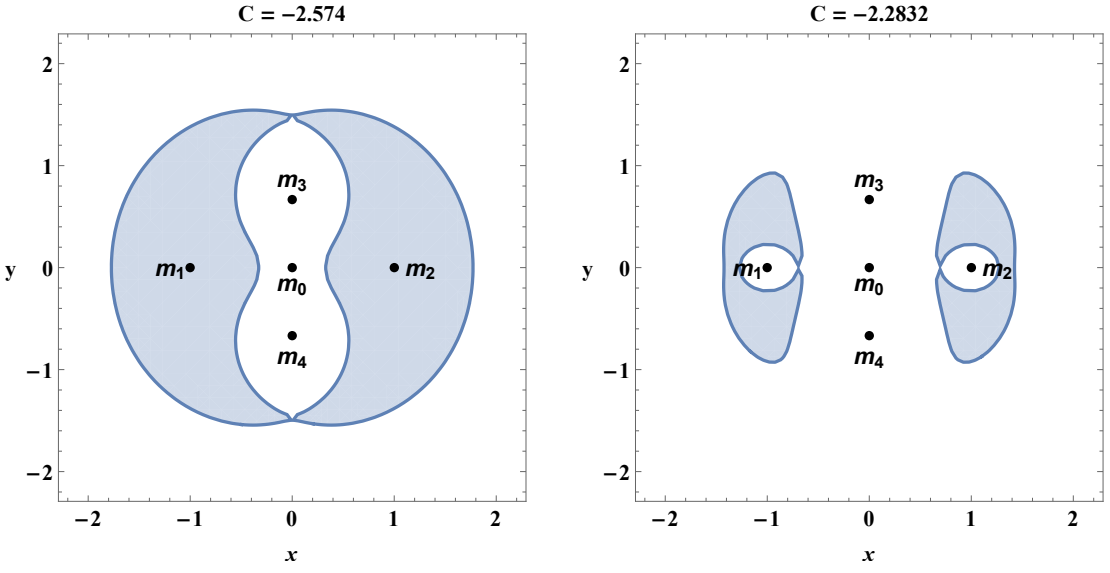

(iii) (iv)

FIGURE 4.3: The regions of motion of m_5 (white region) when $b = 0.67$, (iii) $C = -2.574$ and (iv) $C = -2.2832$.

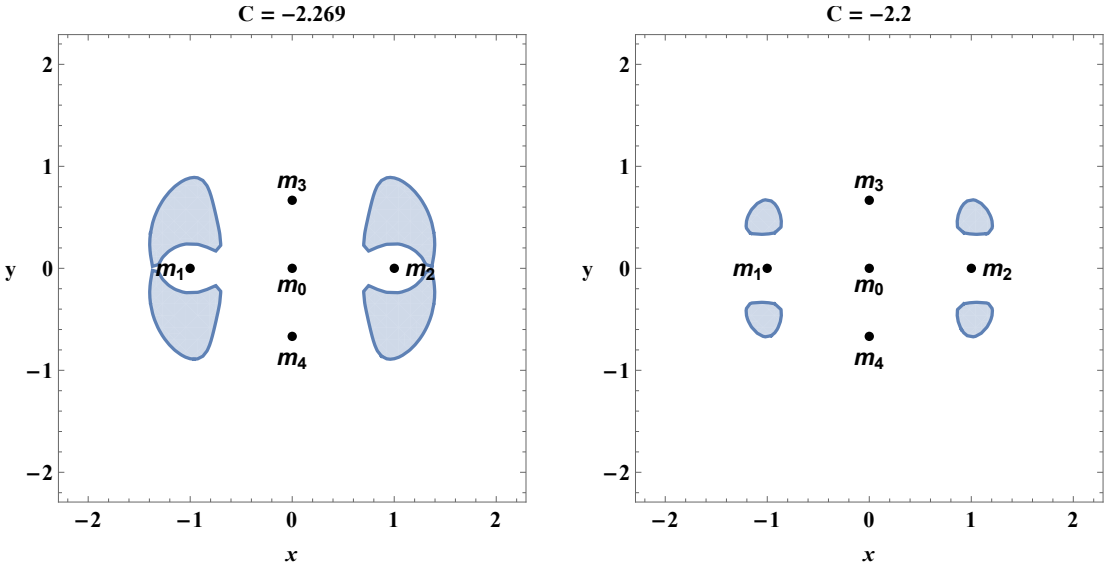

(v) (vi)

FIGURE 4.3: The regions of motion of m_5 (white region) when $b = 0.67$, (v) $C = -2.269$ and (vi) $C = -2.2$.

For the increasing values of C the allowed region of motion (white region) become partially connecting at $C = -2.574, -3.328, -3.342$ and completely connected at $C = -3.2, -3.9, -3.5$. It can be seen from Figures 4.3 to 4.5 that the transition of motion from totally disconnected to completely connected occurs in six stages for $b = 0.67, 0.97, 1.13$. For these values of b, m_5 can freely move in the gravitational field of CC region for $C \geq -2.2, -2.85, -2.56$ and cannot reach any of the primaries for $C \leq -3.2, -3.9, -3.5$.

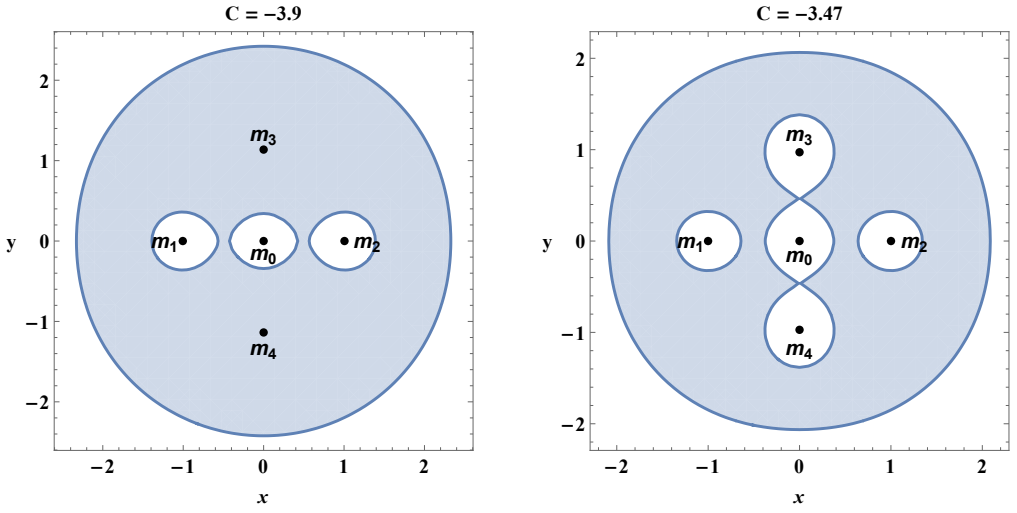

(i) (ii)

FIGURE 4.4: The regions of motion of m_5 (white region) when $b = 0.97$, (i) $C = -3.9$ and (ii) $C = -3.47$.

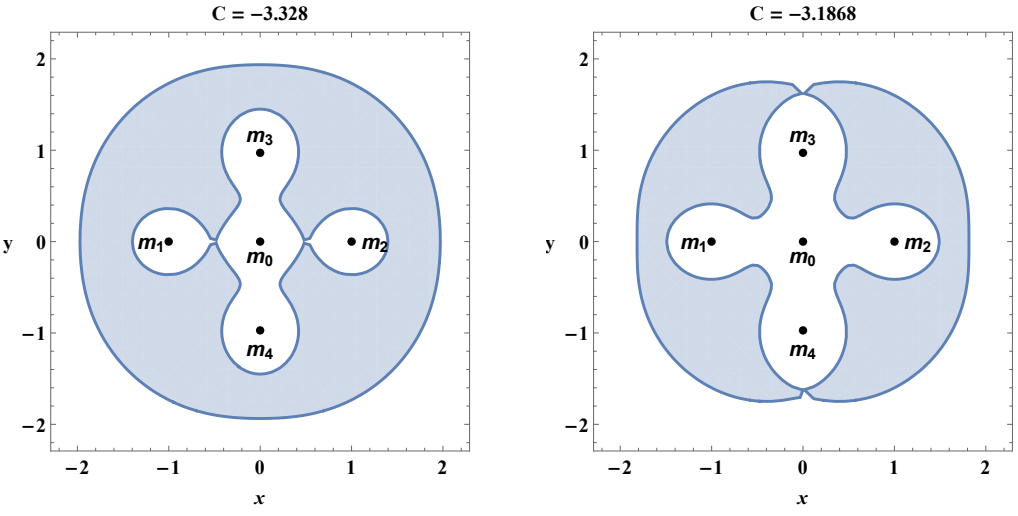

(iii) (iv)

FIGURE 4.4: The regions of motion of m_5 (white region) when $b = 0.97$, (iii) $C = -3.328$ and (iv) $C = -3.1868$.

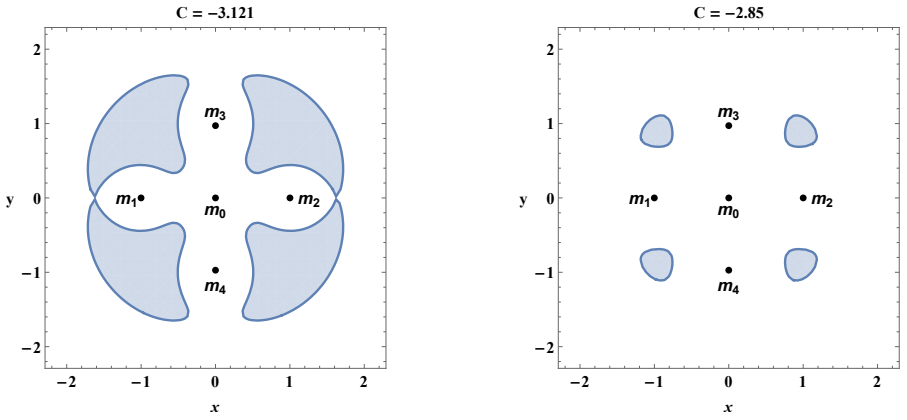

(v) (vi)

FIGURE 4.4: The regions of motion of m_5 (white region) when $b = 0.97$, (v) $C = -3.121$ and (vi) $C = -2.85$.

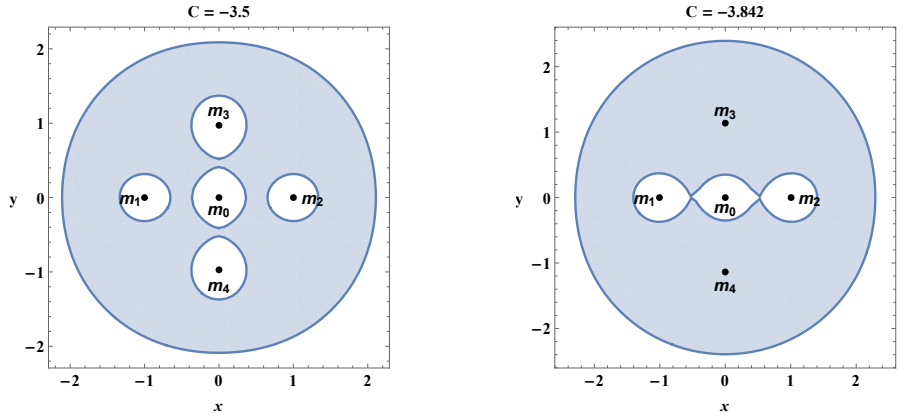

(i) (ii)

FIGURE 4.5: The regions of motion of m_5 (white region) when $b = 1.13$, (i) $C = -3.5$ and (ii) $C = -3.842$.

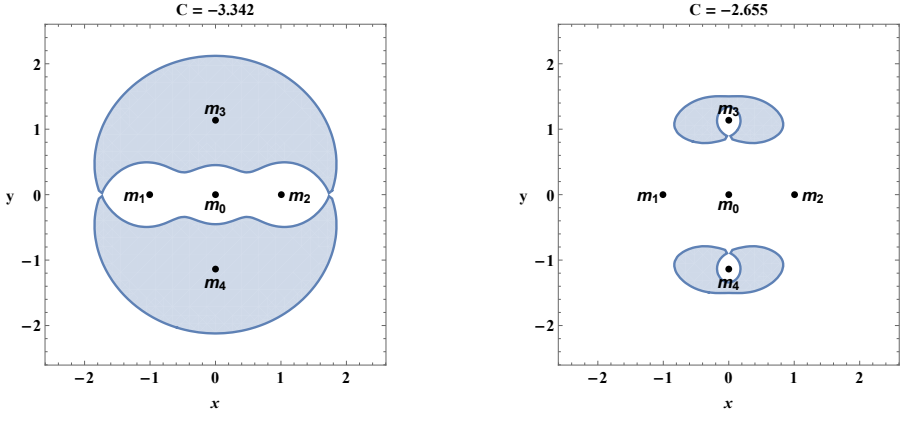

(iii) (iv)

FIGURE 4.5: The regions of motion of m_5 (white region) when $b = 1.13$, (iii) $C = -3.342$ and (iv) $C = -2.655$.

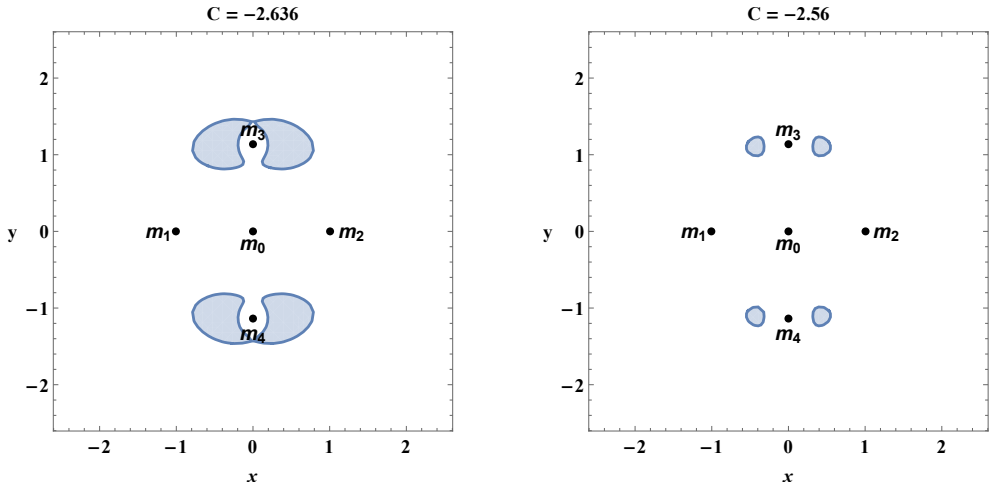

(v) (vi)

FIGURE 4.5: The regions of motion of m_5 (white region) when $b = 1.13$, (v) $C = -2.636$ and (vi) $C = -2.56$.

4.2.1.2 Equilibrium Solutions

Equilibrium solutions of the RR6BP are the solutions of $U_x(x, y) = 0$ and $U_y(x, y) = 0$. The derivative U_x and U_y of the effective potential, given in Equation (4.3) are found as below

$$\begin{aligned} U_x &= x - \frac{mx}{(x^2+y^2)^{3/2}} - m\left(\frac{x-a}{((x-a)^2+y^2)^{3/2}} + \frac{x+1}{((x+1)^2+y^2)^{3/2}}\right) \\ &\quad -\widetilde{m}x\left(\frac{1}{((y-b)^2+x^2)^{3/2}} + \frac{1}{((y+b)^2+x^2)^{3/2}}\right), \end{aligned} \tag{4.8}$$

$$\begin{aligned} U_y &= y - \frac{my}{(x^2+y^2)^{3/2}} - my\left(\frac{1}{((x-1)^2+y^2)^{3/2}} + \frac{1}{((x+1)^2+y^2)^{3/2}}\right) \\ &\quad -\tilde{m}\left(\frac{y-b}{((y-b)^2+x^2)^{3/2}} + \frac{b+y}{((y+b)^2+x^2)^{3/2}}\right). \end{aligned} \tag{4.9}$$

4.2.1.3 Equilibrium Solutions on the Coordinates Axes

Since the potential given in Equation (4.3) is invariant under the symmetry, $(x, -y)$, $(-x, y)$ and $(-x, -y)$ we will restrict our computation to the first quadrant: $x \geq 0$ and $y \geq 0$. Initially we study the existence and number of equilibrium

solutions on the axes and then off the coordinate axes.

To study the equilibrium solutions on the y-axis, let $x = 0$, then Equations (4.8) and (4.9) are given as

$$\left.\begin{aligned} U_x &= 0, \\ U_y &= y - \frac{my}{(y^2)^{3/2}} - \frac{2my}{(1+y^2)^{3/2}} \\ &\quad - \tilde{m}\left(\frac{y-b}{((y-b)^2)^{3/2}} + \frac{b+y}{((y+b)^2)^{3/2}}\right). \end{aligned}\right\} \tag{4.10}$$

To solve $U_y = 0$, divide y into sub-intervals $0 < y < b$ and $y > b$.

$0 < y < b$; $1/\sqrt{3} < b < 1.1394282249562009$

Rewrite the right hand side of Equation (4.9) by taking into account that $y \in (0, b)$

$$f_1(y) = y - \frac{m}{y^2} - \frac{2my}{(1+y^2)^{3/2}} + \tilde{m}\left(\frac{1}{(y-b)^2} - \frac{1}{(y+b)^2}\right). \tag{4.11}$$

At $y \approx 0$, $f_1(y) < 0$ and $y \approx b$, $f_1(y) > 0$ therefore by the mean value theorem there is at least one zero of $f_1(y)$ when $y \in (0, b)$. The derivative of $f_1(y)$ is given by

$$\begin{aligned} \frac{df_1(y)}{dy} &= 1 + 2m\left(\frac{1}{y^3} + \frac{1}{(y^2+1)^{3/2}} - \frac{3y^2}{(y^2+1)^{5/2}}\right) \\ &\quad + 2\widetilde{m}\left(\frac{1}{(y+b)^3} - \frac{1}{(y-b)^3}\right) \end{aligned} \tag{4.12}$$

The only term $\left(-\dfrac{3y^2}{(y^2+1)^{5/2}}\right)$ that can make $\dfrac{df_1(y)}{dy}$ negative for $y \in (0, b)$ is dominated by the rest of the term in Equation (4.10), therefore $\dfrac{df_1(y)}{dy} > 0$. This proves the existence of unique equilibrium solution inside rhombus on the y axis.

y > b

Now consider the case $y > b$. Using Equation (4.10) and rewriting as

$$f_2(y) = y - \frac{m}{y^2} - \frac{2my}{(1+y^2)^{3/2}} - \tilde{m}\left(\frac{1}{(y-b)^2} + \frac{1}{(y+b)^2}\right). \tag{4.13}$$

At $y \approx b$, $f_2(y) < 0$ and $y \approx \infty$, $f_2(y) > 0$, therefore by mean value theorem there is at least one zero of $f_2(y)$ when $y \in (b, \infty)$. The derivative of $f_2(y)$ is given by

$$\begin{aligned}\frac{df_2(y)}{dy} &= 1 + 2m\left(\frac{1}{y^3} + \frac{1}{(y^2+1)^{3/2}} - \frac{3y^2}{(y^2+1)^{5/2}}\right) \\ &\quad +2\tilde{m}\left(\frac{1}{(y+b)^3} + \frac{1}{(y-b)^3}\right)\end{aligned} \tag{4.14}$$

Following the same procedure as given for $0 < y < b$, one can easily prove the uniqueness of equilibrium solution for $y > b$.

We discuss here two special cases of CC for $b \in (\frac{1}{\sqrt{3}}, 1.1394282249562009)$. When $b = \frac{1}{\sqrt{3}}$, then the masses on the horizontal axis are zero, i.e., $m = 0$. In this case we only get the two equilibrium points along y-axis. When $b = 1.1394282249562009$, then $\tilde{m} = 0$. In this case we get four equilibrium points along x-axis. The positions of the masses and the corresponding equilibrium points for the these two cases are shown in Figure 4.6. The stability of these cases will be discussed in Section 4.2.1.5.

4.2.1.4 Equilibrium Solutions Off the Coordinates Axes

It is numerically confirmed that for $b = 0.67, 0.97, 1.13$ there are always a total of 12 equilibrium points. As shown in Figure 4.7 four of the equilibrium points are on the x-axis, four on the y-axis and remaining four of the equilibrium points are off the axes. Since the gravitational field is a function of mass parameters $m(b)$ therefore the equilibrium points change their positions around the primaries for changing values of b. It is numerically confirmed that majority of equilibrium points are around the primaries along the horizontal axis if b is around $1/\sqrt{3}$ as

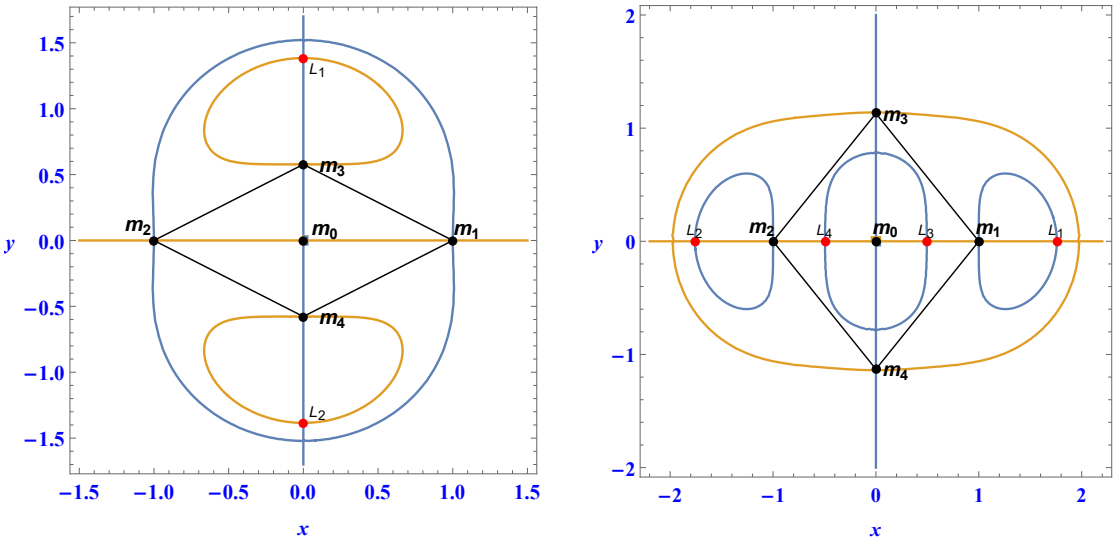

(i) (ii)

FIGURE 4.6: (i) Equilibrium points (red color) along y-axis when $m = 0$ (ii) Equilibrium points (red color) along x-axis when $\tilde{m} = 0$

the masses on the horizontal axis are dominant (see Figure 4.7 (i)). For $b \geq 1$ the equilibrium points concentrated around the primaries on vertical axis (see Figure 4.7 (ii)).

4.2.1.5 Stability Analysis

To study the stability of the equilibrium points obtained in the previous section we will follow the standard linearization procedure by linearizing the equation of motion of infinitesimal mass. Let the location of an equilibrium point in the RR6BP be denoted by (x, y) and consider a small displacement (X, Y) from the point such that $x + X$ and $y + Y$ is the new position of the infinitesimal. Using the Taylor's series expansion in Equations (4.2), gives a new set of second order linear differential equations:

$$\ddot{X} - 2\dot{Y} = XU_{xx} + YU_{xy}, \tag{4.15}$$

$$\ddot{Y} + 2\dot{X} = XU_{xy} + YU_{yy}. \tag{4.16}$$

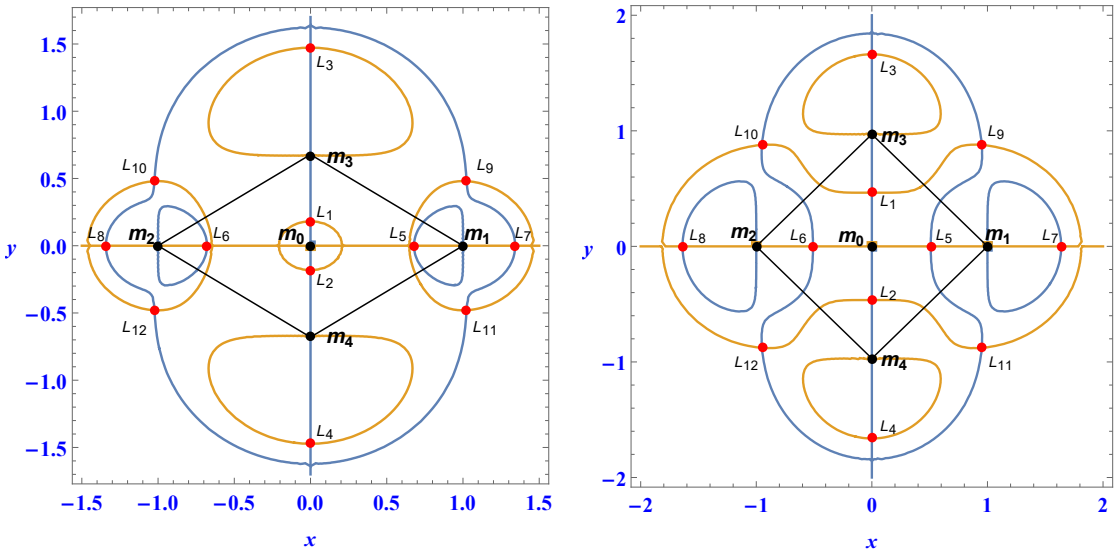

(i) (ii)

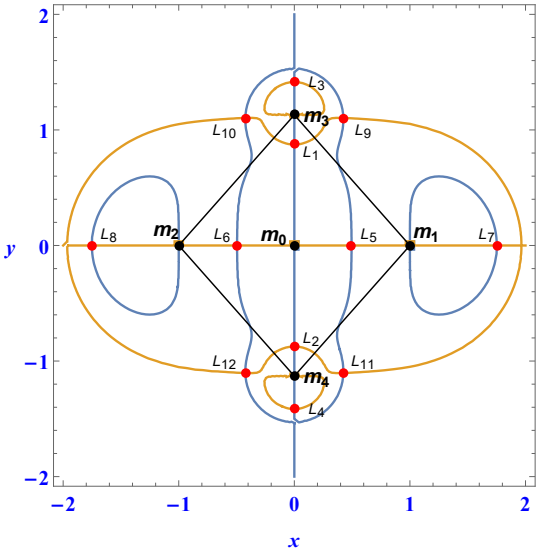

(iii)

FIGURE 4.7: 12 equilibrium points (red dots) for different values of $b = 0.67, 0.97, 1.13$ respectively and masses are given in black dots.

The matrix form of the linearized equations is

$$\begin{pmatrix} \dot{X} \\ \dot{Y} \\ \ddot{X} \\ \ddot{Y} \end{pmatrix} = \begin{pmatrix} 0 & 0 & 1 & 0 \\ 0 & 0 & 0 & 1 \\ U_{xx} & U_{xy} & 0 & 2 \\ U_{xy} & U_{yy} & -2 & 0 \end{pmatrix} \begin{pmatrix} X \\ Y \\ \dot{X} \\ \dot{Y} \end{pmatrix} \tag{4.17}$$

These equations can also be written in the following matrix form

$$\dot{\mathbf{\Psi}} = \mathcal{A}\mathbf{\Psi} \tag{4.18}$$

where

$$\dot{\mathbf{\Psi}} = \begin{pmatrix} \dot{X} \\ \dot{Y} \\ \ddot{X} \\ \ddot{Y} \end{pmatrix} \quad \text{and} \quad \mathcal{A} = \begin{pmatrix} 0 & 0 & 1 & 0 \\ 0 & 0 & 0 & 1 \\ U_{xx} & U_{xy} & 0 & 2 \\ U_{xy} & U_{yy} & -2 & 0 \end{pmatrix}. \tag{4.19}$$

The characteristic polynomial for $\mathcal{A}$ is

$$\Lambda^4 + \alpha\Lambda^2 + \beta = 0 \tag{4.20}$$

where $\alpha = 4 - U_{xx} - U_{yy}$ and $\beta = U_{xx}U_{yy} - U_{xy}^2$. Let $\Lambda^2 = \lambda$, then Equation (4.20) reduces to

$$\lambda^2 + \alpha\lambda + \beta = 0. \tag{4.21}$$

Now in order for a Lagrange point to be linearly stable to a small perturbation, all four roots, Λ of Equation (4.20) must be purely imaginary. Thus in turn, implies that the two roots of Equation (4.21) must be real and negative.

$$\lambda_{\pm} = \frac{-\alpha \pm \sqrt{\alpha^2 - 4\beta}}{2} \tag{4.22}$$

For $\lambda_{\pm} < 0$, we must have:

$$(i)\ \alpha > 0 \ \text{ and } \ 0 < \beta < \frac{\alpha^2}{4},$$

or

$$(ii)\ \ \alpha > 0 \ \text{ and } \ \alpha^2 - 4\beta = 0.$$

We will numerically identify regions when either condition (i) or condition (ii) is satisfied. Figure 4.8 (left to right) gives the stability region in case (i) and case

(ii) and their projections for $b = 0.67$, $b = 1$ and $b = 1.13$ are shown in Figures 4.9 and 4.10 respectively.

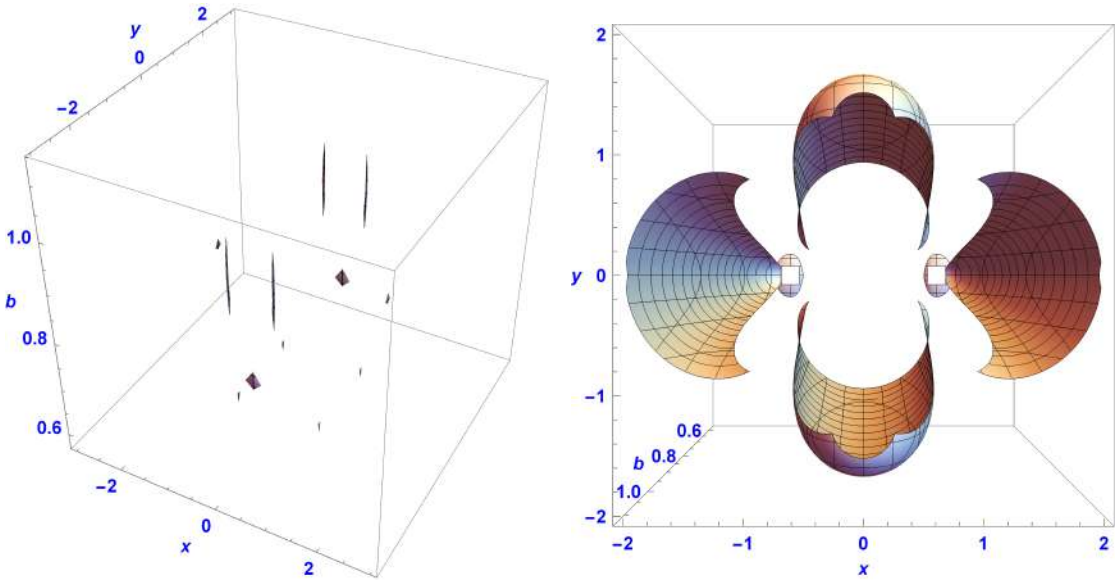

(a) (b)

FIGURE 4.8: Left to right: Shaded regions represent stability regions for case (i) and (ii) respectively

We have tested a large number of equilibrium points for many values of b and found all of them unstable. In other words the intersection of $U_x = 0$ and $U_y = 0$ within $\{\alpha > 0 \text{ and } 0 < \beta < \alpha^2/4\}$ and $\{\alpha > 0 \text{ and } \alpha^2 - 4\beta = 0\}$ is an empty set. Representative examples are given in Tables 4.1 to 4.3.

TABLE 4.1: Equilibrium points and stability analysis for $b = 0.67$

Equilibrium Point	Eigenvalues	stability
$L_{1,2} = (\pm 1.342241, 0)$	$\pm 1.660648, \pm 1.525769i$	unstable
$L_{3,4} = (\pm 0.678932, 0)$	$\pm 1.943106, \pm 1.168505i$	unstable
$L_{5,6} = (0, \pm 1.472145)$	$\pm 1.218669, \pm 1.351617i$	unstable
$L_{7,8} = (0, \pm 0.180864)$	$\pm 6.347782, \pm 4.5925990i$	unstable
$L_{9,10,11,12} = (\pm 1.023953, \pm 0.479505)$	$\mp 0.913372 \pm 0.998959i$	unstable

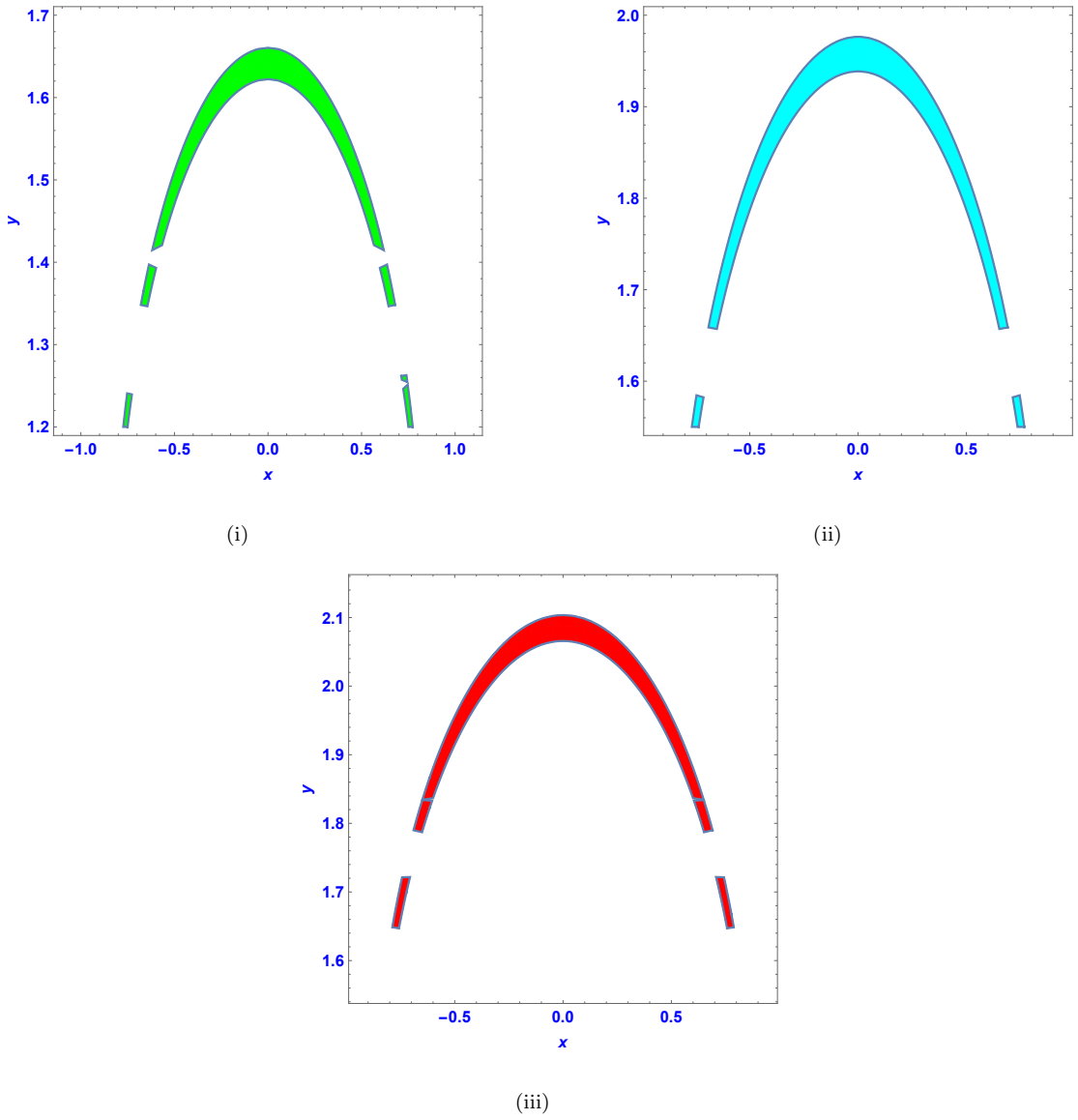

FIGURE 4.9: Projection of stability regions for fixed values of the parameter $b = 0.67,\ 1,\ 1.13$.

TABLE 4.2: Equilibrium points and stability analysis for $b = 0.97$

Equilibrium Point	Eigenvalues	stability
$L_{1,2} = (\pm 1.637980, 0)$	$\pm 1.480313, \pm 1.458732i$	unstable
$L_{3,4} = (\pm 0.509436, 0)$	$\pm 3.583445, \pm 2.544469i$	unstable
$L_{5,6} = (0, \pm 1.660744)$	$\pm 1.454216, \pm 1.451670i$	unstable
$L_{7,8} = (0, \pm 0.464669)$	$\pm 4.047077, \pm 2.908229i$	unstable
$L_{9,10,11,12} = (\pm 0.950136, \pm 0.874620)$	$\mp 0.909938 \pm 0.998607i$	unstable

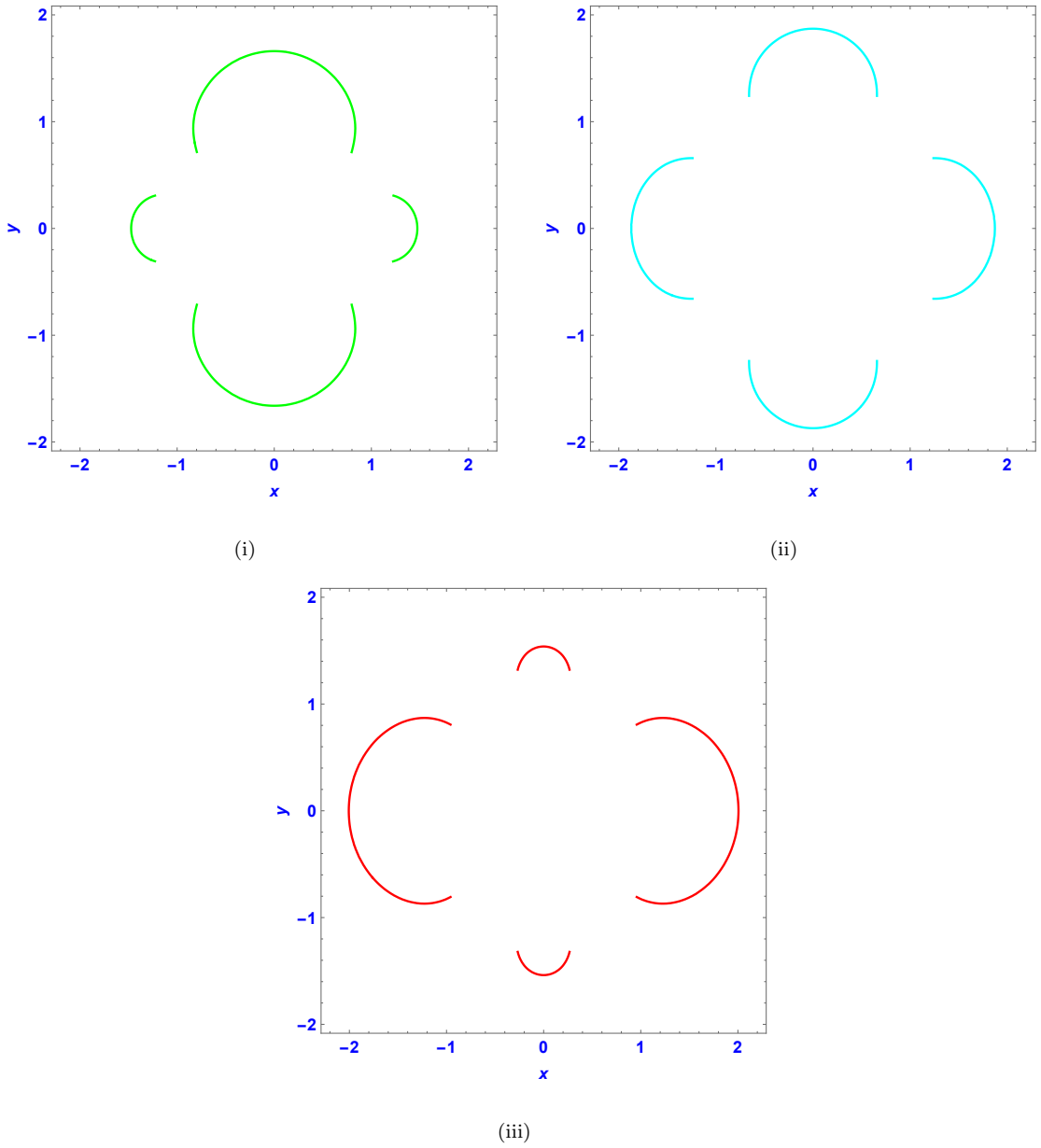

(i) (ii)

(iii)

FIGURE 4.10: Case (ii): Projection of stability regions for fixed values of the parameter $b = 0.67,\ 1,\ 1.13$

TABLE 4.3: Equilibrium points and stability analysis for $b = 1.13$

Equilibrium Point	Eigenvalues	stability
$L_{1,2} = (\pm 1.751564, 0)$	$\pm 1.5080962, \pm 1.499923i$	unstable
$L_{3,4} = (\pm 0.495101, 0)$	$\pm 4.863781, \pm 3.594754i$	unstable
$L_{5,6} = (0, \pm 1.413901)$	$\pm 1.797668, \pm 1.600502i$	unstable
$L_{7,8} = (0, \pm 0.874617)$	$\pm 2.535781, \pm 1.929722i$	unstable
$L_{9,10,11,12} = (\pm 0.423616, \pm 1.103657)$	$\mp 0.903618 \pm 0.9990127i$	unstable

4.2.2 Case-II: $m_1 = m_2 = m$, $m_3 = m_4 = \widetilde{m}$, $m_0 \neq m \neq \widetilde{m}$

In this section the equations of motion of the infinitesimal body, m_5, are derived using the Equation 4.1. When compared to the masses of the primaries, the sixth body, m_5, has a significantly smaller mass. i.e., ($m_5 << m_i$), where $i = 0,...,4$ as in Section 4.2.1, but the gravitation field has changed due to the change in the masses of the primaries. The equations will now be changed due to the change in the effective potential. As a result, the equations of motion of the m_5 in corotating coordinates x and y [114] are

$$\left.\begin{aligned} \ddot{x} - 2\dot{y} &= U_x, \\ \ddot{y} + 2\dot{x} &= U_y, \end{aligned}\right\} \tag{4.23}$$

where

$$U(x,y) = \frac{(x^2+y^2)}{2} + \frac{m_0}{r_{50}} + m\left(\frac{1}{r_{51}} + \frac{1}{r_{52}}\right) + \widetilde{m}\left(\frac{1}{r_{53}} + \frac{1}{r_{54}}\right) \tag{4.24}$$

is the effective potential, where the mutual distances are

$$\left.\begin{aligned} r_{50} &= \sqrt{x^2+y^2} \quad , \quad r_{51} = \sqrt{(x-a)^2+y^2}, \\ r_{52} &= \sqrt{(x+a)^2+y^2} \quad , \quad r_{53} = \sqrt{x^2+(y-b)^2}, \\ r_{54} &= \sqrt{x^2+(y+b)^2}. \end{aligned}\right\} \tag{4.25}$$

The effective potential is shown in Figures 4.13 and 4.14 for the four different cases of rhomboidal restricted 6-body problem. We define the first Jacobian type integral constant by

$$C = \frac{1}{2}\left(\dot{x}^2 + \dot{y}^2\right) - U. \tag{4.26}$$

By demonstrating that $\dot{C}(x,y) = 0$, it is now straight forward to establish that $C(x,y)$ is the first integral of motion of system (4.23). The Equation (4.26) shows

that $C + U \geq 0$. Then $U = -C$ will establish a boundary between both the allowed and forbidden regions and $U = -C$ presents the zero velocity curves for various values of C.

4.2.2.1 The Spheres of Influence

Spheres of influence or gravitational spheres of influence are areas surrounding celestial objects where other celestial objects experience greatest pull and can become satellites of the huge celestial object relative to its mass; these regions are also known as Hill's regions, after *George William Hill*. The zero velocity curves (ZVC) are the contours of the Jacobian constant C as mentioned above, and they are available in Figure 4.11 (i) for $a = 0.68$ and $b = 0.58$, (ii) for $a = 0.68$ and $b = 0.60$, and in Figure 4.12 (i) for $a = 0.78$ and $b = 0.67$, (ii) for $a = 0.62$ and $b = 0.80$.

The Hill's regions are tightly packed circular regions surrounding primaries; Figure 4.11 and 4.12 show that the spheres of influence shrink as the particle mass decreases and vice versa.

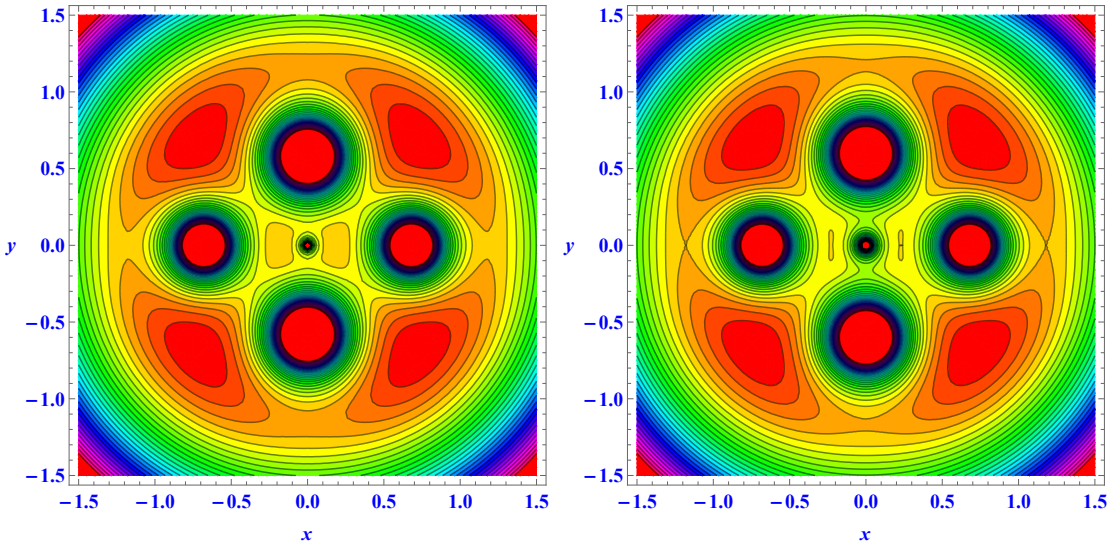

(i) (ii)

FIGURE 4.11: The evolution of zero velocity curves. (i) $a = 0.68$ and $b = 0.58$, (ii) $a = 0.68$ and $b = 0.60$

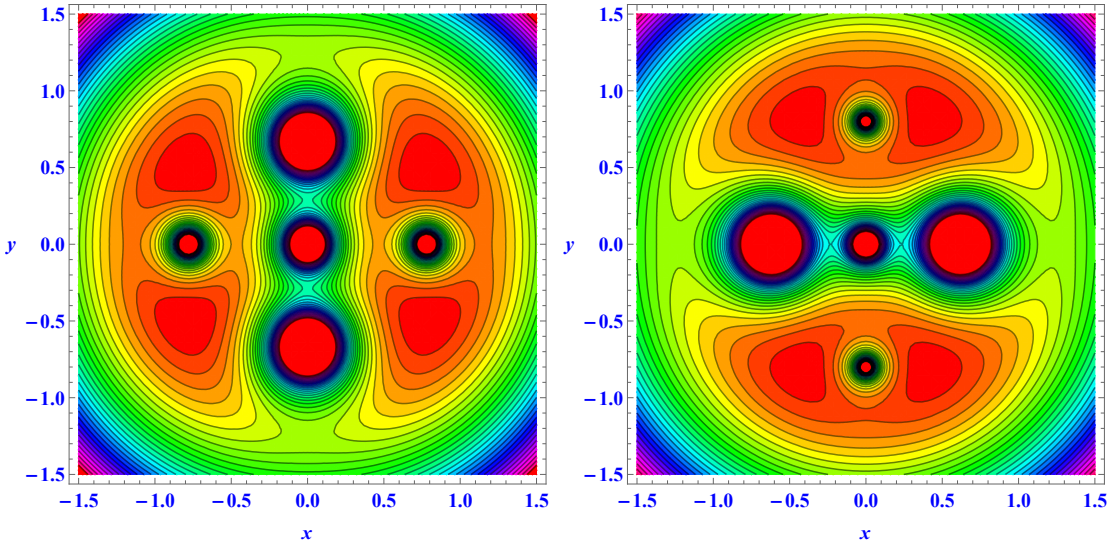

(i) (ii)

FIGURE 4.12: The evolution of zero velocity curves. (i) $a = 0.78$ and $b = 0.67$, (ii) $a = 0.62$ and $b = 0.80$

Figures 4.13 (i) $a = 0.68$ and $b = 0.58$, (ii) $a = 0.68$ and $b = 0.60$ illustrate the effective potentials, while Figures 4.14 (i) $a = 0.78$ and $b = 0.67$, (ii) $a = 0.62$ and $b = 0.80$ where the closely packed circular regions around the potentials of each mass, which resemble chimneys, can be seen clearly.

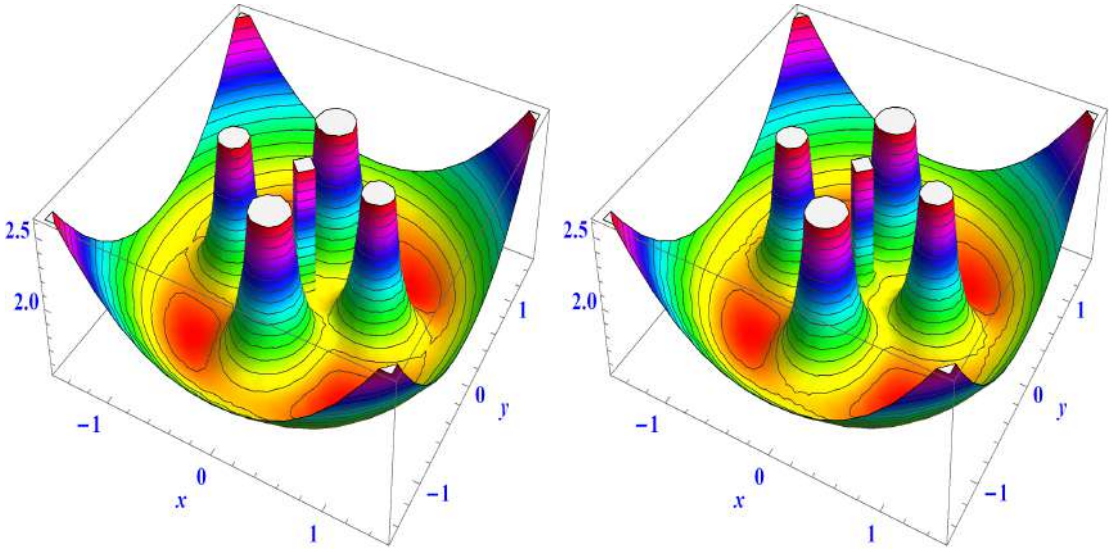

(i) (ii)

FIGURE 4.13: The effective potential.(i) $a = 0.68$ and $b = 0.58$, (ii) $a = 0.68$ and $b = 0.60$

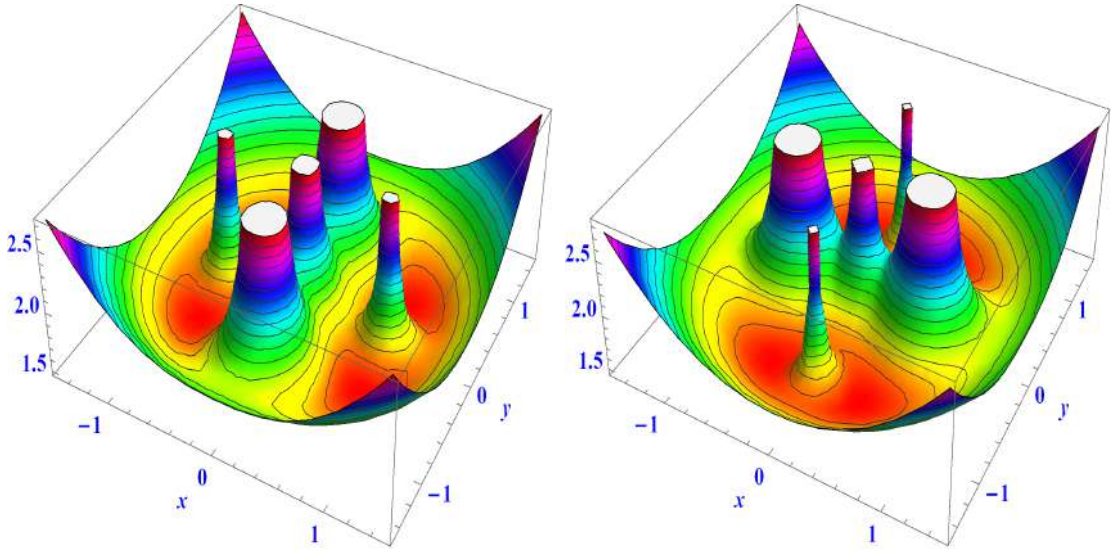

(i) (ii)

FIGURE 4.14: The effective potential. (i) $a = 0.78$ and $b = 0.67$, (ii) $a = 0.62$ and $b = 0.80$

The permissible regions of motion for the infinitesimal mass m_5 are shown in Figures 4.15−4.26 for each of the four cases for different values of mass parameters a and b. Six figures for each of the four cases show the forbidden (shaded) and permissible (white) regions of motion of m_5 for various values of C.

The regions of motion that are permitted have the same behaviour in all four cases, i.e., the permissible region increases as the value of C decreases. It has also been numerically confirmed that the permissible regions of motion are connected and are around the primaries for higher values of C, i.e., at $C = -1.66,\ -1.97,\ -2.47,\ -2.59,$ and -3.49. The permissible motion regions are mainly around the four primary and are isolated from one another at $C = -1.78$, and for the above values of C the motion of m_5 will be bounded around any of the four primaries and will not be able to escape form there normally. The permitted regions become totally detached when $C \leq -1.58$, and the infinitesimal mass m_5 may freely move in the gravitational field of the primaries.

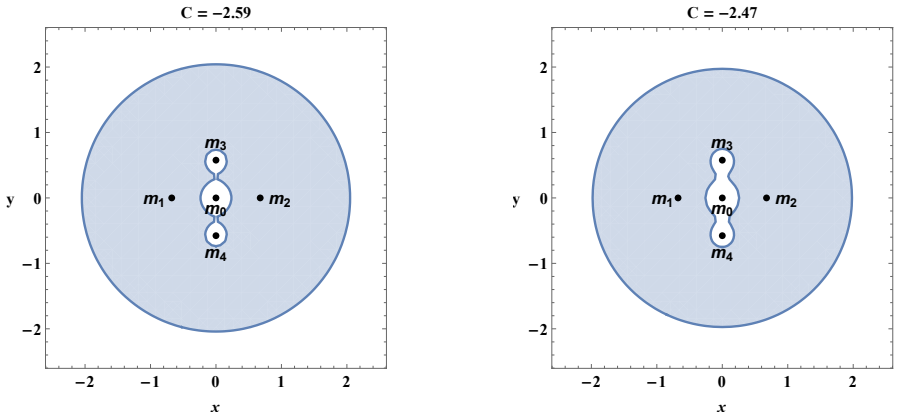

(i) (ii)

FIGURE 4.15: The regions of motion (white region) when $a = 0.68$ and $b = 0.58$ (i) $C = -2.59$ (ii) $C = -2.47$

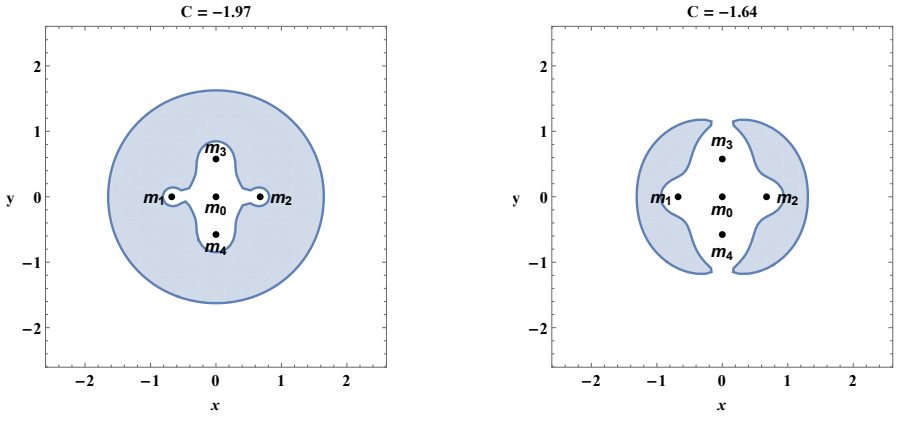

(i) (ii)

FIGURE 4.16: The regions of motion (white region) when $a = 0.68$ and $b = 0.58$ (i) $C = -1.97$ (ii) $C = -1.64$

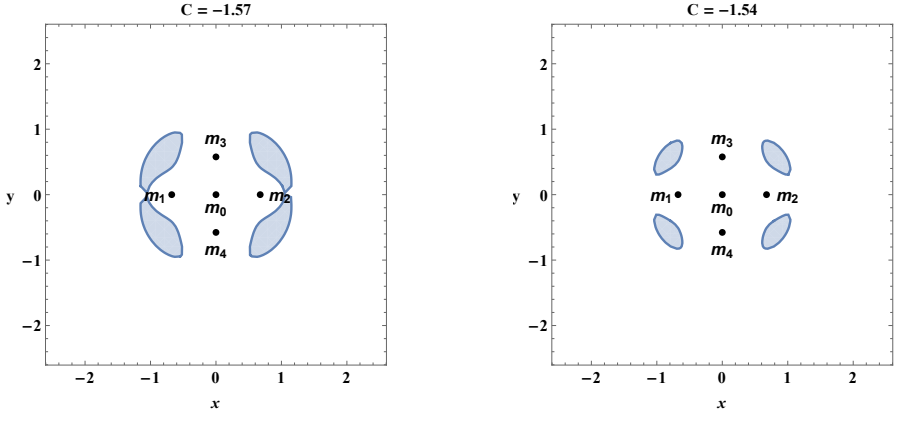

(i) (ii)

FIGURE 4.17: The regions of motion (white region) when $a = 0.68$ and $b = 0.58$ (i) $C = -1.57$ (ii) $C = -1.54$

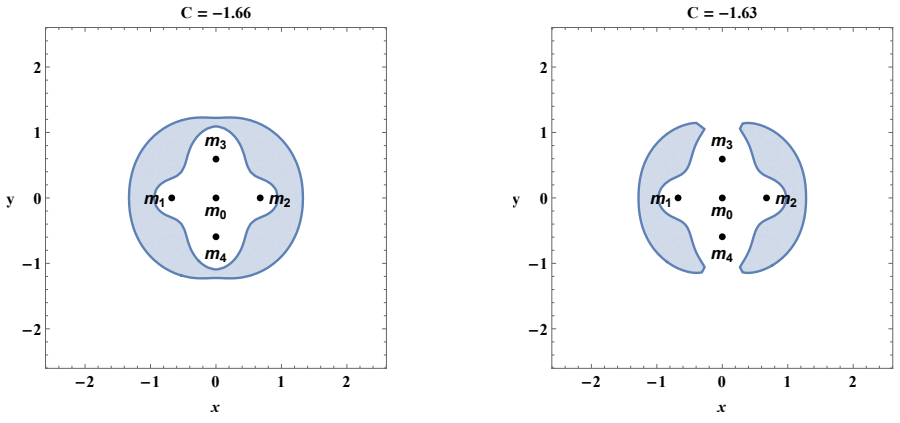

(i) (ii)

FIGURE 4.18: The regions of motion (white region) when $a = 0.68$ and $b = 0.60$ (i) $C = -1.66$ (ii) $C = -1.63$

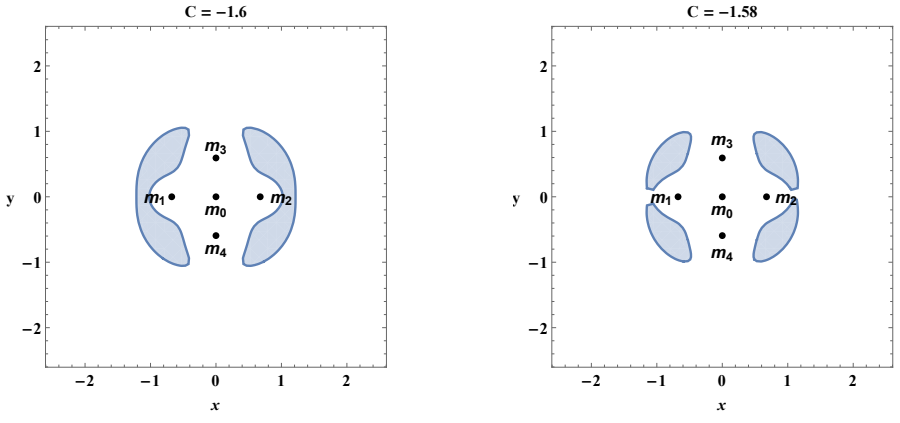

(i) (ii)

FIGURE 4.19: The regions of motion (white region) when $a = 0.68$ and $b = 0.60$ (i) $C = -1.6$ (ii) $C = -1.58$

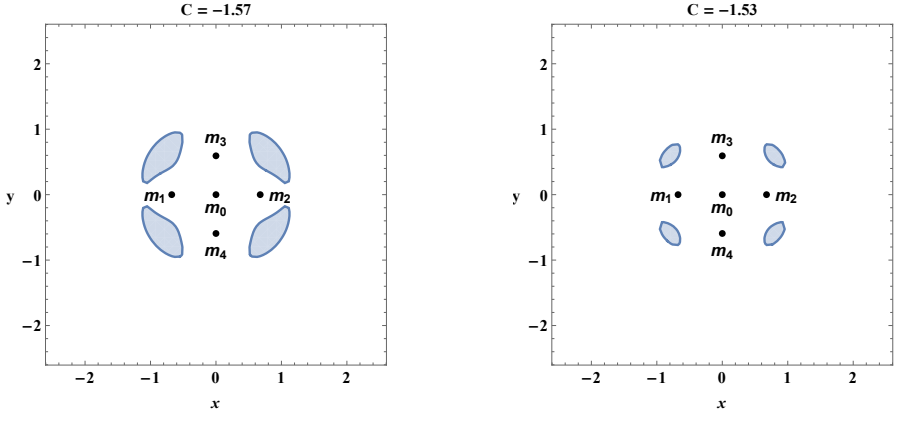

(i) (ii)

FIGURE 4.20: The regions of motion (white region) when $a = 0.68$ and $b = 0.60$ (i) $C = -1.57$ (ii) $C = -1.53$

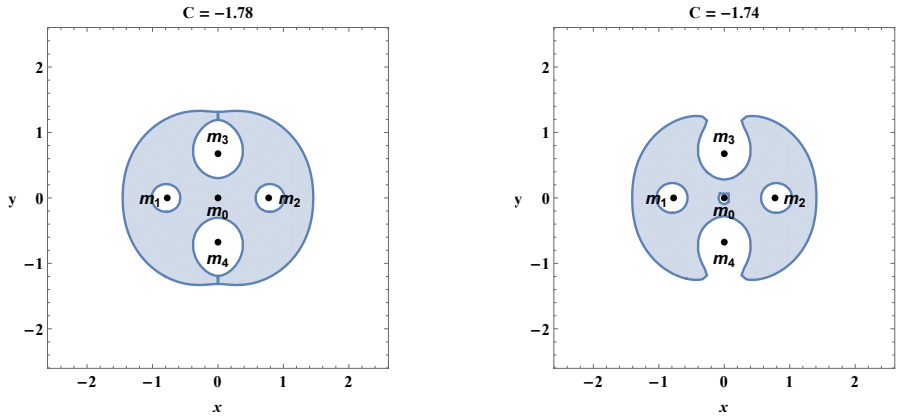

(i) (ii)

FIGURE 4.21: The regions of motion (white region) when $a = 0.78$ and $b = 0.68$ (i) $C = -1.78$ (ii) $C = -1.74$

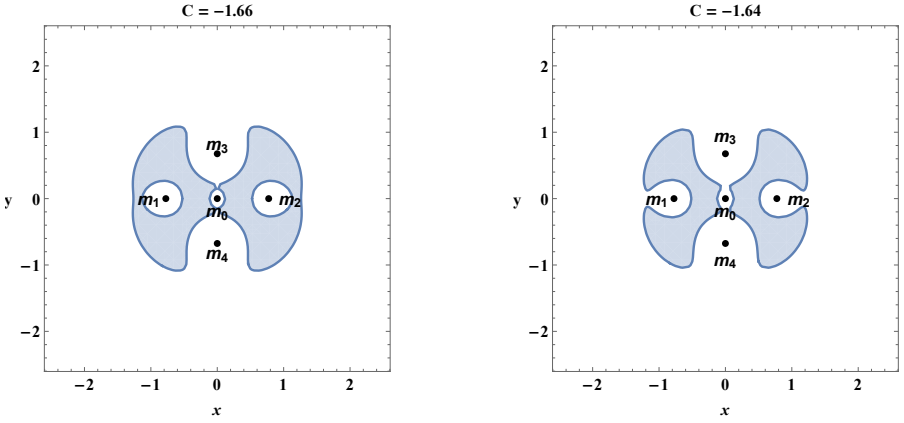

(i) (ii)

FIGURE 4.22: The regions of motion (white region) when $a = 0.78$ and $b = 0.68$ (i) $C = -1.66$ (ii) $C = -1.64$

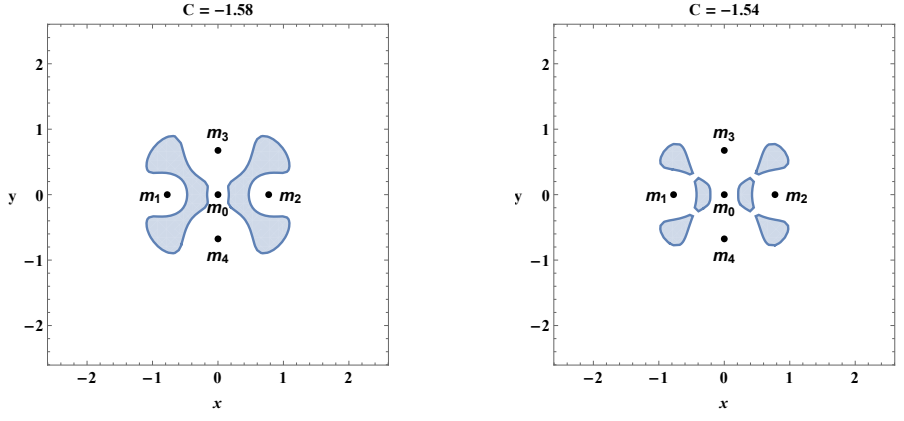

(i) (ii)

FIGURE 4.23: The regions of motion (white region) when $a = 0.78$ and $b = 0.68$ (i) $C = -1.58$ (ii) $C = -1.54$

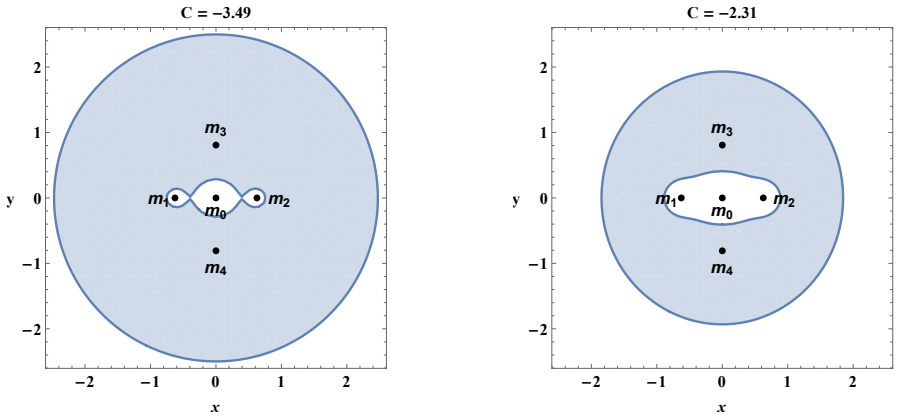

(i) (ii)

FIGURE 4.24: The regions of motion (white region) when $a = 0.62$ and $b = 0.80$ (i) $C = -3.49$ (ii) $C = -2.31$

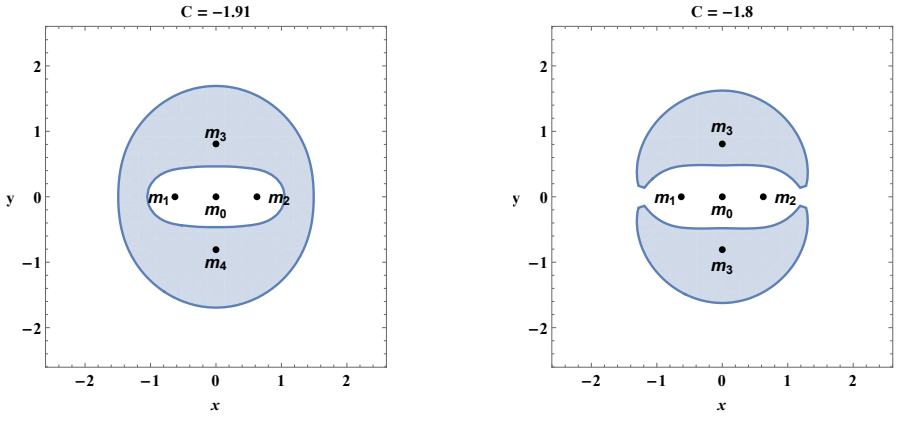

(i) (ii)

FIGURE 4.25: The regions of motion (white region) when $a = 0.62$ and $b = 0.80$ (i) $C = -1.91$ (ii) $C = -1.80$

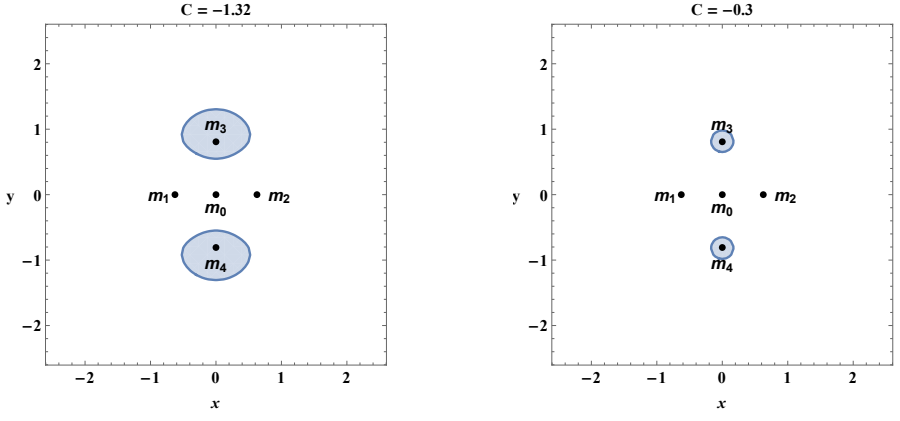

(i) (ii)

FIGURE 4.26: The regions of motion (white region) when $a = 0.62$ and $b = 0.80$ (i) $C = -1.32$ (ii) $C = -0.30$

4.2.2.2 Equilibrium solutions

All rates of change should be zero for equilibrium solutions, hence the right hand side of the system in (4.23) can be set to zero, i.e., $U_x = 0$ and $U_y = 0$ and the solution of resulting equations will give the problem's equilibrium solutions . The U_x and U_y are

$$U_x = x - \frac{m_0 x}{(y^2+x^2)^{3/2}} - m\left(\frac{x-a}{((x-a)^2+y^2)^{3/2}} + \frac{a+x}{((a+x)^2+y^2)^{3/2}}\right) - \widetilde{m}\left(\frac{x}{((y-b)^2+x^2)^{3/2}} + \frac{x}{((b+y)^2+x^2)^{3/2}}\right), \tag{4.27}$$

$$U_y = y - \frac{m_0 y}{(y^2+x^2)^{3/2}} - m\left(\frac{y}{((x-a)^2+y^2)^{3/2}} + \frac{y}{((a+x)^2+y^2)^{3/2}}\right) - \widetilde{m}\left(\frac{y-b}{((y-b)^2+x^2)^{3/2}} + \frac{b+y}{((b+y)^2+x^2)^{3/2}}\right). \tag{4.28}$$

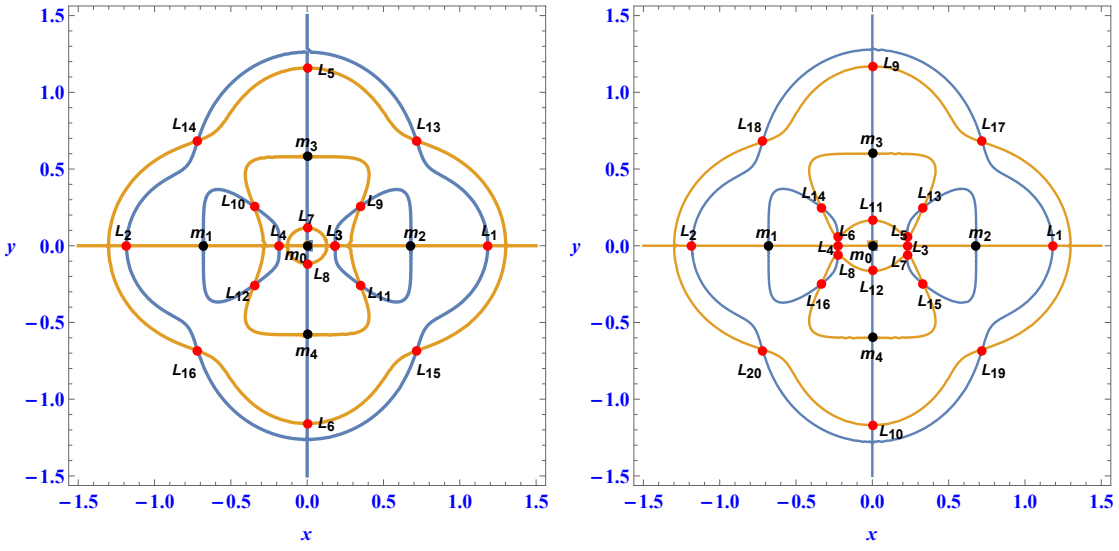

(i) (ii)

FIGURE 4.27: The equilibrium points (red dots) and masses (black dots) when (i) $a = 0.68$ and $b = 0.58$, (ii) $a = 0.68$ and $b = 0.60$

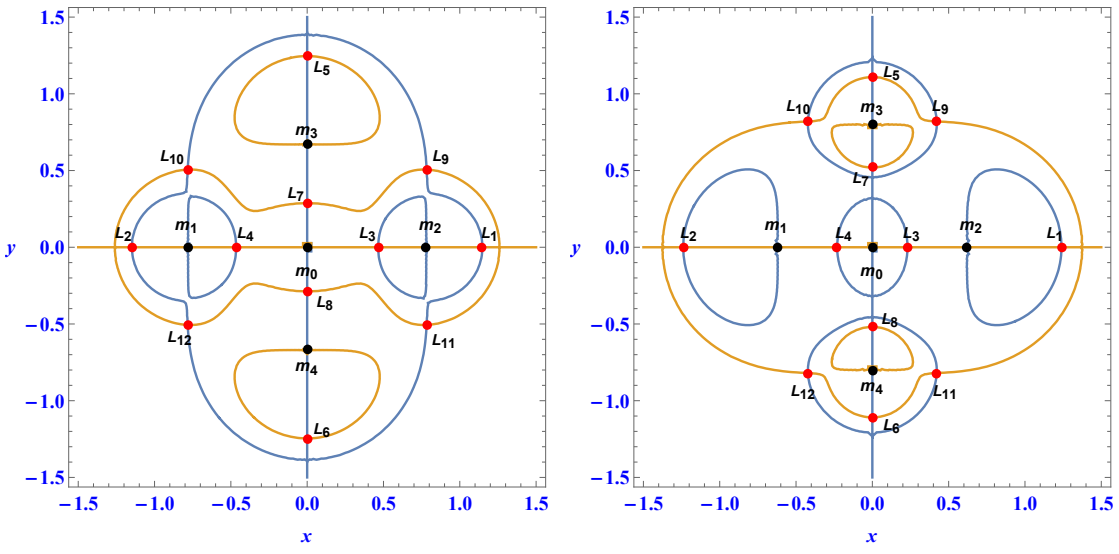

(i) (ii)

FIGURE 4.28: The equilibrium points (red dots) and masses (black dots) when (i) $a = 0.78$ and $b = 0.67$, (ii) $a = 0.62$ and $b = 0.80$

We considered four cases with different values of a and b that show a significant change in the number and location of equilibrium points, namely $a = 0.68$ and $b = 0.58$ for case-I, $a = 0.68$ and $b = 0.60$ for case-II, $a = 0.78$ and $b = 0.67$ for case-III and $a = 0.62$ and $b = 0.80$ for case-IV. The corresponding equilibrium points can be seen in Figure 4.27 and 4.28.

The black dots indicate masses and are represented by the symbol m_i; $i = 0, 1, 2, 3, 4$, the red dots represent equilibrium points and are denoted by L_i; $i = 1, 2, ..., 20$. There are 16 equilibrium points in case-I, 20 equilibrium points in case-II and 12 equilibrium points in both case-III and case-IV (see Figure 4.27 and 4.28).

4.2.2.3 Equilibrium Solutions: on the Coordinate Axes

We shall limit our investigation to the first quadrant, $x \geq 0$ and $y \geq 0$, because the potential given in Equation (4.23) is unchanged under the symmetry $(x, -y)$, $(-x, y)$, and $(-x, -y)$. To determine the presence and number of equilibrium solutions on the y-axis, we set $x = 0$ and then write Equations (4.27) and (4.28)

as

$$\left.\begin{aligned} U_x &= 0, \\ U_y &= y - \frac{m_0 y}{(y^2)^{3/2}} - \frac{2my}{(a^2+y^2)^{3/2}} \\ &\quad - \widetilde{m}\left(\frac{y-b}{((y-b)^2)^{3/2}} + \frac{b+y}{((b+y)^2)^{3/2}}\right). \end{aligned}\right\} \tag{4.29}$$

The y-axis is subdivided into $0 < y < b$ and $y > b$ to figure out $U_y = 0$ for equilibrium solutions. $y = b$ means collisions of m_5 with m_3 or m_4 from inside. We will not discuss collisions cases here.

$0 < y < b$

The Equation (4.29) is rewritten as

$$f_1(y) = y - \frac{m_0}{y^2} - \frac{2my}{(a^2+y^2)^{3/2}} - \tilde{m}\left(\frac{1}{(y-b)^2} + \frac{1}{(b+y)^2}\right). \tag{4.30}$$

For $y \in (0, b)$ and $b \in (0.5, 1)$, when $y \approx 0$, $f_1(y) < 0$ and when $y \approx b$, $f_1(y) > 0$, thus the mean value theorem implies that $f_1(y)$ has at least one zero when $y \in (0, b)$.

To verify the existence and uniqueness of equilibrium solutions inside the interval $(0, b)$, we take derivative of Equation (4.30).

$$\begin{aligned} f'_1(y) &= 1 + \frac{2m_0}{y^3} + 2m\left(\frac{3y^2}{(a^2+y^2)^{5/2}} - \frac{1}{(a^2+y^2)^{3/2}}\right) \\ &\quad + 2\tilde{m}\left(\frac{1}{(b+y)^3} + \frac{1}{(y-b)^3}\right) \end{aligned} \tag{4.31}$$

$(a^2 + y^2)^{3/2}$ in Equation (4.31) is the only term that can make the derivative negative for $y \in (0, b)$, as a result, $f'_1(y) > 0$, indicates that the equilibrium points in the interval $(0, b)$ exist and are unique.

y > b

When $y > b$, the Equation (4.29) is rewritten as

$$f_2(y) = y - \frac{m_0}{y^2} - \frac{2my}{(a^2+y^2)^{3/2}} - \tilde{m}\left(\frac{1}{(y-b)^2} + \frac{1}{(b+y)^2}\right). \tag{4.32}$$

For $y \in (b, \infty)$ and $b \in (0.5, 1)$, when $y \approx b$, $f_2(y) < 0$ and when $y \approx \infty$,$f_2(y) > 0$, thus mean value theorem implies that $f_2(y)$ has at least one zero when $y \in (b, \infty)$.

The derivative of Equation (4.32) with respect to y is

$$\begin{aligned} f'_2(y) &= 1 + \frac{2m_0}{y^3} + 2m\left(\frac{3y^2}{(a^2+y^2)^{5/2}} - \frac{1}{(a^2+y^2)^{3/2}}\right) \\ &\quad +2\tilde{m}\left(\frac{1}{(b+y)^3} + \frac{1}{(y-b)^3}\right) \end{aligned} \tag{4.33}$$

The equilibrium solution's uniqueness for $y > b$ can be easily proved using the same technique as for $0 < y < b$.

Then there are total 16 equilibrium points for case-I and out of which $L_{5,6,7,8}$ are along y axis while $L_{1,2,3,4}$ are on x axis; Similarly for case-II, III and IV, there are four equilibrium points on each coordinate axis for distinct values of a and b but the number of equilibrium points is different for other cases which can be seen in Figures 4.27 and 4.28.

4.2.2.4 Equilibrium Solutions: Off the Coordinate Axes

The mass parameters a and b, which we have numerically confirmed, determine the number and location of the equilibrium points, which is illustrated in Figures 4.27 and 4.28.

For case-I, there are eight off-coordinate axis equilibrium points; for case-II, there are 12 off-coordinate axis equilibrium points, the majority of which are clustered

around the central mass m_0. Cases III and IV contain 4 equilibrium points that cluster around m and $\widetilde{m}$ off the coordinate axis.

4.2.2.5 Stability Analysis

We represent the location of an equilibrium point in our problem by the coordinates (x, y), and consider a small displacement from the equilibrium point to be (X, Y) in order to linearize around the equilibrium point, then the new location of the equilibrium points will be $(x + X, y + Y)$. The system in Equations (4.23) is subjected to Taylor series expansion, yielding the following set of linearized equations.

$$\ddot{X} - 2\dot{Y} = XU_{xx} + YU_{xy}, \tag{4.34}$$

$$\ddot{Y} + 2\dot{X} = XU_{xy} + YU_{yy}. \tag{4.35}$$

The matrix form of the linearized equations is

$$\begin{pmatrix} \dot{X} \\ \dot{Y} \\ \ddot{X} \\ \ddot{Y} \end{pmatrix} = \begin{pmatrix} 0 & 0 & 1 & 0 \\ 0 & 0 & 0 & 1 \\ U_{xx} & U_{xy} & 0 & 2 \\ U_{xy} & U_{yy} & -2 & 0 \end{pmatrix} \begin{pmatrix} X \\ Y \\ \dot{X} \\ \dot{Y} \end{pmatrix} \tag{4.36}$$

Let

$$\dot{\mathbf{\Psi}} = \begin{pmatrix} \dot{X} \\ \dot{Y} \\ \ddot{X} \\ \ddot{Y} \end{pmatrix} \quad \text{and} \quad \mathcal{A} = \begin{pmatrix} 0 & 0 & 1 & 0 \\ 0 & 0 & 0 & 1 \\ U_{xx} & U_{xy} & 0 & 2 \\ U_{xy} & U_{yy} & -2 & 0 \end{pmatrix}. \tag{4.37}$$

The Equation in (4.36) can be written as

$$\dot{\mathbf{\Psi}} = \mathcal{A}\mathbf{\Psi} \tag{4.38}$$

From $\mathcal{A}$, the characteristic polynomial is

$$\Lambda^4 + \alpha\Lambda^2 + \beta = 0, \tag{4.39}$$

where $\alpha = 4 - U_{xx} - U_{yy}$ and $\beta = U_{xx}U_{yy} - U_{xy}^2$.

Let $\Lambda^2 = \lambda$, then equation (4.39) reduces to

$$\lambda^2 + \alpha\lambda + \beta = 0. \tag{4.40}$$

For an Equilibrium point to be linearly stable under a slight disturbance, all four roots of Equation (4.39) must be completely imaginary. As a result, the two roots of Equation (4.40)

$$\lambda_{\pm} = \frac{-\alpha \pm \sqrt{\alpha^2 - 4\beta}}{2} \tag{4.41}$$

must be real and negative. For $\lambda_{\pm} < 0$, we must have:

$$(i)\ \alpha > 0 \ \text{ and } \ 0 < \beta < \alpha^2/4, \text{or}$$
$$(ii)\ \ \alpha > 0 \ \text{ and } \ \alpha^2 - 4\beta = 0.$$

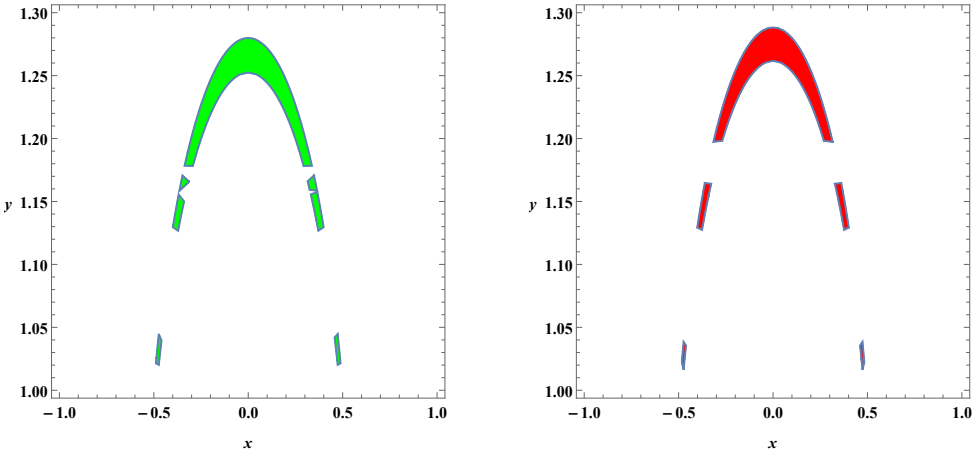

(i) (ii)

FIGURE 4.29: Condition(i): Projection of stability regions (i) $b = 0.58$ and $a = 0.68$; (ii) $b = 0.60$ and $a = 0.68$.

The regions of stability when either condition (i) or (ii) holds true have been determined and presented in Figures 4.29–4.32.

The stability areas corresponding to the four cases for different values of a and b are shown in Figures 4.33−4.34, where b is fixed at 0.58, 0.60, 0.67, and 0.80, and the regions are projected across the whole domain of the mass parameter a, i.e., $0.5 < a < 1$. We investigated the stability of the equilibrium points found in the preceding section for each of the four different cases, and many off-coordinate stable equilibrium points were discovered; the results are reported in Tables 4.4−4.7.

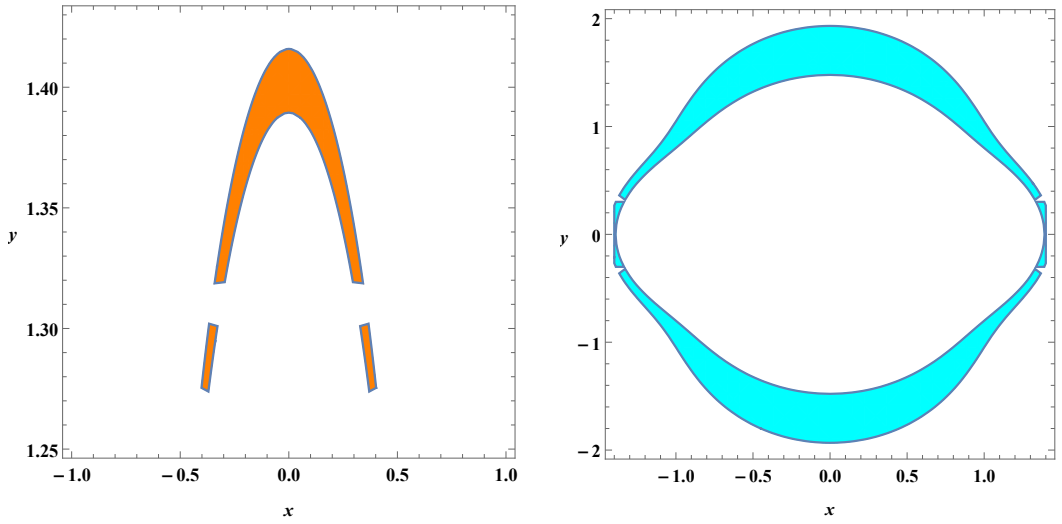

(i) (ii)

FIGURE 4.30: Condition(i): Projection of stability regions (i) $b = 0.67$ and $a = 0.78$; (ii) $b = 0.80$ and $a = 0.62$.

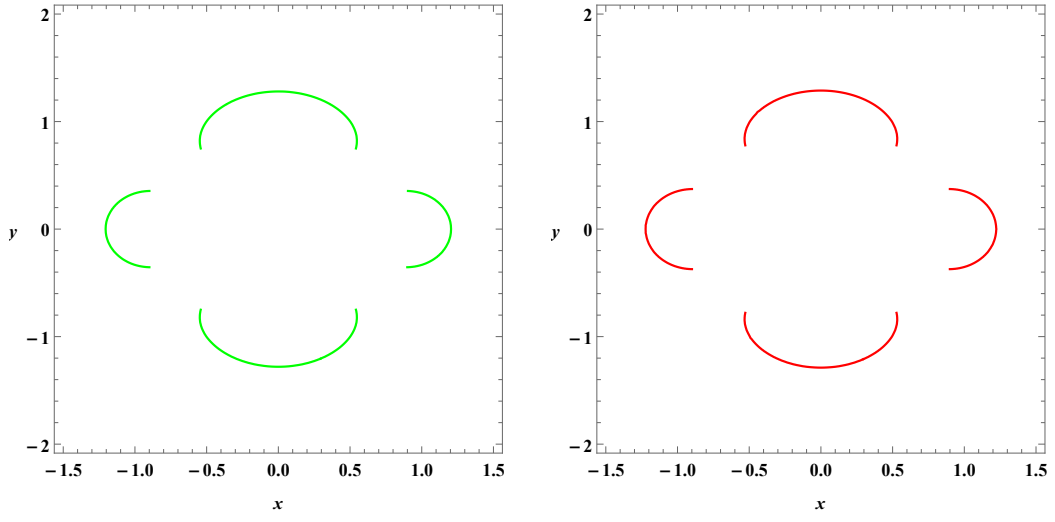

(i) (ii)

FIGURE 4.31: Condition(ii): Projection of stability regions (i) $b = 0.58$ and $a = 0.68$; (ii) $b = 0.60$ and $a = 0.68$.

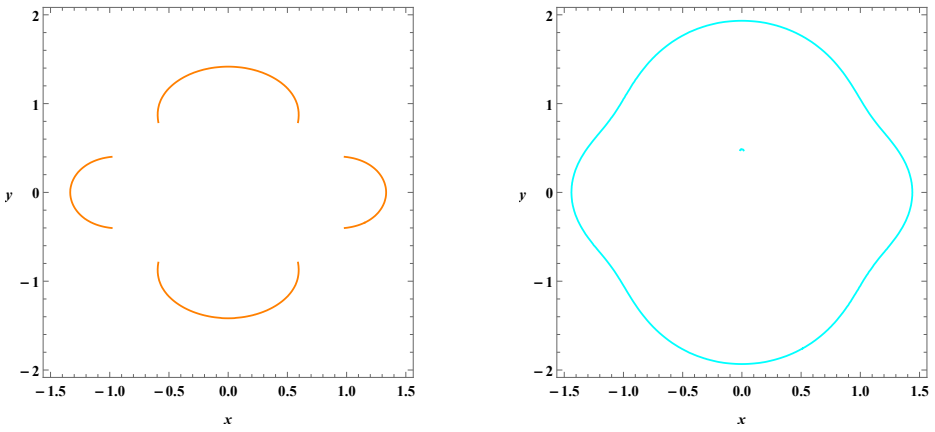

(i) (ii)

FIGURE 4.32: Condition(ii): Projection of stability regions (i) $b = 0.67$ and $a = 0.78$; (ii) $b = 0.80$ and $a = 0.62$.

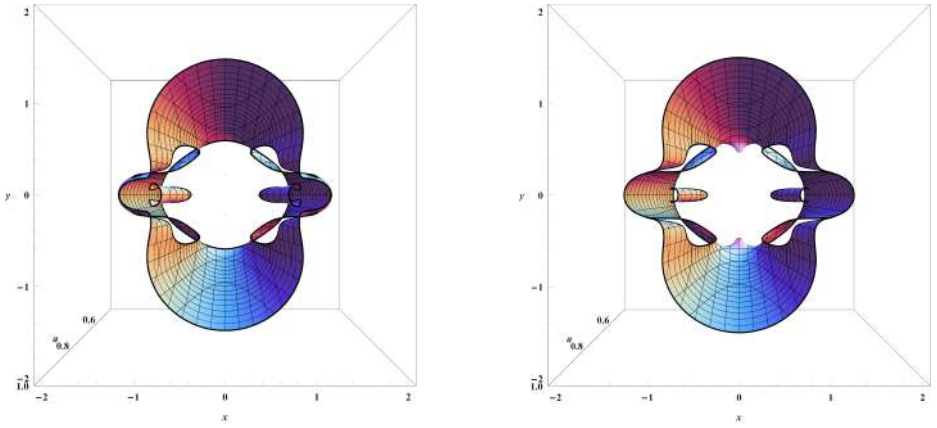

(i) (ii)

FIGURE 4.33: Stability regions (shaded) (i) $b = 0.58$ and $0.5 < a < 1$; (ii) $b = 0.60$ and $0.5 < a < 1$.

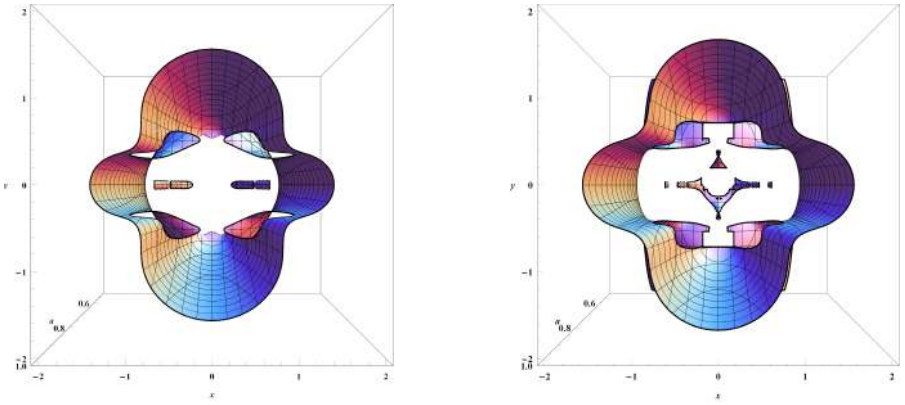

(i) (ii)

FIGURE 4.34: Stability regions (shaded) (i) $b = 0.67$ and $0.5 < a < 1$; (ii) $b = 0.80$ and $0.5 < a < 1$.

TABLE 4.4: Equilibrium points, Eigenvalues and stability status when $b = 0.58$ and $a = 0.68$

On the Coordinate Axis		
Equilibrium Point	Eigenvalues	Stability
$L_{1,2} = (\pm 1.183771, 0)$	$\pm 0.067596, \pm 2.670587i$	unstable
$L_{3,4} = (\pm 0.183968, 0)$	$\pm 7.279086, \pm 10.945510i$	unstable
$L_{5,6} = (0, \pm 1.158556)$	$\pm 0.500651, \pm 2.791424i$	unstable
$L_{7,8} = (0, \pm 0.116046)$	$\pm 15.176878, \pm 21.692684i$	unstable
Off the Coordinate Axis		
Equilibrium Point	Eigenvalues	Stability
$L_{9,10,11,12} = (0.347976, \pm 0.256131)$	$\pm 1.138065i, \pm 3.593599i$	stable
$L_{13,14,15,16} = (\pm 0.716623, \pm 0.684335)$	$\mp 0.479573i, \pm 2.668968i$	stable

TABLE 4.5: Equilibrium points, Eigenvalues and stability status when $b = 0.60$ and $a = 0.68$

On the Coordinate Axis		
Equilibrium Point	Eigenvalues	Stability
$L_{1,2} = (\pm 1.183772, 0)$	$\pm 0.209362, \pm 2.693806i$	unstable
$L_{3,4} = (\pm 0.228309, 0)$	$\pm 5.091753, \pm 8.027477i$	unstable
$L_{9,10} = (0, \pm 1.169283)$	$\pm 0.500956, \pm 2.792577i$	unstable
$L_{11,12} = (0, \pm 0.164938)$	$\pm 8.849253, \pm 12.907057i$	unstable
Off the Coordinate Axis		
Equilibrium Point	Eigenvalues	Stability
$L_{5,6,7,8} = (0.228064, \pm 0.058906)$	$\pm 4.765442, \pm 7.656460i$	unstable
$L_{13,14,15,16} = (\pm 0.334768, \pm 0.250108)$	$\mp 1.088025i, \pm 3.645851i$	stable
$L_{17,18,19,20} = (\pm 0.716623, \pm 0.684335)$	$\mp 0.508226i, \pm 2.666074i$	stable

.

TABLE 4.6: Equilibrium points Eigenvalues and stability status when $b = 0.67$ and $a = 0.78$

On the Coordinate Axis		
Equilibrium Point	Eigenvalues	Stability
$L_{1,2} = (\pm 1.147893, 0)$	$\pm 1.125396, \pm 3.220510i$	unstable
$L_{3,4} = (\pm 0.465536, 0)$	$\pm 1.381845, \pm 3.742671i$	unstable
$L_{5,6} = (0, \pm 1.245704)$	$\pm 0.715462, \pm 2.911764i$	unstable
$L_{7,8} = (0, \pm 0.287148)$	$\pm 2.273632, \pm 4.422842i$	unstable
Off the Coordinate Axis		
Equilibrium Point	Eigenvalues	Stability
$L_{9,10,11,12} = (\pm 0.782825, \pm 0.505983)$	$\mp 0.673476i, \pm 2.735112i$	stable

TABLE 4.7: Equilibrium points, Eigenvalues and stability status when $b = 0.80$ and $a = 0.62$

On the Coordinate Axis		
Equilibrium Point	Eigenvalues	Stability
$L_{1,2} = (\pm 1.239106, 0)$	$\pm 0.646502, \pm 2.834110i$	unstable
$L_{3,4} = (\pm 0.230153, 0)$	$\pm 9.177227, \pm 13.194850i$	unstable
$L_{5,6} = (0, \pm 1.108360)$	$\pm 3.715368, \pm 3.365771i$	unstable
$L_{7,8} = (0, \pm 0.519657)$	$\pm 2.864727, \pm 3.088526i$	unstable
Off the Coordinate Axis		
Equilibrium Point	Eigenvalues	Stability
$L_{9,10,11,12} = (\pm 0.421763, \pm 0.819726)$	$\mp 2.317673, \pm 3.0801580i$	unstable

4.3 Summary

The motion of the test particle, as compared to primaries, is discussed in this chapter. The test particle, m_5 moves under the gravitational field of primaries, and during its course it experiences some points that may or may not hold it. These points are called equilibrium points, which may be stable or unstable. Equilibrium points for both of the central configurations, which have been discussed in the previous chapter, were found and tested for their possible stability. It has been found that for the first case there are always 12 equilibrium points, and all are proved to be unstable. The second case yielded 16, 20 and 12 equilibrium points for different values of a and b.

When:

- $a = 0.68$ and $b = 0.58$ then there are eight off the coordinated axes stable equilibrium points;
- $a = 0.68$ and $b = 0.60$ then there are also eight off the coordinated axes stable equilibrium points;
- $a = 0.78$ and $b = 0.67$ then there are four off the coordinated axes stable equilibrium points;
- $a = 0.62$ and $b = 0.80$ then there are no stable equilibrium points.

Further regions of stability and the regions of possible motion of the test particle have also been given based on Jacobian constant. The permissible region of motion increases with increases in the Jacobian constant.

Chapter 5

Conclusions and Future Work

5.1 Conclusions

The research focuses on the rhomboidal central configuration model of the five bodies, with one body at the origin of the coordinate axis, that is, the intersection of the two diagonals of a rhombus, and the other four bodies at the vertices of a rhombus. The primaries always move in the rhomboidal configuration. The existence and linear stability of the equilibrium points were examined. In this regard, the regions for the possible motion of the body with infinitesimal mass have been configured. The equilibrium points have been found qualitatively and verified numerically.

In Chapter 3 of this dissertation, the setting up of the rhomboidal central configuration is discussed with four masses, m_1, m_2, m_3 and m_4 at the vertices of the rhombus, and a fifth mass, m_0 at the intersection of the two diagonals. The origin of the coordinate axis is considered to be the location of the m_0. The two different cases have been discussed with regards to the CC of the five masses. In the *first case*, the masses m_0, m_1, and m_2 at the locations $(0,0)$, $(a,0)$, and $(-a,0)$ respectively are assumed to be equal, i.e., $m_0 = m_1 = m_2 = m$, and the masses at the locations $(0,b)$ and $(0,-b)$ are assumed to be equal, i.e., $m_3 = m_4 = \widetilde{m}$. The central configuration equations of motion show that masses depend on the values

of lengths parameters a and b, i.e., by changing the values of a and b the values of masses change, which ultimately changes the configuration. Setting the parameter $a = 1$, it has been proved that the central configuration holds and the shape is a rhombus through the motion of primaries for $b \in (1/\sqrt{3}, 1.3944282249562009)$.

Three specific cases were discussed for different values of a and b, one of which is that the configuration will be a square when $a = b = 1$ and all the masses are also unity. The CC degenerates in two cases: when $b = \frac{1}{\sqrt{3}}$ and the masses in the horizontal axis become zero, i.e., $m = 0$, and when $b = 1.1394282249562009$ and the $\widetilde{m} = 0$.

In the *second case*, the four primaries form a rhombus by sitting on its vertices, while the fifth mass, m_0, is situated at the origin of the coordinate axis, which is also the point of intersection of the two diagonals of the rhombus. The masses m_1 and m_2 are assumed to be equal, i.e., $m_1 = m_2 = m$ and are located along the horizontal axis, while the masses m_3 and m_4 are considered same, i.e., $m_3 = m_4 = \widetilde{m}$ and are placed on the vertical axis. It has also been assumed that the sum of all the masses is 1, i.e., $m_0 + 2(m + \widetilde{m}) = 1$. We also write in this case the masses, m_0, m and $\widetilde{m}$ in terms of a and b.

It is found that both the mass parameters a and b vary in the interval $(0.5, 1)$ for the existence of the central configuration which is shown graphically and verified numerically. Then by fixing the value of b from the interval $(0.5, 1)$ and varying the value of a in the same interval it has been verified that the equation $m_0 + 2(m + \widetilde{m}) = 1$ always hold in this interval. In this case by the change in the size of masses changed the gravitational field that gave quite interesting results which are discusses in the Chapter 4.

In Chapter 4, the dynamics of the very small test mass, m_5 having an infinitesimal mass as compared to the primaries forming the central configuration of the system are discussed as it moves in the gravitational field of the primaries. This chapter also contains two sections. In the first section, the equation of motion of the sixth mass, m_5 was found with respect to the first model, which has been discussed in the previous chapter.

The relation for the first integral of motion, i.e., the Jacobian constant (C), is discovered, and the relation $U = -C$ represents the boundaries between the possible permissible region of motion of m_5 around the primaries, where U represents the m_5's effective potential. It was determined that the permissible region of motion increases when C is increased.

The equilibrium solutions of m_5 are discovered qualitatively and verified numerically by setting all rates of change appearing in the equation of motion for m_5 equal to zero. The equilibrium points are the locations in space where the gravitational force of the primaries becomes equal for a body with infinitesimal mass; they are also known as Lagrange points, after Joseph-Louis Lagrange [4], who wrote about them in 1772.

In the first section of the chapter 4, where, m_5 is supposed to move under the gravitational influence of the CC model when $m_0 = m_1 = m_2 = m$ and $m_3 = m_4 = \widetilde{m}$. It has been seen that by fixing the parameter $a = 1$ and $b \in (1/\sqrt{3}, 1.3944282249562009)$ the total number of equilibrium points are always 12. Out of the 12 equilibrium points 4 are on the x-axis and 4 are on the y-axis. As the mass parameters varies the equilibrium points also changes their positions around the five primaries and the number of equilibrium points remain same. The linear stability analysis revealed that none of the equilibrium points are stable.

In the second section a significant shift in the position and number of equilibrium points were found in four cases with the variations of mass parameters a and b. Case-I to IV have 16, 20, 12, and 12 equilibrium points respectively, with case-I and case-II have eight off-the-coordinate-axis stable equilibrium points, case-III have four off-the-coordinate-axis stable equilibrium points, and case-IV have no on or off-the-coordinate-axis stable equilibrium points.

A linear stability analysis has been done around equilibrium points. In both cases, the regions of possible motion of m_5 have been discussed, and it has been discovered that as the Jacobian constant 'C' increases, so does the permissible region of motion. The value of 'C', for which the regions of possible motion become disconnected or partially disconnected, has also been discovered.

5.2 Future Work

Understanding the four-, five-, and six-body problems is very important, as it is known that approximately two-thirds of stars in our galaxy are part of multi-stellar systems. The study of central configurations plays an important role in understanding the gravitational N-body problems. In this dissertation, we have developed a symmetrically restricted rhomboidal central configuration of five-body problem called the RR6BP, however, the multi-stellar system can take any quadrilateral or N-Gon shape in the universe. We can understand the Newtonian gravitational field and future work in the above configurations for primaries and then understand the motion of the test particle in these configurations. We can also discuss the Lagrange points and the stability of the test particle in these configurations. With the variation of the Jacobi Constant, we can also discuss the regions of possible motions of the infinitesimal.

Understanding different configurations can pave the way for sending new space missions into the solar system and interstellar space. Recently, the **JWST** has been sent to the L_2 point of the Sun-Earth restricted three-body problem. The **JWST** is designed to investigate the entire life cycle of the solar system, from the first flashes of light following the Big Bang to the formation of solar systems capable of supporting life on planets like Earth. L_2 is also the future home of **Euclid**, **WFIRST**, **LiteBIRD** [115–117].

Bibliography

[1] W. H. Goodyear, "Completely general closed-form solution for coordinates and partial derivative of the two-body problem," *Astronomical Journal, Vol. 70, p. 189*, vol. 70, p. 189, 1965.

[2] I. Newton and N. Chittenden, *Newton's principia: The mathematical principles of natural philosophy.* Geo. P. Putnam, 1850.

[3] L. Euler, "De motu rectilineo trium corporum se mutuo attrahentium," *Novi commentarii academiae scientiarum Petropolitanae*, pp. 144–151, 1767.

[4] J.-L. Lagrange, "Essay on the three-body problem," *Prix de l'académie royale des Sciences de paris*, vol. 9, p. 292, 1772.

[5] S. Ramesh, "Uncovering the new mysteries of our universe: The origins of the james webb space telescope," *Berkeley Scientific Journal*, vol. 26, no. 2, 2022.

[6] S. B. Nicholson, "The trojan asteroids," *Leaflet of the Astronomical Society of the Pacific*, vol. 8, p. 239, 1961.

[7] R. Broucke, "Stability of periodic orbits in the elliptic, restricted three-body problem." *AIAA journal*, vol. 7, no. 6, pp. 1003–1009, 1969.

[8] R. Dvorak, "Critical orbits in the elliptic restricted three-body problem," *Astronomy and Astrophysics*, vol. 167, pp. 379–386, 1986.

[9] H. D. Curtis, *Orbital mechanics for engineering students.* Butterworth-Heinemann, 2013.

[10] A. Plastino and A. Plastino, "Robe's restricted three-body problem revisited," *Celestial Mechanics and Dynamical Astronomy*, vol. 61, no. 2, pp. 197–206, 1995.

[11] M. Hénon, *Generating families in the restricted three-body problem*. Springer Science & Business Media, 2003, vol. 52.

[12] G. Gómez, W. S. Koon, M. Lo, J. E. Marsden, J. Masdemont, and S. D. Ross, "Connecting orbits and invariant manifolds in the spatial restricted three-body problem," *Nonlinearity*, vol. 17, no. 5, p. 1571, 2004.

[13] J. Nagler, "Crash test for the restricted three-body problem," *Physical Review E*, vol. 71, no. 2, p. 026227, 2005.

[14] P. Albers, U. Frauenfelder, O. V. Koert, and G. P. Paternain, "Contact geometry of the restricted three-body problem," *Communications on pure and applied mathematics*, vol. 65, no. 2, pp. 229–263, 2012.

[15] E. I. Abouelmagd and J. L. Guirao, "On the perturbed restricted three-body problem," *Applied Mathematics and Nonlinear Sciences*, vol. 1, no. 1, pp. 123–144, 2016.

[16] U. Frauenfelder and O. Van Koert, *The restricted three-body problem and holomorphic curves*. Springer, 2018.

[17] S. D. Ross and D. J. Scheeres, "Multiple gravity assists, capture, and escape in the restricted three-body problem," *SIAM Journal on Applied Dynamical Systems*, vol. 6, no. 3, pp. 576–596, 2007.

[18] S. Campagnola, P. Skerritt, and R. P. Russell, "Flybys in the planar, circular, restricted, three-body problem," *Celestial Mechanics and Dynamical Astronomy*, vol. 113, no. 3, pp. 343–368, 2012.

[19] R. I. Paez and M. Guzzo, "A study of temporary captures and collisions in the circular restricted three-body problem with normalizations of the levi-civita hamiltonian," *International Journal of Non-Linear Mechanics*, vol. 120, p. 103417, 2020.

[20] J. M. Sánchez-Cerritos and E. Pérez-Chavela, "Hyperbolic regularization of the restricted three–body problem on curved spaces," *Analysis and Mathematical Physics*, vol. 12, no. 1, pp. 1–26, 2022.

[21] G. GOMIERO, "Manifold dynamics in the restricted three body problem and applications to orbital mechanics."

[22] C. Fernández de Heredia Pérez de Zabalza, "Trajectory optimization in the circular restricted three body problem," B.S. thesis, 2019.

[23] M. Álvarez-Ramírez and C. Vidal, "Dynamical aspects of an equilateral restricted four-body problem," *Mathematical Problems in Engineering*, vol. 2009, 2009.

[24] C. D. Murray and S. F. Dermott, *Solar system dynamics*. Cambridge university press, 1999.

[25] D. G. Saari, "On the role and the prooperties of n-body central configuration," *Celestial Mechanics*, vol. 21, no. 1, pp. 9–20, 1980.

[26] F. Pacella, "Central configurations of the n-body problem via equivariant morse theory," *Archive for Rational Mechanics and Analysis*, vol. 97, no. 1, pp. 59–74, 1987.

[27] R. Moeckel, "On central configurations," *Mathematische Zeitschrift*, vol. 205, no. 1, pp. 499–517, 1990.

[28] E. E. Slaminka and K. D. Woerner, "Central configurations and a theorem of palmore," *Celestial Mechanics and Dynamical Astronomy*, vol. 48, no. 4, pp. 347–355, 1990.

[29] Z. Xia, "Central configurations with many small masses," *Journal of Differential Equations*, vol. 91, no. 1, pp. 168–179, 1991.

[30] J. Casasayas, J. Llibre, and A. Nunes, "Central configurations of the planar 1+ n body problem," *Celestial Mechanics and Dynamical Astronomy*, vol. 60, no. 2, pp. 273–288, 1994.

[31] A. Albouy, "On a paper of moeckel on central configurations," *Regular and chaotic dynamics*, vol. 8, no. 2, pp. 133–142, 2003.

[32] J. M. Cors, J. Llibre, and M. Ollé, "Central configurations of the planar coorbitalsatellite problem," *Celestial Mechanics and Dynamical Astronomy*, vol. 89, no. 4, pp. 319–342, 2004.

[33] Y. Long and S. Sun, "Collinear central configurations and singular surfaces in the mass space," *Archive for rational mechanics and analysis*, vol. 173, no. 2, pp. 151–167, 2004.

[34] Z. Xia, "Convex central configurations for the n-body problem," *Journal of Differential Equations*, vol. 200, no. 2, pp. 185–190, 2004.

[35] M. Hampton, "Stacked central configurations: new examples in the planar five-body problem," *Nonlinearity*, vol. 18, no. 5, p. 2299, 2005.

[36] M. Arribas, A. Elipe, and T. Kalvouridis, "Central configuration in the planar (n+ 1) body problem with generalized forces," *Monogr. Real Acad. Ci. Zaragoza*, vol. 28, pp. 1–8, 2006.

[37] M. Corbera and J. Llibre, "Infinitely many periodic orbits for the rhomboidal five-body problem," *Journal of mathematical physics*, vol. 47, no. 12, p. 122701, 2006.

[38] M. Celli, "The central configurations of four masses x,- x, y,- y," *Journal of Differential Equations*, vol. 235, no. 2, pp. 668–682, 2007.

[39] M. Hampton and M. Santoprete, "Seven-body central configurations: a family of central configurations in the spatial seven-body problem," *Celestial Mechanics and Dynamical Astronomy*, vol. 99, no. 4, pp. 293–305, 2007.

[40] J. Llibre and L. F. Mello, "New central configurations for the planar 5-body problem," *Celestial Mechanics and Dynamical Astronomy*, vol. 100, no. 2, pp. 141–149, 2008.

[41] J. Llibre, L. F. Mello, and E. Perez-Chavela, "New stacked central configurations for the planar 5-body problem," *Celestial Mechanics and Dynamical Astronomy*, vol. 110, no. 1, pp. 43–52, 2011.

[42] A. Siluszyk, "On the relative equilibrium configurations in the planar five-body problem," *Opuscula Mathematica*, vol. 30, no. 4, pp. 495–506, 2010.

[43] J. Shi and Z. Xie, "Classification of four-body central configurations with three equal masses," *Journal of Mathematical Analysis and Applications*, vol. 363, no. 2, pp. 512–524, 2010.

[44] Z. Xie, "Super central configurations of the n-body problem," *Journal of Mathematical Physics*, vol. 51, no. 4, p. 042902, 2010.

[45] V. Paraschiv, "Central configurations and homographic solutions for the quasihomogeneous n-body problem," *Journal of mathematical physics*, vol. 53, no. 12, p. 122902, 2012.

[46] Z. Xie, "Isosceles trapezoid central configurations of the newtonian four-body problem," *Proceedings of the Royal Society of Edinburgh Section A: Mathematics*, vol. 142, no. 3, pp. 665–672, 2012.

[47] M. Shoaib, I. Faye, and A. Sivasankaran, "Some special solutions of the rhomboidal five-body problem," in *AIP Conference Proceedings*, vol. 1482, no. 1. American Institute of Physics, 2012, pp. 496–501.

[48] M. Marchesin and C. Vidal, "Spatial restricted rhomboidal five-body problem and horizontal stability of its periodic solutions," *Celestial Mechanics and Dynamical Astronomy*, vol. 115, no. 3, pp. 261–279, 2013.

[49] J. Llibre, "On the central configurations of the n-body problem," *Applied Mathematics and Nonlinear Sciences*, vol. 2, no. 2, pp. 509–518, 2017.

[50] Y. Deng, B. Li, and S. Zhanga, "Four-body central configurations with adjacent equal masses," *Journal of Geometry and Physics*, vol. 114, pp. 329–335, 2017.

[51] M. Corbera, J. M. Cors, J. Llibre, and E. Pérez-Chavela, "Trapezoid central configurations," *Applied Mathematics and Computation*, vol. 346, pp. 127–142, 2019.

[52] M. Corbera, J. M. Cors, and G. E. Roberts, "Classifying four-body convex central configurations," *Celestial Mechanics and Dynamical Astronomy*, vol. 131, no. 7, pp. 1–27, 2019.

[53] M. Álvarez-Ramírez and J. Llibre, "Hjelmslev quadrilateral central configurations," *Physics Letters A*, vol. 383, no. 2-3, pp. 103–109, 2019.

[54] M. Moczurad and P. Zgliczyński, "Central configurations in planar n-body problem with equal masses for $n = 5, 6, 7$," *Celestial Mechanics and Dynamical Astronomy*, vol. 131, no. 10, pp. 1–28, 2019.

[55] L. Ding, J. M. Sánchez-Cerritos, and J. Wei, "Eulerian collinear configuration for 3-body problem," *arXiv preprint arXiv:1910.00367*, 2019.

[56] O. Hénot and C. Rousseau, "Spiderweb central configurations," *Qualitative theory of dynamical systems*, vol. 18, no. 3, pp. 1135–1160, 2019.

[57] M. Hampton, "Planar n-body central configurations with a homogeneous potential," *Celestial Mechanics and Dynamical Astronomy*, vol. 131, no. 5, pp. 1–27, 2019.

[58] L. Ding, J. Wei, and S. Zhang, "The central configuration of the planar (n+1)-body problem with a regular n-polygon," *arXiv preprint arXiv:2005.07487*, 2020.

[59] Y. Deng and M. Hampton, "Equilateral chains and cyclic central configurations of the planar 5-body problem," *arXiv preprint arXiv:2112.06755[math.DS]*, 2021.

[60] A. C. Fernandes, L. F. Mello, L. Ruiz dos Santos, and C. Vidal, "Planar central configurations of six bodies," *Journal of Mathematical Physics*, vol. 63, no. 6, p. 062701, 2022.

[61] Z. Wang, "On the centered co-circular central configurations for the n-body problem," *arXiv preprint arXiv:2211.14820*, 2022.

[62] X. Su and C. Deng, "On the symmetric central configurations for the planar 1+ 5-body problem with small arbitrary masses," *Celestial Mechanics and Dynamical Astronomy*, vol. 134, no. 3, pp. 1–17, 2022.

[63] G. Libourel and C. M. Corrigan, "Asteroids: New challenges, new targets," *Elements*, vol. 10, no. 1, pp. 11–17, 2014.

[64] "Where Is Webb? NASA/Webb — webb.nasa.gov," https://webb.nasa.gov/content/webbLaunch/whereIsWebb.html, [Accessed 28-09-2023].

[65] E. Belbruno, "A new family of periodic orbits for the restricted problem," *Celestial mechanics*, vol. 25, no. 2, pp. 195–217, 1981.

[66] A. A. Ansari and Z. A. Alhussain, "The restricted five-body problem with cyclic kite configuration," *Journal of Dynamical Systems and Geometric Theories*, vol. 17, no. 1, pp. 91–107, 2019.

[67] A. Ollongren, "On a particular restricted five-body problem an analysis with computer algebra," *Journal of symbolic computation*, vol. 6, no. 1, pp. 117–126, 1988.

[68] C. Liu and L. Dong, "Stabilization of lagrange points in circular restricted three-body problem: a port-hamiltonian approach," *Physics Letters A*, vol. 383, no. 16, pp. 1907–1914, 2019.

[69] R. Lara and A. Bengochea, "A restricted four-body problem for the eight figure choreography," *arXiv preprint arXiv:1910.12822*, 2019.

[70] P. Meena and R. Kishor, "First order stability test of equilibrium points in the planar elliptic restricted four body problem with radiating primaries," *Chaos, Solitons & Fractals*, vol. 150, p. 111138, 2021.

[71] M. Alvarez-Ramírez and M. Medina, "Overview and comparison of approaches towards the planar restricted five-body problem with primaries

forming an axisymmetric four-body central configuration," *Astrophysics and Space Science*, vol. 365, no. 2, pp. 1–10, 2020.

[72] J. A. Zepeda Ramírez, M. Alvarez-Ramírez, and A. García, "Nonlinear stability of equilibrium points in the planar equilateral restricted mass-unequal four-body problem," *International Journal of Bifurcation and Chaos*, vol. 31, no. 11, p. 2130031, 2021.

[73] A. Alsaedi, F. Yousef, S. Bushnaq, and S. Momani, "New styles of periodic solutions of the classical six-body problem," *Mathematics and Computers in Simulation*, vol. 159, pp. 183–196, 2019.

[74] M. J. Idrisi and M. S. Ullah, "Central-body square configuration of restricted six-body problem," *New Astronomy*, p. 101381, 2020.

[75] M. J. Idrisi, M. S. Ullah, and A. Sikkandhar, "Effect of perturbations in coriolis and centrifugal forces on libration points in the restricted six-body problem," *The Journal of the Astronautical Sciences*, vol. 68, no. 1, pp. 4–25, 2021.

[76] M. Kulesza, M. Marchesin, and C. Vidal, "Restricted rhomboidal five-body problem," *Journal of Physics A: Mathematical and Theoretical*, vol. 44, no. 48, 2011.

[77] J. Waldvogel, "The rhomboidal symmetric four-body problem," *Celestial Mechanics and Dynamical Astronomy*, vol. 113, no. 1, pp. 113–123, 2012.

[78] M. Marchesin and C. Vidal, "Stability in a rhomboidal 5-body problem with generalized central forces," *Journal of Mathematical Physics*, vol. 54, no. 10, p. 102902, 2013.

[79] M. Marchesin, "Stability of a rhomboidal configuration with a central body," *Astrophysics and Space Science*, vol. 362, no. 1, 2017.

[80] S. Smale, "Mathematical problems for the next century," *The mathematical intelligencer*, vol. 20, no. 2, pp. 7–15, 1998.

[81] A. E. Roy, *Orbital motion*. CRC Press, 2020.

[82] M. Alonso and E. J. Finn, *Fundamental university physics*. Addison-Wesley Reading, MA, 1967, vol. 2.

[83] F. R. Moulton, *An introduction to celestial mechanics*. Courier Corporation, 1970.

[84] Y. Zhu, "Interaction of gravitational field and orbit in sun-planet-moon system," 2021.

[85] D. Cline, *Variational principles in classical mechanics*. University of Rochester River Campus Librarie, 2017.

[86] C. Q. Choi, "First asteroid companion of earth discovered at last," *Space. com. Retrieved*, vol. 27, 2011.

[87] T. Santana-Ros, M. Micheli, L. Faggioli, R. Cennamo, M. Devogèle, A. Alvarez-Candal, D. Oszkiewicz, O. Ramírez, P.-Y. Liu, P. G. Benavidez *et al.*, "Orbital stability analysis and photometric characterization of the second earth trojan asteroid 2020 xl5," *Nature Communications*, vol. 13, no. 1, p. 447, 2022.

[88] M.-T. Hui, P. A. Wiegert, D. J. Tholen, and D. Föhring, "The second earth trojan 2020 xl5," *The Astrophysical Journal Letters*, vol. 922, no. 2, p. L25, 2021.

[89] R. A. Freitas Jr and F. Valdes, "A search for natural or artificial objects located at the earth-moon libration points," *Icarus*, vol. 42, no. 3, pp. 442–447, 1980.

[90] "List Of Neptune Trojans — minorplanetcenter.net," https://minorplanetcenter.net//iau/lists/NeptuneTrojans.html, [Accessed 28-09-2023].

[91] L. D. Schmadel and L. D. Schmadel, *Dictionary of minor planet names*. Springer, 2012.

[92] G. Borisov, A. Christou, F. Colas, S. Bagnulo, A. Cellino, and A. DellOro, "(121514) 1999 uj7: A primitive, slow-rotating martian trojan," *Astronomy & Astrophysics*, vol. 618, p. A178, 2018.

[93] G. Borisov, A. Christou, S. Bagnulo, A. Cellino, and A. DellOro, "The lunar-like mineralogy of the martian trojan asteroid (101429) 1998 vf31," in *EPSC-DPS Joint Meeting 2019*, vol. 2019, 2019, pp. EPSC–DPS2019.

[94] "MPEC 2007-O03 : 2007 NS2 — minorplanetcenter.net," https://www.minorplanetcenter.net/mpec/K07/K07O03.html, [Accessed 28-09-2023].

[95] J. Blunck, *Solar system moons: Discovery and mythology*. Springer Science & Business Media, 2009.

[96] F. Roques, "Formation and dynamic history of the solar system," *The Solar System 2: External Satellites, Small Bodies, Cosmochemistry, Dynamics, Exobiology*, pp. 205–256, 2021.

[97] D. G. Saari, "Central Configurations-A problem for the Twenty-first Century," *Exped. Math. MAA Spectrum*, pp. 283–295, 2011.

[98] F. Yan-ning and S. Yi-sui, "The homographic solutions in the n-body problem with a general attraction," *Chinese astronomy and astrophysics*, vol. 17, no. 4, pp. 442–448, 1993.

[99] A. Wintner, "The analytical foundations of celestial mechanics," *Princeton*, 1941.

[100] D. G. Saari, "On the role and the properties of n-body central configurations," *Celestial mechanics*, vol. 21, no. 1, pp. 9–20, 1980.

[101] A. Albouy and A. Chenciner, "The n-body problem and mutual distances," *Inventiones mathematicae*, vol. 131, no. 1, pp. 151–184, 1997.

[102] D. Schmidt, "Central configurations and relative equilibria for the n-body problem, classical and celestial mechanics (recife, 1993/1999)," 2002.

[103] D. Saari, *Collisions, Rings, and Other Newtonian N-Body Problems*. American Mathematical Soc., 2005, no. 104.

[104] R. Moeckel, "On central configurations," *Mathematics Zeitschrift*, vol. 205, no. 1, pp. 499–517, 1990.

[105] A. Albouy and V. Kaloshin, "Finiteness of central configurations of five bodies in the plane," *Annals of Mathematics*, vol. 176, pp. 1–54, 2012.

[106] R. Moeckel, J. Libre, and C. Simó, *Central Configurations, Periodic Orbits, and Hamiltonian Systems*. Springer Link, 2015.

[107] M. Marchesin, "Stability of a rhomboidal configuration with a central body," *Astrophysics and Space Science*, vol. 362, no. 1, p. 1, 2017.

[108] A. Albouy, "The symmetric central configurations of four equal masses," *Contemporary Mathematics*, vol. 198, pp. 131–136, 1996.

[109] C. Simo, "Relative equilibrium solutions in the four body problem," *Celestial Mechanics*, vol. 18, no. 2, pp. 165–184, 1978.

[110] M. Shoaib, A. R. Kashif, and I. Szücs-Csillik, "On the planar central configurations of rhomboidal and triangular four-and five-body problems," *Astrophysics and Space Science*, vol. 362, no. 10, p. 182, 2017.

[111] J. L. Cornelio, M. Alvarez-Ramírez, and J. M. Cors, "Central configurations in the five-body problem: Rhombus plus one," *Qualitative theory of dynamical systems*, vol. 20, no. 2, pp. 1–13, 2021.

[112] M. S. Suraj, S. S. Alhowaity, and R. Aggarwal, "Fractal basins of convergence in the restricted rhomboidal six-body problem," *New Astronomy*, p. 101798, 2022.

[113] M. S. Suraj, S. Alhowaity, R. Aggarwal, M. C. Asique, and A. Alahmadi, "On the rhomboidal restricted five-body problem: Analysis of the basins of convergence," *New Astronomy*, p. 101893, 2022.

[114] R. Broucke, "Periodic orbits in the restricted three body problem with earth-moon masses," Tech. Rep., 1968.

[115] "Euclid overview — esa.int," https://www.esa.int/Science_Exploration/Space_Science/Euclid_overview, [Accessed 28-09-2023].

[116] R. Akeson, L. Armus, E. Bachelet, V. Bailey, L. Bartusek, A. Bellini, D. Benford, D. Bennett, A. Bhattacharya, R. Bohlin *et al.*, "The wide field infrared survey telescope: 100 hubbles for the 2020s," *arXiv preprint arXiv:1902.05569*, 2019.

[117] M. Hazumi, P. A. Ade, A. Adler, E. Allys, K. Arnold, D. Auguste, J. Aumont, R. Aurlien, J. Austermann, C. Baccigalupi *et al.*, "Litebird satellite: Jaxa's new strategic l-class mission for all-sky surveys of cosmic microwave background polarization," in *Space Telescopes and Instrumentation 2020: Optical, Infrared, and Millimeter Wave*, vol. 11443. SPIE, 2020, pp. 431–450.